Computational approach to the Schottky problem

Eddy Brandon de Leon Aguilar

Université de Bourgogne Franche-Comté
Institut de Mathématiques de Bourgogne
École doctorale Carnot-Pasteur

THÈSE

pour l'obtention du grade de

Docteur de l'Université de Bourgogne

en Mathématiques

présentée et soutenue publiquement par

Eddy Brandon DE LEÓN AGUILAR

le 5 juillet 2023

Computational approach to the Schottky problem

Directeur de thèse : **Christian KLEIN**

Jury composé de

Simonetta ABENDA	University of Bologna	Rapporteuse
Samuel GRUSHEVSKY	Stony Brook University	Rapporteur
Jörg FRAUENDIENER	University Of Otago	Examinateur
Türkü ÇELIK	Boğaziçi University	Examinatrice
Jean-Marc COUVEIGNES	Université de Bordeaux	Président du Jury
Dmitri KOROTKIN	Concordia University	Examinateur
Nikola STOILOV	Université de Bourgogne	Examinateur
Christian KLEIN	Université de Bourgogne	Directeur

Abstract

We present a computational approach to the classical Schottky problem based on Fay's trisecant identity for genus $g \geq 4$. For a given Riemann matrix $\Omega \in \mathbb{H}^g$, the Fay identity establishes linear dependence of secants in the Kummer variety if and only if the Riemann matrix corresponds to a Jacobian variety as proved by Krichever. The theta functions in terms of which these secants are given depend on the Abel maps of four arbitrary points on a Riemann surface. To establish linear dependence of the secants, four components of these Abel maps are conveniently chosen. The remaining components are determined by a Newton iteration to minimize the residual of the Fay identity. Krichever's theorem assures that if this residual vanishes within the finite numerical precision for a generic choice of input data, then the Riemann matrix is with this numerical precision in the Jacobi locus.

The algorithm is compared in genus 4 for some examples to the Schottky-Igusa modular form known to give the Jacobi locus in this case. In genera 5, 6 and 7, we discuss known examples of Riemann matrices and perturbations thereof for which the Fay identity is not satisfied.

To illustrate the importance of Jacobian varieties in areas outside of mathematics, we present algebro-geometric solutions of the Ernst equation that solve the Einstein field equations for stationary axisymmetric spacetimes. These solutions have not been studied extensively in simulations, due to the computational cost of calculating theta functions. Thus, we present a series of numerical techniques in order to approach the numerical simulations efficiently, which would allow further studies of these solutions.

Résumé

Nous présentons une approche numérique du problème de Schottky classique basée sur l'identité trisécante de Fay pour le genre $g \geq 4$. Pour une matrice de Riemann $\Omega \in \mathbb{H}^g$ donnée, l'identité de Fay établit une dépendance linéaire des sécantes dans la variété de Kummer si et seulement si la matrice de Riemann correspond à une variété jacobienne comme le prouve Krichever. Les fonctions thêta sous forme desquelles ces sécantes sont données dépendent des applications d'Abel de quatre points arbitraires sur une surface de Riemann. Pour établir la dépendance linéaire des sécantes, quatre composants de ces applications d'Abel sont choisis. Les composants restants sont déterminés par une itération de Newton pour minimiser le résidu de l'identité de Fay. Le théorème de Krichever assure que si ce résidu disparaît avec précision numérique finie pour un choix générique de données d'entrée, alors la matrice de Riemann est avec cette précision numérique dans le lieu de Jacobi.

L'algorithme est comparé en genre 4 pour quelques exemples à la forme modulaire de Schottky-Igusa donnant le lieu de Jacobi dans ce cas. Dans les genres 5, 6 et 7, nous discutons des exemples connus de matrices de Riemann et de leurs perturbations pour lesquelles l'identité de Fay n'est pas satisfaite.

De plus, pour souligner l'importance des variétés jacobiennes dans des domaines en dehors des mathématiques, nous présentons des solutions algébro-géométriques de l'équation d'Ernst qui résolvent les équations de champ d'Einstein pour des espaces-temps stationnaires et à symétrie axiale. Ces solutions n'ont pas été largement étudiées dans les simulations, en raison du coût de calcul des fonctions thêta. Ainsi, nous présentons une série de techniques numériques afin d'aborder efficacement les simulations numériques, ce qui permettrait d'approfondir l'étude de ces solutions.

Acknowledgements

I would like to start by expressing my gratitude to mi advisor, Christian Klein. None of this would have been possible without all your support. Thanks to your guidance I have been able to explore different areas in both physics and mathematics. I am also grateful for the opportunity you gave me to meet other collaborators and traveling the world while working on topics of my interest.

I want to thank Dmitri Korotkin for hosting me in Montreal and giving me the opportunity to work on a topic linking relativity and algebraic geometry in whose development he played an important role.

I am thankful to Jörg Frauendiener for sharing all his years of experience in general relativity and for his valuable suggestions on how to approach my numerical simulations.

I am fortunate to have met the other PhD students at the IMB. It has been a amazing experience to have shared these years with people from all over the world and learning that life goes beyond mathematics.

I thank my siblings —Paulina, Denilson, Nancy and Leslie— for all these years we spent growing up together.

I am infinitely grateful to my parents —Elsa and Obispo— for believing in me when nobody else did. Thank you for feeding my curiosity since my early childhood and for having done the impossible to support my dream of studying science and mathematics.

I thank for the financial support provided by the EIPHI Graduate School (contract ANR-17-EURE-0002), the Bourgogne-Franche-Comté Region, the European fund FEDER, and the European Union Horizon 2020 research and innovation program under the Marie Sklodowska-Curie RISE 2017 grant agreement no. 778010 IPaDE-GAN.

Activités de vulgarisation

Tout au long de mes années de doctorat, j'ai participé en tant que tuteur à une série d'écoles d'été appelées «French+Sciences» organisées par l'EIPHI Graduate School. Le but de ces écoles était de permettre aux étudiants internationaux d'apprendre le français tout en assistant à des cours sur les recherches menées à l'Université Bourgogne-Franche-Comté. C'est, en outre, un événement entre Dijon et Besançon. Ma contribution à cet événement s'est déroulée dans le cours «Mathematics for applied physics: an application in health sciences» où j'ai présenté la partie sur les méthodes numériques. Plus précisément, j'ai donné une brève introduction aux méthodes spectrales. Ces méthodes on différents domaines d'application, notamment aux équations aux dérivées partielles avec des conditions au bord.

La première école était organisée en 2021, mais l'événement sur place a été annulé en raison de la pandémie. Par conséquent, les cours ont été enregistrés en format vidéo afin de lancer une version virtuelle de l'école d'été.

Puis, en avril 2022, l'EIPHI Graduate School a organisé l'école en coopération avec l'Université ITS d'Indonésie, pendant laquelle nous avons enseigné les mêmes cours, mais cette fois en présentiel.

En juin 2022, le programme normal des écoles d'été a repris et des étudiants internationaux de différents pays ont pu venir en France. J'ai de nouveau participé au cours sur l'application des mathématiques à l'imagerie médicale. Plus précisément, j'ai expliqué comment les méthodes spectrales peuvent etre appliquées au problème de la tomographie par impédance électrique (Electrical Impedance Tomography). À chaque occasion, j'ai présenté des exemples simples à comprendre mais liés au problème initial. Le problème de la tomographie par impédance électrique consiste à trouver le potentiel électrique à l'intérieur d'un corps à partir de valeurs limites données. L'un des exemples que j'ai présenté était de trouver le potentiel à l'extérieur de deux conducteurs sphériques à partir du potentiel aux surfaces. L'idée est la même mais elle est beaucoup plus simple à comprendre et donc plus adaptée aux étudiants. Je l'ai résolu en utilisant des méthodes spectrales et j'ai montré son efficacité par rapport à d'autres schémas numériques.

Lors de l'école d'été organisée en juin 2023, les cours proposés ont changé. A cette occasion j'ai participé au cours «Non-linear fiber optics» et j'ai à nouveau présenté le cours sur les méthodes spectrales, mais cette fois je me suis concentré sur ses applications physiques. Dans tous ces cours en présentiel, j'ai présenté le logiciel open source Octave et j'ai laissé aux étudiants quelques exercices prêts à l'emploi afin qu'ils puissent voir comment fonctionne le schéma numérique en modifiant certains paramètres sur les conditions des équations différentielles.

Enfin, lors de la dernière partie de ma thèse j'ai travaillé sur les techniques de simulation d'images dans des espaces-temps en rotation. Bien que le but de ce travail soit d'étudier le mouvement de la lumière et de générer des images d'objets dans des espaces-temps plutôt généraux, il permet également de construire des exemples pédagogiques pour montrer au grand public des phénomènes intéressants qui se produisent dans les espaces-temps autour des trous noirs. Ce qui est l'exemple le plus étudié parmi les espaces-temps en rotation. Nous pouvons donc montrer plusieurs simulations d'images et même des animations de mouvement de particules individuelles, afin d'observer les effets d'un fort champ gravitationnel de manière très visuelle, adaptée aux objectifs de vulgarisation scientifique.

Contents

List of Figures

List of Symbols

$\mathcal{R}$	Riemann surface
$H_1(\mathcal{R}, \mathbb{Z})$	First homology group of $\mathcal{R}$
$H^0(\mathcal{R}, \Omega^1_{\mathcal{R}})$	Space of holomorphic differentials on $\mathcal{R}$
$\mathbb{B}$	Period matrix of a Riemann surface
Ω	Riemann matrix
$\mathbb{C}^g$	g-dimensional complex space
$\Lambda_\Omega = \mathbb{Z}^g + \Omega\mathbb{Z}^g$	Full-rank lattice in $\mathbb{C}^g$
$\mathrm{Jac}(\mathcal{R})$	Jacobian variety of $\mathcal{R}$
ϑ	Riemann theta function
Θ	Theta divisor of the function ϑ
$\alpha(P)$	Abel map of $P \in \mathcal{R}$
$\int_b^a$	Difference of Abel maps $\alpha(b) - \alpha(a)$
$\mathbb{H}^g$	Siegel halfspace of degree g
$\mathcal{J}_g$	Jacobi locus
$\mathcal{M}_g$	Moduli space of Riemann surfaces
$\mathcal{A}_g$	Moduli space of principally polarized Abelian varieties
$\mathrm{Sp}(2g, \mathbb{Z})$	Symplectic group
$g_{\mu\nu}$	Metric coefficients in local coordinates
$\langle \cdot, \cdot \rangle$	Euclidean scalar product

Chapter 1

Introduction

Riemann surfaces play an eminent role in mathematics and physics. They are of special importance in the context of integrable systems. The first success beyond elliptic surfaces was the integration of the Kovaleskaya top [Kow88] in terms of theta functions on a hyperelliptic surface of genus 2. Bianchi [Bia94] in principle showed the integrability of the surfaces named after him by introducing a spectral parameter in the Gauss-Weingarten equations for these surfaces. It is interesting to note that solutions of the stationary axisymmetric Einstein equations in vacuum can be constructed from solutions to the Ernst equation [Ern68] which can be seen as a Bianchi surface, see for instance [KR05]. In the 1970s, quasiperiodic solutions to completely integrable partial differential equations (PDEs) were given in terms of multidimensional theta functions. First the Korteweg-de Vries equation was treated with this approach which led to the Its-Matveev formula for KdV in terms of hyperelliptic theta functions. In 1977 Krichever solved the Kadomtsev-Petviashvili (KP) equation in terms of theta functions on arbitrary compact Riemann surfaces, see [Bel+94; Dub81] for a historic account of the development.

The success in applying Riemann surfaces to integrable systems raised the question of the computability of the solutions. The theta functions in terms of which these solutions are defined depend on the period matrix of the Riemann surface, which is a symmetric matrix with positive imaginary part (called Riemann matrix). However, a simple parametrization of the solutions via the components of the Riemann matrix fails due to the fact that not all such matrices entering Krichever's solution arise from Riemann surfaces. Novikov conjectured that Krichevers's formula gives solutions to KP if and only if Riemann matrices being the matrix of periods of a Riemann surface are used. This would provide a characterization of the classical *Schottky problem* to identify in the space of all symmetric matrices with positive definite imaginary part the ones that are periods of a Riemann surface (known as the *Jacobi locus*). Novikov's conjecture was eventually proven by Shiota [Shi86].

The question remained open whether Novikov's idea to use KP solutions to solve the Schottky problem can be applied in practice, i.e., in a computational approach. This means, is there a way to decide numerically for a given Riemann matrix at least with finite precision whether it is in the Jacobi locus? Finding solutions to the KP equation is a computationally challenging task when the only given data is the Riemann matrix. However, Shiota's proof led to a result of greater practical significance. In this thesis, we provide an implementation of such a result for genus up to 7.

More concretely the topological classification of compact Riemann surfaces is given by one single number g, which is known as the genus of the surface. We say

that a Riemann surface $\mathcal{R}$ has genus g if it is homeomorphic to a sphere with g-handles. If $\mathcal{R}$ has genus g, then the rank of its first homology group is $2g$. Loosely speaking, the basis elements of the first homology group are cycles that cannot be deformed one into another. Let us denote such a basis by $\{a_1, b_1, ..., a_g, b_g\}$. The space of holomorphic differentials of a genus-g Riemann surface is g-dimensional and its basis is denoted by $\{\omega_1, \ldots, \omega_g\}$. Moreover, it is possible to consider a basis normalized with respect to the a-cycles, namely, the basis elements can be chosen such that $\int_{a_j} \omega_k = \delta_{jk}$. With this normalization, the $g \times g$ matrix $\mathbb{B}$ with components $\mathbb{B}_{jk} = \int_{b_j} \omega_k$ is defined as the period matrix of $\mathcal{R}$. This matrix has some interesting properties: it turns out that $\mathbb{B}$ is symmetric and its imaginary part is positive definite. The Jacobian variety of $\mathcal{R}$ is defined as the complex torus

$$\mathrm{Jac}(\mathcal{R}) := \mathbb{C}^g / \Lambda_{\mathbb{B}} = \mathbb{C}^g / (\mathbb{Z}^g + \mathbb{B} \cdot \mathbb{Z}^g).$$

Together with the divisor (zero set) of the theta function

$$\vartheta_{\mathbb{B}}(\mathbf{z}) = \sum_{\mathbf{n} \in \mathbb{Z}^g} \exp(\pi \mathrm{i} \langle \mathbf{n}, \mathbb{B}\mathbf{n} \rangle + 2\pi \mathrm{i} \langle \mathbf{n}, \mathbf{z} \rangle),$$

denoted $\Theta_{\mathbb{B}}$, the Jacobian variety $\mathrm{Jac}(\mathcal{R})$ defines a principally polarized Abelian variety (the precise definition is given in Chapter 2). In general, PPAVs are parametrized by symmetric matrices with positive definite imaginary part. This set is known as the Siegel's halfspace of degree g and denoted by $\mathbb{H}^g$. The dimension of this space is clearly $\frac{1}{2}g(g+1)$. On the other hand, it is known that isomorphism classes of Riemann surfaces are parametrized by one (complex) parameter if $g = 1$ and $3g - 3$ parameters if $g > 1$. Thus not all Riemann matrices follow from a Riemann surface.

The locus of PPAVs that are defined by the period matrix of a Riemann surface is denoted by $\mathcal{J}_g$ and known as the Jacobi locus. The formulation of the Schottky problem we are interested in is: given a Riemann matrix determine whether it is in the Jacobi locus or not. Although the problem goes back to Riemann, the first person to give a partial solution was Schottky (1888) for the case $g = 4$. He found a modular form $\Sigma : \mathbb{H}^4 \to \mathbb{C}$ that vanishes on $\mathcal{J}_4$. Igusa (1981) proved rigorously that the zero locus of such modular forms coincides with the Jacobi locus, namely, $\Sigma(\Omega) = 0$ if and only if Ω is the Riemann surface of some suitable Riemann surface of genus g. Finding a higher dimensional analogous of this solution is hard and only partial results exist to date.

Another formulation of the Schottky problem is the following: provide a characterization of the Jacobi locus. Namely, give conditions on $\Omega \in \mathbb{H}^g$, or its associated PPAV, such that it defines a Jacobian variety.

As mentioned above, a different approach to the Schottky problem was provided when Krichever [Kri77] gave algebro-geometric solutions to the KP equation in terms of theta functions of Jacobian varieties. In this context, an effective characterization of Jacobian varieties is given by Shiota's solution of the Novikov conjecture. The difference with respect to Schottky-Igusa's solution is that it requires extra parameters that are non-trivial to determine. Thus, using this characterization to determine explicitly whether a given Riemann matrix is in the Jacobi locus is a difficult task in practice.

Another approach was inspired by the celebrated Fay identity (although it is closely related to the former). Fay's identity is a relation between theta functions on

a Jacobian variety in dependence of four arbitrary points on its defining Riemann surface. A corollary of this identity due to Mumford [Mum83] is that it parametrizes a four-dimensional family of non-identical collinear points in the Kummer variety (the embedding of the Jacobian variety into projective space). Gunning [Gun82] then proved that given three parameters in a PPAV satisfying some non-degeneracy conditions, the existence of a one-dimensional family of collinear points in the Kummer variety characterizes Jacobians. This was further developed by Welters [Wel84] in terms of flexes (collinear points up to order two). The main result we are interested in is due to Krichever [Kri10] in which he proved that the existence of only one trisecant in the Kummer variety of the PPAV is a characterization of Jacobian varieties. This is the most important solution to date to determine in practice whether a given $\Omega \in \mathbb{H}^g$ is a period matrix.

The goal is to set up an algorithm to look exhaustively for trisecant points in the Kummer variety defined by Ω. Extending Fay's identity to the whole complex torus, we set up a locally holomorphic function of the form $F : \mathbb{C}^n \to \mathbb{C}^m$, where $n, m \in \mathbb{Z}$, such that $F(\mathbf{x}) = 0$ if and only if there exist non-identical trisecant points in the Kummer variety (the precise definition of this is given in Chapter 2). In terms of this function, Krichever's theorem translates to: a matrix $\Omega \in \mathbb{H}^g$ is the period matrix of some Riemann surface of genus g if and only if the zero set of its associated function F is non-empty. Taking advantage of the analyticity of F, we use Newton's method to perform the extensive search of zeros efficiently. The way this method works is that given an initial guess $\mathbf{x}^{(0)}$, we look for another point in its neighborhood such that $F(\mathbf{x}^{(1)})$ is closer to be a zero and the process is repeated until a zero is found. The holomorphic property of F stabilizes the iterative process, namely, if $\mathbf{x}^{(n)}$ is close to a zero, the iteration will converge in just a few steps. The only downside is that this a local method, which implies that if the initial guess is far from a zero, then the iteration might fail to converge.

Another approach is to express the search for trisecant points as an optimization problem. Namely, set up a function $f : S \subset \mathbb{R}^{2n} \to \mathbb{R}$, where S is a compact subset, such that $\min_{\mathbf{x} \in S}(f) = 0$ if and only if there exist non-identical trisecant points. This type of problems can be approached by global optimization methods, such as *simulated annealing*. The particularity of this method is that it accepts less optimal points with some probability in order to perform an extensive search at the beginning of the iteration. As the iteration progresses, this acceptance probability goes to zero and the method becomes a local optimizer, but the iteration is expected to be in the neighborhood of a local minimum by then.

Overall, based on our numerical experiments, it is much more effective using Newton's method, since we can take advantage of the knowledge we have from Fay's identity about trisecant points to set up starting points in the neighborhood of a zero and then assure convergence.

We present some numerical experiments using the algorithm with Newton's method. We start by studying the stability of the method applied to this specific type of problems, by considering a Riemann matrix that is known to be in the Jacobi locus and with known Abel maps. This means that we can test with points in the neighborhood of a zero. As expected, this method converges to a zero up to machine precision in just a few steps.

Then we focus on the simplest non-trivial case for which an explicit solution exists. Namely, in $g = 4$ we compare the Schottky-Igusa form to the minimum residual obtained by our method. The residual is defined as $\|f(x^{(n)}) - f(x_*)\|$, where $f(x_*)$

is the result we are looking for and since we are interested in zeros of this function, $f(x_*) = 0$. Then, the residual is just $\|f(x^{(n)})\|$. We consider the family of Riemann matrices given by [GM18] and add perturbations that lead to Riemann matrices outside of the Jacobi locus. The following is the graph obtained by performing the search using our method compared to the norm of the Schottky-Igusa form.

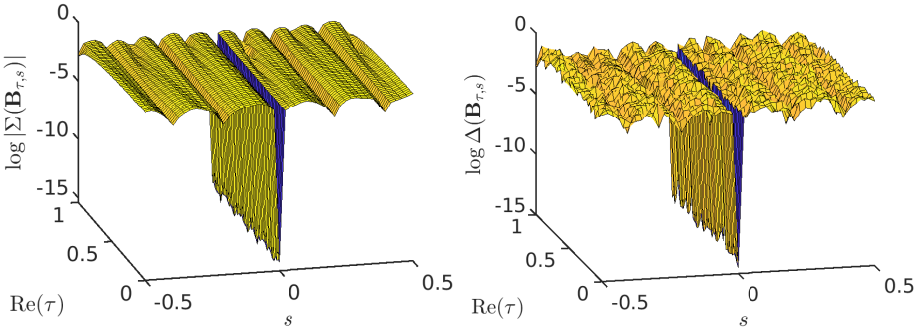

FIGURE 1.1: Schottky-Igusa form on the left and the smallest attained residual of f on the right.

It can be observed that only the Riemann matrices that correspond to Riemann surfaces converge to zero to machine precision. Adding even smaller perturbations, the smallest residual can be used as an indicator of the accuracy of the period matrix (if it is computed numerically, as it is usually the case). Although we show experiments with double precision, this algorithm is general enough to be implemented in different programming languages and with various numerical precisions.

As mentioned above, some of the oldest completely integrable models arose in surface theory. In Chapter 6 we discuss a special example, the Ernst equation, an important integrable system with applications in general relativity. We will see the importance of Jacobi varieties in a field seemingly disconnected to algebraic geometry, namely, stationary axisymmetric vacuum spacetimes. The rotating Kerr black hole is the most popular representant of this class [Ker63]. The Einstein field equations describe the geometry of a 4-dimensional Lorentzian manifold (known as *spacetime*). In general, these equations are not integrable, but imposing extra symmetries gives rise to integrable systems. For instance, if the metric is axisymmetric and time independent, solutions of the Einstein equations can be constructed from solutions to the Ernst equation via quadratures. The particularity of this integrable system with respect to nonlinear evolution equations such as KdV and KP is that the solutions in terms of theta functions do not show periodicity properties since the modular dependence is important here. Whereas the algebro-geometric solutions of KdV and KP equations are generated on a constant Jacobian variety, the solutions to Ernst's equation are given on a family of Riemann surfaces where some of the branch points depend on the physical coordinates.

These solutions have not been extensively studied due to the computational cost of computing theta functions, the period matrices and the Abel maps. However, the Kerr solution can be obtained as the solitonic limit of a particular class of solutions. This is the most prominent stationary axisymmetric spacetime since it models rotating black holes, the most interesting type of black holes from an astrophysical point of view [EHT19]. We use this solution as a test case to develop approximation

techniques to study geodesics in general Weyl-Lewis-Papepetrou metrics for which the Ernst equation is defined. This would allow further studies of the class of solutions obtained via algebro-geometric methods. For instance, the class of solutions obtained by Korotkin [Kor88] and the disk solutions in [FK01b], both of which are given in terms of multidimensional theta functions.

The thesis is organized as follows. In Chapter 2 we present concepts on Riemann surfaces, principally polarized Abelian varieties and theta functions that will be useful throughout the thesis. In Chapter 3 we present the Fay identity in its many different forms and its role in characterizing the Schottky problem. In Chapter 4 we adapt the Fay identity for computational purposes; we also present the numerical tools to perform the search of trisecant points. In Chapter 5 we apply the algorithm to determine whether a given Riemann matrix defines a Jacobian variety up to $g = 7$. In Chapter 6 we discuss the physical importance of stationary axisymmetric vacuum spacetimes and present a solution to the Ernst equation in terms of theta functions, which gives rise to solutions of the Einstein equations. In Chapter 7 we present the ray-tracing technique applied to an equivalent form of the Kerr solution given by the Ernst equation and present a completely numerical method to analyze more general solutions.

Chapter 2

Preliminaries

In this chapter we recall some basic mathematical facts that will be needed throughout the thesis. We start by defining important quantities for Riemann surfaces and how they generate complex tori, which is an Abelian variety. Then we introduce multidimensional theta functions, which have played an important role in the study of Riemann surfaces and their Jacobian varieties. For further discussions, see [Mir94; FK80] for theory on Riemann surfaces, [BL04; Tai97] for the theory on complex Abelian varieties and [Igu81; Mum83] for the theory on theta functions.

The chapter is organized as follows. In Section 2.1 we present some definitions about Riemann surfaces and how they define Jacobian varieties. In Section 2.2 we introduce general principally polarized Abelian varieties and their equivalence classes. In Section 2.3 we present the theta functions and their role in PPAVs.

2.1 Riemann surfaces

In this section we recall some concepts on Riemann surfaces.

Definition 2.1.1. *A Riemann surface $\mathcal{R}$ is a one-dimensional connected complex analytic manifold.*

This means that the surface $\mathcal{R}$ must be given together with a complex structure, i.e., a set of local coordinates

$$\phi_\alpha : U_\alpha \to \mathbb{C},$$

such that $\{U_\alpha; \alpha \in A\}$ covers the entire $\mathcal{R}$, namely, $\mathcal{R} = \cup_{\alpha\in A} U_\alpha$. The analyticity of the complex manifold means that either $U_\alpha \cap U_\beta = \emptyset$ or the transition functions

$$\phi_{\alpha\beta} := \phi_\alpha \circ \phi_\beta^{-1} : \phi_\beta(U_\alpha \cap U_\beta) \to \phi_\alpha(U_\alpha \cap U_\beta),$$

must be biholomorphic, namely, $\phi_{\alpha\beta}$ is bijective and both this function and its inverse are holomorphic.

Some examples include:

- The complex plane $\mathbb{C}$ with the identity map $\phi : z \mapsto z$.
- The Riemann sphere $\mathbb{C}_\infty := \mathbb{C} \cup \{\infty\}$ with the maps $\phi_0 : z \mapsto z$ and $\phi_\infty : z \mapsto 1/z$ on $\mathbb{C}$ and $\mathbb{C}_\infty \backslash \{\infty\}$ respectively.
- The complex torus $\mathbb{C}/(\mathbb{Z} + \tau\mathbb{Z})$, where $\Im(\tau) > 0$, with the quotient topology.
- The smooth elliptic curve $\{(x, y) \in \mathbb{C}^2 \mid f(x, y) = y^2 - (x^2 + cx + d) = 0; c, d \in \mathbb{C}\}$ with the maps $\phi_x : (x, y) \mapsto x$ if $\partial f/\partial y \neq 0$ and $\phi_y : (x, y) \mapsto y$ if $\partial f/\partial x \neq 0$.

In the sequel, we will always consider compact Riemann surfaces. Topologically, they can be classified by their genus.

Definition 2.1.2 (Genus)**.** *A compact Riemann surface $\mathcal{R}$ homeomorphic to a sphere with g handles is said to have genus g.*

The space of holomorphic differentials $H^0(\mathcal{R}, \Omega^1_{\mathcal{R}})$ of a genus-g Riemann surface is g-dimensional and the first homology group $H_1(\mathcal{R}, \mathbb{Z})$ is of rank $2g$. The basis $\{a_1, b_1, ..., a_g, b_g\}$ of $H_1(\mathcal{R}, \mathbb{Z})$ is said to be canonical if their intersection numbers are $a_j \circ b_k = \delta_{jk}$ and $a_j \circ a_k = b_j \circ b_k = 0$ for all $j, k = 1, \ldots, g$.

Definition 2.1.3 (Period matrix)**.** *Let $\mathcal{R}$ be a compact Riemann matrix of genus g, $\{a_1, b_1, ..., a_g, b_g\}$ a canonical basis of the first homology group $H_1(\mathcal{R}, \mathbb{Z})$ and $\{\omega_1, ..., \omega_g\}$ a normalized basis of $H^0(\mathcal{R}, \Omega^1_{\mathcal{R}})$ with respect to the a_j cycles, namely, $\int_{a_j} \omega_k = \delta_{jk}$. Then, the period matrix of $\mathcal{R}$ is defined as the $g \times g$ complex matrix with components*

$$\mathbb{B}_{jk} := \int_{b_j} \omega_k. \tag{2.1}$$

Using the Riemann bilinear relations it can be proved that

- $\mathbb{B}^\top = \mathbb{B}$.
- $\Im(\mathbb{B})$ is positive definite.

With this we define the Jacobian variety of $\mathcal{R}$.

Definition 2.1.4 (Jacobian variety)**.** *The Jacobian variety of the Riemann surface $\mathcal{R}$, with a canonical basis for its first homology group and a normalized basis of holomorphic differentials as in Definition 2.1.3, is defined as the quotient*

$$\mathrm{Jac}(\mathcal{R}) := \mathbb{C}^g / \Lambda_{\mathbb{B}}, \tag{2.2}$$

where $\Lambda_{\mathbb{B}}$ is the full-rank lattice defined by the period matrix $\mathbb{B}$ of $\mathcal{R}$,

$$\Lambda_{\mathbb{B}} = \mathbb{Z}^g + \mathbb{B}\mathbb{Z}^g := \{\mathbf{n} + \mathbb{B}\mathbf{m} \;\big|\; \mathbf{n}, \mathbf{m} \in \mathbb{Z}^g\}.$$

2.1.1 Abel Map

Definition 2.1.5. *The Abel map with base point $p_0 \in \mathcal{R}$ is defined as*

$$\begin{aligned} \alpha_{p_0} : \mathcal{R} &\to \mathrm{Jac}(\mathcal{R}), \\ p &\mapsto \int_{p_0}^{p} \omega \mod \Lambda, \end{aligned} \tag{2.3}$$

where $\omega := (\omega_1, ..., \omega_g)$ is the vector formed by the basis $\{\omega_1, ..., \omega_g\}$ of $H^0(\mathcal{R}, \Omega^1_{\mathcal{R}})$ and

$$\int_{p_0}^{p} \omega := \left(\int_{\gamma_p} \omega_1, ..., \int_{\gamma_p} \omega_g \right).$$

This integral is path-dependent, but since the difference of any two paths γ_p, γ'_p is closed and

$$\gamma_p - \gamma'_p \sim \sum_j n_j a_j + m_j b_j$$

in $H^1(\mathcal{R}, \mathbb{Z})$, the Abel map is a well-defined in the quotient $\mathbb{C}^g/\Lambda$.

Remark 2.1.6. *Another definition of the Jacobian of $\mathcal{R}$, which is isomorphic to the one given above, is*

$$\mathrm{Jac}(\mathcal{R}) := H^0(\mathcal{R}, \Omega)^\vee / H^1(\mathcal{R}),$$

where $H^0(\mathcal{R}, \Omega)^\vee$ is the dual of $H^0(\mathcal{R}, \Omega)$. $H^1(\mathcal{R}, \mathbb{Z})$ is injected into $H^0(\mathcal{R}, \Omega)^\vee$ via

$$\sum_j n_j a_j + m_j b_j \mapsto \sum_j n_j \int_{a_j} \cdot + m_j \int_{b_j} \cdot$$

However, since we are interested in the computational implementation, when referring to $\mathrm{Jac}(\mathcal{R})$, we mean the definition (2.2).

2.2 Principally polarized Abelian varieties

In this section we define principally polarized Abelian varieties (PPAV) from the complex analytic point of view. We start by defining Abelian varieties, which we express in terms of complex tori. Then we define what a polarization is and in particular, a principal polarization.

2.2.1 Abelian varieties

An Abelian variety is a complex torus X admiting a positive line bundle L, we denote it by the pair (X, L). This is known to be equivalent to the complex torus satisfying the Riemann relations, thus we focus our attention on complex tori with this property.

Definition 2.2.1 (Complex torus)**.** *A complex torus is the quotient V/Λ, where V is a g-dimensional complex space and Λ is a discrete subgroup of rank $2g$ (a full-rank lattice).*

V/Λ is a connected complex manifold and it is compact as well. We say that Λ is a full-rank lattice if its generators $\lambda_1, ..., \lambda_{2g}$ are $\mathbb{R}$-linearly independent or equivalently, if $\Lambda \cong \mathbb{Z}^{2g}$. Since we are interested in a computational application, we will always consider $V = \mathbb{C}^g$

Let Λ and Λ' be two full-rank lattices such that $\Lambda = M\Lambda'$, where $M \in \mathrm{GL}(g, \mathbb{C})$. Namely, the generators of these two lattice are related by $\lambda_j = \Lambda\lambda'_j$ for all $j = 1, ..., 2g$. Then, the complex tori $\mathbb{C}^g/\Lambda$ and $\mathbb{C}^g/\Lambda'$ are isomorphic since there exist a holomorphic mapping $\phi_M : \mathbb{C}^g/\Lambda' \to \mathbb{C}^g/\Lambda$, which is inherited from the linear transformation $M : \mathbb{C}^g \to \mathbb{C}^g$.

Remark 2.2.2. *Due to this equivalence, we will always consider complex tori $\mathcal{A}_\mathbb{B} = \mathbb{C}^g/\Lambda_\Omega$ with a lattice of the form*

$$\Lambda_\Omega = \mathbb{Z}^g + \Omega\mathbb{Z}^g = \{\mathbf{n} + \Omega\mathbf{m} \mid \mathbf{n}, \mathbf{m} \in \mathbb{Z}^g\}. \tag{2.4}$$

It is known that X_Ω is an Abelian variety if and only if the defining matrix Ω is symmetric and its imaginary part is positive definite (Riemann relations), namely, Ω is in the Siegel halfspace. Thus, we will refer to Abelian varieties and complex tori of this form as the same objects.

Definition 2.2.3 (Siegel halfspace)**.** *The Siegel halfspace of degree g is defined as the subspace of complex matrices*

$$\mathbb{H}^g = \{\Omega \in \mathrm{M}(g, \mathbb{C}) \mid \Omega^\top = \Omega, \Im(\Omega) \succ 0\}. \tag{2.5}$$

For $g = 1$, this is just the upper half plane $\mathbb{H}$. An important definition for the numerical computations is the following domain.

Definition 2.2.4. *A fundamental domain of the complex torus $\mathbb{C}^g/\Lambda$ is a subset $U_\Omega \subset \mathbb{C}^g$ such that there does not exist two different points inside U_Ω differing by a lattice vector and its closure $\overline{U}_\Omega$ covers the entire complex torus under the quotient map.*

For computational purposes, we will always consider the following fundamental domain:

$$U_\Omega := \{\mathbf{z} \in \mathbb{C}^g \mid \mathbf{z} = \mathrm{q} + \Omega \mathrm{p}\}, \tag{2.6}$$

where $\mathrm{p}, \mathrm{q} \in \mathbb{R}^g$ with components $\mathrm{p}_j, \mathrm{q}_j \in (-1/2, 1/2)$ for $j = 1, \ldots, g$.

2.2.2 Polarized Abelian varieties

The polarization of the Abelian variety (X, L) is the first Chern class $c_1(L)$ of its line bundle L. However, there exists a 1-to-1 correspondence between $c_1(L)$ and the alternating form $E : \Lambda \times \Lambda \to \mathbb{Z}$ defined from the automorphic forms η_λ that generate the line bundle L. We recall that if $u : \mathbb{C}^g \to \mathbb{C}$ is a holomorphic function such that $u(\mathbf{z} + \lambda) = \eta_\lambda(\mathbf{z})u(\mathbf{z})$ for a non-vanishing holomorphic function $\eta_\lambda : \mathbb{C}^g \to \mathbb{C}$, it corresponds to a section of the line bundle L on $\mathbb{C}^g/\Lambda$ with automorphic form η_λ. Moreover, there exists a suitable basis (known as symplectic basis) $\{\lambda_1, \ldots, \lambda_{2g}\}$ of Λ in which E can be represented as

$$E = \begin{pmatrix} 0 & D \\ -D & 0 \end{pmatrix}, \tag{2.7}$$

where $D = \mathrm{diag}(d_1, \ldots, d_g)$ with non-negative integers d_j such that d_j divides d_{j+1}. For the lattice (2.4), this basis is simply $\{e_1, \ldots, e_g, \Omega e_1, \ldots, \Omega e_g\}$, where e_j is the vector with 1 in the j-th position and 0 everywhere else.

Definition 2.2.5 (Polarization)**.** *Let (X, L) be an Abelian variety with the alternating form* (2.7)*. Then, its polarization type is said to be $(d_1, \ldots, d_g)$ or simply D.*

If $D = \mathbb{I}_g$, then we say that the Abelian variety (X, L) has a principal polarization. They are known in the literature as *principally polarized Abelian varieties* (PPAV).

2.2.3 Modular transformations

Even if we consider lattices of the form $\Lambda_\Omega = \mathbb{Z}^g + \Omega\mathbb{Z}^g$ it is possible finding lattices such that $\Lambda = M\Lambda'$ for some $M \in \mathrm{GL}(g, \mathbb{C})$. For example, let us consider $\tau \in \mathbb{H}$ for the case $g = 1$ and

$$\tau' = \tau + 1, \quad \tau'' = -\frac{1}{\tau}. \tag{2.8}$$

Notice that $\Lambda = \Lambda'$ and $\Lambda = \tau\Lambda'$, i.e., they define equivalent complex tori. The succesive application of (2.8) also gives equivalent complex tori, namely,

$$\tau' = \begin{pmatrix} a & b \\ c & d \end{pmatrix} \circ \tau = \frac{a\tau + b}{c\tau + d}, \tag{2.9}$$

with

$$\begin{pmatrix} a & b \\ c & d \end{pmatrix} \in \mathrm{PSL}(2, \mathbb{Z}),$$

where $\mathrm{PSL}(2, \mathbb{Z})$ is known as the *modular group* and it is defined as the projection $\mathrm{SL}(2, \mathbb{Z}) \to \mathrm{PSL}(2, \mathbb{Z})$ where the matrices A and $-A$ are identified. The group $\mathrm{SL}(2, \mathbb{Z})$ is generated by $\begin{pmatrix} 1 & 1 \\ 0 & 1 \end{pmatrix}$ and $\begin{pmatrix} 0 & 1 \\ -1 & 0 \end{pmatrix}$. Notice that (2.8) is the action of these generators on τ. The transformation (2.9) is known as *modular transformation*.

Definition 2.2.6 (Modular fundamental domain)**.** *The fundamental domain $\mathcal{F}$ of $\mathbb{H}$ is the subspace $\mathcal{F}$ such that there does not exist two $\tau, \tau' \in \mathbb{H}$ related by a modular transformation and the closure $\overline{\mathcal{F}}$ generates the whole space $\mathbb{H}$ via modular transformations.*

It can be observed from the transformations (2.8) that

$$\mathcal{F} = \{\tau \in \mathbb{H} \mid |\tau| > 1, |\Re(\tau)| < 1/2\} \tag{2.10}$$

satisfies the first condition and in fact $\overline{\mathcal{F}}$ generates the whole $\mathbb{H}$ (see [FK01a]). The domains delimited by the curves in Figure 2.1 are other fundamental domains of $\mathrm{PSL}(2, \mathbb{Z})$.

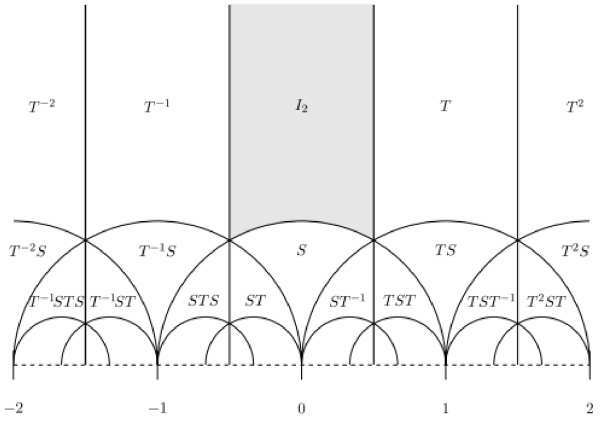

FIGURE 2.1: Fundamental domains of $\mathrm{PSL}(2, \mathbb{Z})$.
Source: [Con].

It is not trivial finding a fundamental domain in higher dimensions, thus we say that $\tilde{\mathcal{F}}$ is approximate fundamental domain if it only satisfies the second condition, i.e.,

Definition 2.2.7. *An approximate fundamental domain $\tilde{\mathcal{F}}$ is a subset of $\mathbb{H}$ such that any $\tau \in \mathbb{H}$ is modularly equivalent to some $\tau' \in \tilde{\mathcal{F}}$.*

For the previous example, an approximate fundamental domain would be

$$\tilde{\mathcal{F}} = \{\tau \in \mathbb{H} \mid \Im(\tau) > \sqrt{3}/2, |\Re(\tau)| < 1/2\},$$

where $\sqrt{3}/2$ is the minimal $\Im(\tau)$ of (2.10). Notice that the intersection of the unitary circle with the line with constant real part $\Re(\tau) = 1/2$ is $\tau = 1/2 + \mathrm{i}\sqrt{3}/2$.

Modular transformations in higher dimensions

Analogously, this can be extended to the Siegel halfspace $\mathbb{H}^g$. Two Riemann matrices $\Omega, \tilde{\Omega} \in \mathbb{H}^g$ can define isomorphic PPAVs if they define equivalent complex tori, both of them principally polarized. $\mathcal{A}_{\tilde{\Omega}}$ and $\mathcal{A}_{\Omega}$ are equivalent as complex tori if there exists an invertible homomorphism $\mathbb{C}^g/\tilde{\Lambda} \to \mathbb{C}^g/\Lambda$. This is equivalent to the existence of an invertible linear transformation $\mathcal{M} : \mathbb{C}^g \to \mathbb{C}^g$ with $\mathcal{M}(\tilde{\Lambda}) = \Lambda$ and a matrix

$$R = \begin{pmatrix} A & B \\ C & D \end{pmatrix} \in M(2g, \mathbb{Z}) \tag{2.11}$$

such that

$$\mathcal{M}(\tilde{\Omega}, \mathbb{I}_g) = (\Omega, \mathbb{I}_g) R^\top, \tag{2.12}$$

holds. Additionally, the principal polarization must be preserved, i.e., the alternating form (2.7) must be the same in the new basis. This is equivalent to the requirement

$$\begin{pmatrix} A & B \\ C & D \end{pmatrix}^\top \begin{pmatrix} 0_g & \mathbb{I}_g \\ -\mathbb{I}_g & 0_g \end{pmatrix} \begin{pmatrix} A & B \\ C & D \end{pmatrix} = \begin{pmatrix} 0_g & \mathbb{I}_g \\ -\mathbb{I}_g & 0_g \end{pmatrix}, \tag{2.13}$$

which means that $R \in \mathrm{Sp}(2g, \mathbb{Z})$. Thus, two matrices in $\mathbb{H}^g$ conjugated under the action of the symplectic (also called modular) group $\mathrm{Sp}(2g, \mathbb{Z})$ define equivalent PPAVs, where the action of $\mathrm{Sp}(2g, \mathbb{Z})$ on $\mathbb{H}^g$ is given by (2.12), which is equivalent to

$$\tilde{\Omega} = R \cdot \Omega = (A\Omega + B)(C\Omega + D)^{-1}, \tag{2.14}$$

which we call modular transformation. In Section 2.3 we will see that theta functions converge faster if we use a representative of the equivalence class of Ω with the maximal shortest vector $y_{\min}$ defined as

$$y_{\min} := \min_{\mathbf{n} \in \mathbb{Z}^g \setminus \{0\}} \langle \mathbf{n}, \Im(\Omega)\mathbf{n} \rangle. \tag{2.15}$$

For this we will consider matrices in Siegel's fundamental domain.

Siegel [Sie89] gave the following fundamental domain for the modular group:

Definition 2.2.8. *Siegel's fundamental domain is the subset of* $\mathbb{H}^g$ *such that* $\mathbb{B} = X + \mathrm{i}Y \in \mathbb{H}^g$ *satisfies:*

1. $|X_{nm}| \leq 1/2$, $n, m = 1, \ldots, g$,
2. Y *is in the fundamental region of Minkowski reductions [Min91; Min11],*
3. $|\det(C\Omega + D)| \geq 1$ *for all* C, D *(2.13).*

Moduli spaces

As mentioned above, the topological classification of compact Riemann surfaces is uniquely given by its genus g. However, the classification of their isomorphism classes given by one (complex) parameter if $g = 1$ and $3g - 3$ (complex) parameters if $g > 1$. Their moduli space is denoted by $\mathcal{M}_g$. On the other hand, PPAVs are parametrized by points in the Siegel halfspace $\mathbb{H}^g$ of degree g and since two symplectically equivalent matrices define equivalent PPAVs, the moduli space of PPAVs $\mathcal{A}_g$ is isomorphic to $\mathbb{H}^g/\mathrm{Sp}(2g,\mathbb{Z})$. Then,

$$\begin{aligned}\dim_{\mathbb{C}}(\mathcal{M}_g) &= \begin{cases} 1, & \text{if} \quad g = 1, \\ 3g-3, & \text{if} \quad g > 1, \end{cases} \\ \dim_{\mathbb{C}}(\mathcal{A}_g) &= \frac{1}{2}g(g+1).\end{aligned}$$

Thus, it is clear that Jacobian varieties $\mathcal{J}_g$ are just a subclass of $\mathcal{A}_g$. The Schottky problem is concerned with the identification of this subset amongst all PPAVs. Up to $g = 3$, every PPAV is a Jacobian. However, starting with $g = 4$ it is necessary to consider additional constraints. We extend this discussion in Chapter 3.

2.3 Theta functions

The multidimensional theta function takes values on the g-dimensional complex space and the Siegel halfspace of degree g to $\mathbb{C}$. Namely,

$$\vartheta : \mathbb{C}^g \times \mathbb{H}^g \to \mathbb{C}.$$

It is defined by the Fourier series

$$\vartheta(\mathbf{z},\Omega) := \sum_{\mathbf{n}\in\mathbb{Z}^g} \exp\left(\pi \mathrm{i}\langle \mathbf{n}, \Omega\mathbf{n}\rangle + 2\pi\mathrm{i}\langle \mathbf{n}, \mathbf{z}\rangle\right), \tag{2.16}$$

where $\langle\cdot,\cdot\rangle$ denotes the Euclidean scalar product. For a fixed matrix Ω, it is the function

$$\vartheta(\cdot,\Omega) : \mathbb{C}^g \to \mathbb{C}.$$

Since $\Omega \in \mathbb{H}^g$, the series (2.16) converges uniformly for all $\mathbf{z} \in \mathbb{C}^g$; thus it is an entire function. It also satisfies the quasi-periodicity properties on the latice (2.4),

$$\begin{aligned}\vartheta(\mathbf{z}+\mathbf{n},\Omega) &= \vartheta(\mathbf{z},\Omega), \\ \vartheta(\mathbf{z}+\Omega\mathbf{m},\Omega) &= \exp(-\pi\mathrm{i}\langle\mathbf{m},\Omega\mathbf{m}\rangle - 2\pi\mathrm{i}\langle\mathbf{m},\mathbf{z}\rangle)\cdot\vartheta(\mathbf{z},\Omega),\end{aligned} \tag{2.17}$$

This means that the zero set

$$\Theta_\Omega = \{\mathbf{z}\in\mathbb{C}^g \,|\, \vartheta(\mathbf{z},\Omega) = 0\} \tag{2.18}$$

is a well-defined divisor on $\mathbb{C}^g/\Lambda_\Omega$.

Remark 2.3.1. *In general, any holomorphic function u on $\mathbb{C}^g$ with the property*

$$u(\mathbf{z}+\lambda) = \eta_\lambda(\mathbf{z})\cdot u(\mathbf{z}), \tag{2.19}$$

where the function $\eta_\lambda(\mathbf{z})$ is never zero and satisfies the compatibility condition

$$\eta_{\lambda+\lambda'}(\mathbf{z}) = \eta_{\lambda'}(\mathbf{z}+\lambda)\cdot\eta_\lambda(\mathbf{z}), \tag{2.20}$$

is a section of a line bundle on $\mathbb{C}^g/\Lambda_\Omega$. The line bundle itself is generated by the automorphic forms $\eta_\lambda(\mathbf{z})$ (see [Tai97; BL04]).

Therefore, the function (2.16) has the automorphic form

$$\eta_\lambda(z) = \exp(-\pi\mathrm{i}\langle\mathbf{m},\Omega\mathbf{m}\rangle - 2\pi\mathrm{i}\langle\mathbf{m},\mathbf{z}\rangle), \tag{2.21}$$

where $\lambda = \mathbf{n}+\Omega\mathbf{m}$. Thus, it defines a line bundle on $\mathcal{A}_\mathbb{B}$, which is denoted by Θ. Moreover, $(\mathcal{A}_\mathbb{B},\Theta_\Omega)$ is a principally polarized Abelian variety since (2.21) defines the alternating form $E = \begin{pmatrix} 0 & \mathbb{I}_g \\ -\mathbb{I}_g & 0 \end{pmatrix}$.

2.3.1 Theta function with characteristics

The theta function with characteristics $\delta \in \mathbb{R}^{2g}$ is defined as

$$\vartheta[\delta](\mathbf{z},\Omega) = \vartheta\left[\begin{smallmatrix}\mathrm{p}\\ \mathrm{q}\end{smallmatrix}\right](\mathbf{z},\Omega) = \sum_{\mathbf{n}\in\mathbb{Z}^g} \exp\left[\pi\mathrm{i}\langle\Omega(\mathbf{n}+\mathrm{p}),\mathbf{n}+\mathrm{p}\rangle + 2\pi\mathrm{i}\langle\mathbf{n}+\mathrm{p},\mathbf{z}+\mathrm{q}\rangle\right]. \tag{2.22}$$

This function is just the translation of the zero-characteristic theta function with an exponential factor, i.e.,

$$\vartheta\left[\begin{smallmatrix}\mathrm{p}\\ \mathrm{q}\end{smallmatrix}\right](\mathbf{z},\Omega) = \alpha_\delta\cdot\beta_\delta(\mathbf{z})\cdot\vartheta(\mathbf{z}+\mathrm{q}+\Omega\mathrm{p},\Omega), \tag{2.23}$$

where

$$\begin{aligned}\alpha_\delta &= \exp(\pi\mathrm{i}\langle\mathrm{p},\Omega\mathrm{p}\rangle + 2\pi\mathrm{i}\langle\mathrm{p},\mathrm{q}\rangle),\\ \beta_\delta(\mathbf{z}) &= \exp(2\pi\mathrm{i}\langle\mathrm{p},\mathbf{z}\rangle).\end{aligned}$$

Using (2.19) and (2.23) we see that

$$\vartheta\left[\begin{smallmatrix}\mathrm{p}\\ \mathrm{q}\end{smallmatrix}\right](\mathbf{z}+\lambda,\Omega) = \eta_\lambda[\delta](\mathbf{z})\cdot\vartheta\left[\begin{smallmatrix}\mathrm{p}\\ \mathrm{q}\end{smallmatrix}\right](\mathbf{z},\Omega) \tag{2.24}$$

with the factor

$$\eta_\lambda[\delta](\mathbf{z}) = \beta_\delta(\lambda)\eta_\lambda(\mathbf{z}+\mathrm{q}+\Omega\mathrm{p}),$$

which also satisfies the compatibility condition (2.20). Thus, it is a factor of automorphy and it generates a line bundle on $\mathbb{C}^g/\Lambda_\Omega$, which is just a translation of (2.18).

2.3.2 Double period theta functions

Definition 2.3.2. *The double period theta functions (or level-two theta functions) are defined as the theta functions with half-integer characteristics*

$$\vartheta_2^\epsilon(\mathbf{z}) := \vartheta\left[\begin{smallmatrix}\epsilon/2\\ 0\end{smallmatrix}\right](2\mathbf{z},2\Omega), \tag{2.25}$$

with $\epsilon \in \mathbb{Z}^g/2\mathbb{Z}^g$.

Thus, we have the relation

$$\vartheta_2^{\epsilon}(\mathbf{z}) = \alpha_\epsilon \cdot \beta_\epsilon(2\mathbf{z}) \cdot \vartheta(2\mathbf{z} + \Omega\epsilon, 2\Omega), \tag{2.26}$$

where $\alpha_\epsilon = \exp(1/2\pi\mathrm{i}\langle\epsilon, \Omega\epsilon\rangle)$ and $\beta_\epsilon(2\mathbf{z}) = \exp(2\pi\mathrm{i}\langle\epsilon, \mathbf{z}\rangle)$. It can be observed that the factor of automorphy of $\vartheta_2^{\epsilon}(\mathbf{z})$ is

$$\tilde{\eta}_\lambda[\epsilon](\mathbf{z}) := \beta_\epsilon(2\lambda)\eta_\lambda^2(\mathbf{z} + \Omega\epsilon/2) = \eta_\lambda^2(\mathbf{z}), \tag{2.27}$$

which means that it is independent of ϵ. These are the generators of the line bundle $\Theta^2 := \Theta \otimes \Theta$, where the tensor product is defined as the product of the generators of Θ, [Tai97]. This is important for the projection of the complex torus into projective space, because it implies that the mapping

$$\begin{aligned} \phi : \mathcal{A}_{\mathbb{B}} &\to \mathbb{P}^N \\ \mathbf{z} &\mapsto [\vartheta_2^{\epsilon_0}(\mathbf{z}) : \cdots : \vartheta_2^{\epsilon_N}(\mathbf{z})], \end{aligned}$$

is well-defined, where $N = 2^g - 1$. To be more precise, evaluating ϕ at translations of $\mathbf{z}$ by a lattice vector we get

$$\phi(\mathbf{z} + \lambda) = [\vartheta_2^{\epsilon}(\mathbf{z} + \lambda)]_{\epsilon \in \mathbb{Z}_2^g} = [\eta_\lambda^2(z) \cdot \vartheta_2^{\epsilon}(\mathbf{z})]_{\epsilon \in \mathbb{Z}_2^g} = \phi(\mathbf{z}).$$

Moreover, there does not exist any $\mathbf{z} \in \mathcal{A}_{\mathbb{B}}$ such that $\vartheta_2^{\epsilon}(\mathbf{z})$ vanish for all $\epsilon \in \mathbb{Z}^g/2\mathbb{Z}^g$, i.e., this system is base-point free. Thus, $\mathcal{A}_{\mathbb{B}}$ can be immersed into projective space.

The following identity is known as the binary addition theorem [Tai97; Dub81] and will be useful in the sequel

$$\vartheta(\mathbf{z} + \mathbf{w}, \Omega)\vartheta(\mathbf{z} - \mathbf{w}, \Omega) = \sum_{\epsilon \in \mathbb{Z}^g/2\mathbb{Z}^g} \vartheta\left[\begin{smallmatrix} \epsilon/2 \\ 0 \end{smallmatrix}\right](2\mathbf{z}, 2\Omega)\vartheta\left[\begin{smallmatrix} \epsilon/2 \\ 0 \end{smallmatrix}\right](2\mathbf{w}, 2\Omega). \tag{2.28}$$

For more general characteristics, it can be proved that

$$\begin{aligned} &\Theta\left[\begin{smallmatrix} \alpha \\ \gamma \end{smallmatrix}\right](\mathbf{z} + \mathbf{w}, \Omega)\Theta\left[\begin{smallmatrix} \beta \\ \delta \end{smallmatrix}\right](\mathbf{z} - \mathbf{w}, \Omega) = \\ &\sum_{\epsilon \in \mathbb{Z}^g/2\mathbb{Z}^g} \Theta\left[\begin{smallmatrix} (\alpha+\beta)/2+\epsilon/2 \\ \gamma+\delta \end{smallmatrix}\right](2\mathbf{z}, 2\Omega)\Theta\left[\begin{smallmatrix} (\alpha-\beta)/2+\epsilon/2 \\ \gamma-\delta \end{smallmatrix}\right](2\mathbf{w}, 2\Omega), \end{aligned} \tag{2.29}$$

by using (2.28) and (2.23)

2.3.3 Kummer variety

For the geometrical interpretation of Fay's identity (which is discussed in Chapter 3), we need to introduce the Kummer variety, which is the embedding of the complex torus into projective space via level-two theta functions.

Definition 2.3.3. *Let $(\mathcal{A}_\Omega, \Theta_\Omega)$ be an indecomposable PPAV. Thus, its Kummer variety is the image of the map*

$$\begin{aligned} \mathrm{Kum} : \mathcal{A}_\Omega/\sigma &\to \mathbb{P}^{2^g-1}, \\ Z &\mapsto \left[\Theta\left[\begin{smallmatrix} \epsilon/2 \\ 0 \end{smallmatrix}\right](2Z, 2\mathbb{B})\right]_{\epsilon \in \mathbb{Z}^g/2\mathbb{Z}^g}, \end{aligned}$$

where $\sigma(Z) = -Z$.

This map is an embedding by Lefschetz' theorem [BL04; Tai97]. We recall that a PPAV $(\mathcal{A}_\Omega, \Theta_\Omega)$ is indecomposable if there do not exist lower dimensional PPAVs $(\mathcal{A}_{\Omega'}, \Theta_{\Omega'})$, $(\mathcal{A}_{\Omega''}, \Theta_{\Omega''})$ such that $\mathcal{A}_\Omega \cong \mathcal{A}_{\Omega'} \times \mathcal{A}_{\Omega''}$ and $\Theta_\Omega \cong \mathcal{A}_{\Omega'} \times \Theta_{\Omega''} + \Theta_{\Omega'} \times \mathcal{A}_{\Omega''}$ (see [Igu81]). In terms of the Riemann matrix Ω, this means there does not exist a symplectically equivalent matrix of the form $\operatorname{diag}[\Omega', \Omega'']$ with $\Omega' \in \mathbb{H}^{g'}$, $\Omega'' \in \mathbb{H}^{g''}$ and $1 \leq g'' \leq g'$.

Jacobian varieties are known to be indecomposable, thus we will also require this condition on general $\Omega \in \mathbb{H}^g$. The following definition will be useful in the upcoming chapters.

Definition 2.3.4. *Let $[V_1]$, $[V_2]$, $[V_3]$ be points in the projective space $\mathbb{P}^n$. They are said to be trisecant or collinear points in $\mathbb{P}^n$ if their representatives $V_1, V_2, V_3 \in \mathbb{C}^{n+1}$ are linearly dependent, i.e., there exist non-zero $c_1, c_2 \in \mathbb{C}$ such that $V_3 = c_1 V_1 + c_2 V_2$.*

In particular, we say the Kummer variety of $(\mathcal{A}_\Omega, \Theta_\Omega)$ admits trisecant points if there exist $\operatorname{Kum}(X), \operatorname{Kum}(Y), \operatorname{Kum}(Z) \in \mathbb{P}^{2^g-1}$ satisfying Definition 2.3.4.

2.3.4 Modular transformations on theta functions

The action of the modular group on theta functions is known, see for instance [Bel+94; Fay73; Mum83; Igu72]. One has

$$\vartheta\left[\begin{smallmatrix}\tilde{\mathrm{p}}\\ \tilde{\mathrm{q}}\end{smallmatrix}\right](\mathcal{M}^{-1}\mathbf{z}, \tilde{\Omega}) = k\sqrt{\det(\mathcal{M})}\exp\left(\frac{1}{2}\sum_{i\leq j} z_i z_j \frac{\partial}{\partial \Omega_{ij}} \ln\det\mathcal{M}\right)\vartheta\left[\begin{smallmatrix}\mathrm{p}\\ \mathrm{q}\end{smallmatrix}\right](\mathbf{z}, \Omega), \quad (2.30)$$

where $\tilde{\mathbb{B}}$ is given by (2.14)) and k in dependence of z, and where

$$\mathcal{M} = C\mathbb{B} + D, \quad \begin{pmatrix}\tilde{\mathrm{p}}\\ \tilde{\mathrm{q}}\end{pmatrix} = \begin{pmatrix} D & -C\\ -B & A\end{pmatrix}\begin{pmatrix}\mathrm{p}\\ \mathrm{q}\end{pmatrix} + \frac{1}{2}\begin{pmatrix}\operatorname{diag}(CD^\top)\\ \operatorname{diag}(AB^\top)\end{pmatrix}, \quad (2.31)$$

with diag denoting the diagonal of the corresponding matrices.

Remark 2.3.5. *Notice from the definition* (2.16) *that this series converges faster the greater the shortest vector $y_{\min}$ is. E.g., consider the Riemann theta function for some $\tau \in \mathbb{H}$*

$$\vartheta(z, \tau) = \sum_{n\in\mathbb{Z}} e^{-\pi y_{\min} n^2} \cdot e^{\pi \mathrm{i} X n^2 + 2\pi \mathrm{i} n z},$$

for an arbitrary $z \in \mathbb{C}$. Considering an equivalent τ' in the fundamental domain (2.10) *will allow a faster convergence since $y'_{\min} \geq y_{\min}$ and thus the factor $e^{-\pi y'_{\min} n^2}$ converges to zero more rapidly. The oscillations $e^{\pi \mathrm{i} X n^2}$ are minimized by taking the real part $X = \Re(\tau)$ in the interval $[-1/2, 1/2]$. This motivates the use of the fundamental domain* (2.10) *for $g = 1$ and the approximation* (2.2.8) *for general g.*

Chapter 3

Fay's identity and the Schottky problem

In the previous chapter we saw that Jacobian varieties are only a subclass of PPAVs, since $\dim(\mathcal{M}_g) < \dim(\mathcal{A}_g)$ for $g \geq 4$. The Schottky problem is concerned with the identification of the subclass of Jacobian varieties amongst all PPAVs. Recall that Riemann matrices $\Omega \in \mathbb{H}^g$ define PPAVs via the identification $\Omega \mapsto (\mathcal{A}_\Omega, \Theta_\Omega)$, the form of the Schottky problem we want to address in this thesis is:

Given a Riemann matrix $\Omega \in \mathbb{H}^g$, determine whether it is the period matrix of some suitable Riemann surface $\mathcal{R}$ of genus g.

The first result in this direction was given by Schottky himself [Sch88] for $g = 4$, where he defined a modular form $\Sigma : \mathbb{H}^4 \to \mathbb{C}$ that vanishes identically on $\mathcal{J}_4$. Igusa [Igu81] proved that a Riemann matrix $\Omega \in \mathbb{H}^4$ is in the Jacobi locus if and only if $\Sigma(\Omega)$ vanishes.

Before discussing further developments of the Schottky problem, we introduce Fay's identity and its role in the obtention of other characterizations of the Jacobi variety. The Fay identity (also called trisecant identity) is a relation between four arbitrary points on a Riemann surface in its Jacobian variety. It is interpreted geometrically as a trisecant in the Kummer variety of the Jacobian, hence its name.

Krichever [Kri10] proved that the existence of only one trisecant in the Kummer variety of a PPAV implies that such PPAV is a Jacobian variety. This was a consequence of other important results characterizing Jacobian varieties, but it is the most practical one for a computational treatment of the Schottky problem, see [Gru11] for an extensive account on the other approaches to this problem.

The chapter is organized as follows. In Section 3.1 we present Fay's identity and its geometrical interpretation as defining trisecant points in the Kummer variety, as well as its extension as a function in general PPAVs. In Section 3.2 we present the different characterizations of Jacobian varieties, in particular those that were derived directly from Fay's identity.

3.1 Fay identity

The Fay identity is a relation between four arbitrary points on a compact Riemann surface $\mathcal{R}$ in terms of theta functions (see [Fay73; Mum83]). First, we need to define the so-called prime form E defined as

$$E(x, y) = \frac{\vartheta^*(\int_y^x)}{h_*(x)h * (y)}$$

with $h_*(x)$ satisfying $h_*^2(x) = \sum_{j=1}^g \frac{\partial\vartheta^*(0)}{\partial z_j}\omega_j(x)$. The theta function $\vartheta^* := \vartheta\left[\begin{smallmatrix}\mathrm{p}^*\\ \mathrm{q}^*\end{smallmatrix}\right]$ is required to have non-singular odd half-integer characteristics $[\mathrm{p}^*, \mathrm{q}^*]$, i.e., $2\mathrm{p}^*, 2\mathrm{q}^* \in \mathbb{Z}^g$ with $4\langle \mathrm{p}^*, \mathrm{q}^*\rangle = 1 \mod 2$ and $\vartheta^*(\alpha(p))$ does not vanish identically on $\mathcal{R}$. E can be considered as a holomorphic section of a line bundle on $\mathcal{R}\times\mathcal{R}$ (see [Mum83]) and some of its properties are:

- $E(x,y) = 0 \Leftrightarrow x = y$
- $E(x,y) = -E(y,x)$
- E has a first order zero along the diagonal $\Delta \subset \mathcal{R}\times\mathcal{R}$

Theorem 3.1.1 (Fay's identity)**.** *Let $\mathcal{R}$ be a compact Riemann surface, $\vartheta(\mathbf{z}, \mathbb{B})$ its associated theta function and $\int_{D'}^{D} = \alpha(D - D')$ its Abel map. Then, the following identity holds*

$$\vartheta\left(\mathbf{z}+\int_a^c\right)\vartheta\left(\mathbf{z}+\int_b^d\right)E(c,b)E(a,d) + \vartheta\left(\mathbf{z}+\int_b^c\right)\vartheta\left(\mathbf{z}+\int_a^d\right)E(c,a)E(d,b) = \vartheta(\mathbf{z})\vartheta\left(\mathbf{z}+\int_{a+b}^{c+d}\right)E(c,d)E(a,b), \tag{3.1}$$

for all $a, b, c, d \in \mathcal{R}$ and $\mathbf{z} \in \mathbb{C}^g$.

Making the substitution $\mathbf{z} \to \mathbf{z} - \frac{1}{2}\int_{a+b}^{c+d}$, we obtain the equivalent form of this identity,

$$\lambda_1\cdot\vartheta\left(\mathbf{z}+\frac{1}{2}\int_{a+d}^{c+b}\right)\vartheta\left(\mathbf{z}-\frac{1}{2}\int_{a+d}^{c+b}\right) + \lambda_2\cdot\vartheta\left(\mathbf{z}+\frac{1}{2}\int_{b+d}^{a+c}\right)\vartheta\left(\mathbf{z}-\frac{1}{2}\int_{b+d}^{a+c}\right) + \lambda_3\cdot\vartheta\left(\mathbf{z}+\frac{1}{2}\int_{a+b}^{c+d}\right)\vartheta\left(\mathbf{z}-\frac{1}{2}\int_{a+b}^{c+d}\right) = 0, \tag{3.2}$$

where $\lambda_1 = E(c,b)E(a,d)$, $\lambda_2 = E(c,a)E(d,b)$ and $\lambda_3 = -E(c,d)E(a,b)$.

Applying the binary addition theorem (2.28) to (3.1), we obtain

$$\sum_{\epsilon\in\mathbb{Z}^g/2\mathbb{Z}^g}\vartheta\left[\begin{smallmatrix}\epsilon/2\\ 0\end{smallmatrix}\right](2\mathbf{z}, 2\mathbb{B})\left[\lambda_1\cdot\vartheta\left[\begin{smallmatrix}\epsilon/2\\ 0\end{smallmatrix}\right]\left(\int_{a+d}^{c+b}, 2\mathbb{B}\right) + \lambda_2\cdot\vartheta\left[\begin{smallmatrix}\epsilon/2\\ 0\end{smallmatrix}\right]\left(\int_{b+d}^{a+c}, 2\mathbb{B}\right) + \lambda_3\cdot\vartheta\left[\begin{smallmatrix}\epsilon/2\\ 0\end{smallmatrix}\right]\left(\int_{a+b}^{c+d}, 2\mathbb{B}\right)\right] = 0, \tag{3.3}$$

for all $\mathbf{z} \in \mathbb{C}^g$. Mumford [Mum83] noted that since the level-two theta functions form a basis of $|2\Theta|$, the latter equality holds if and only if

$$\lambda_1\cdot\vartheta\left[\begin{smallmatrix}\epsilon/2\\ 0\end{smallmatrix}\right]\left(\int_{a+d}^{c+b}, 2\mathbb{B}\right) + \lambda_2\cdot\vartheta\left[\begin{smallmatrix}\epsilon/2\\ 0\end{smallmatrix}\right]\left(\int_{b+d}^{a+c}, 2\mathbb{B}\right) + \lambda_3\cdot\vartheta\left[\begin{smallmatrix}\epsilon/2\\ 0\end{smallmatrix}\right]\left(\int_{a+b}^{c+d}, 2\mathbb{B}\right) = 0, \tag{3.4}$$

for all $\epsilon \in \mathbb{Z}^g/2\mathbb{Z}^g$. The geometric interpretation of this observation is that there exists a four-dimensional family of trisecant (collinear) points in the Kummer variety $\mathrm{Kum}(\mathcal{A}_{\mathbb{B}}/\{\pm 1\}) \subset \mathbb{P}^{2^g-1}$ parametrized by distinct points $a, b, c, d \in \mathcal{R}$. Namely, the

Kummer points $\mathrm{Kum}(X)$, $\mathrm{Kum}(Y)$, $\mathrm{Kum}(Z)$ are collinear if $X, Y, Z \in \mathcal{A}_{\mathbb{B}}/\{\pm 1\}$ are parametrized by

$$X = \frac{1}{2}\int_{a+d}^{c+b}, \quad Y = \frac{1}{2}\int_{b+d}^{a+c}, \quad Z = \frac{1}{2}\int_{a+b}^{c+d}. \tag{3.5}$$

3.1.1 Generalization of the cross-ratio function

Fay's identity can be considered as the generalization to general compact Riemann surfaces of the cross-ratio function $\lambda_0 : \mathbb{C}_\infty^4 \to \mathbb{C}_\infty$, which is defined as

$$\lambda_0(a,b,c,d) = \frac{(c-a)(d-b)}{(c-b)(d-a)}, \tag{3.6}$$

where $a, b, c, d \in \mathbb{C}_\infty$. This function satisfies the identity

$$\lambda_0(a,b,c,d) + \lambda_0(a,c,b,d) = 1. \tag{3.7}$$

Other properties of this function include

$$\begin{aligned} &\lambda_0(a,b,c,d) = \lambda_0(c,d,a,b) = \lambda_0(b,a,d,c) = \lambda_0(d,c,b,a), \\ &\lambda_0(a,b,c,d)\lambda_0(a,d,b,c)\lambda_0(a,c,d,b) = -1, \\ &\lambda_0(a,b,c,d) = \lambda_0(b,a,c,d)^{-1}. \end{aligned} \tag{3.8}$$

Fay's identity can be viewed as an extension of this function to general compact Riemann surfaces by defining λ to be the meromorphic function

$$\lambda(a,b,c,d) = \frac{E(c,a)E(d,b)}{E(c,b)E(d,a)} = \frac{\vartheta^*(\int_a^c)\cdot\vartheta^*(\int_b^d)}{\vartheta^*(\int_b^c)\cdot\vartheta^*(\int_a^d)}, \tag{3.9}$$

Moreover, this ratio is free of the h_* forms in the definition of the prime form E. The properties (3.8) can be readily checked by using the skew-symmetric property of E. With this function, the Fay identity can be rewritten as

$$\begin{aligned} \lambda(a,b,c,d)\cdot\vartheta\left(\mathbf{z}+\int_b^c\right)\vartheta\left(\mathbf{z}+\int_a^d\right) + \lambda(a,c,b,d)\cdot\vartheta(\mathbf{z})\vartheta\left(\mathbf{z}+\int_{a+b}^{c+d}\right) \\ = \vartheta\left(\mathbf{z}+\int_a^c\right)\vartheta\left(\mathbf{z}+\int_b^d\right), \end{aligned} \tag{3.10}$$

which is analogous to the cross-ratio identity (3.7). In terms of the level-two theta functions we obtain,

$$c_1\cdot\vartheta\left[{}^{\epsilon/2}_{0}\right]\left(\int_{b+d}^{a+c}, 2\mathbb{B}\right) + c_2\cdot\vartheta\left[{}^{\epsilon/2}_{0}\right]\left(\int_{a+b}^{c+d}, 2\mathbb{B}\right) + \vartheta\left[{}^{\epsilon/2}_{0}\right]\left(\int_{a+d}^{c+b}, 2\mathbb{B}\right) = 0,$$

where $c_1 = -\lambda(a,b,c,d)$ and $c_2 = -\lambda(a,b,c,d)$.

Notice that this generalization can expressed in many different ways by considering the properties (3.8) satisfied by the function (3.9).

3.1.2 Fay function

Let us extend this identity to a general function on $\tilde{\mathcal{A}}_\Omega \times \tilde{\mathcal{A}}_\Omega \times \tilde{\mathcal{A}}_\Omega$, where $\tilde{\mathcal{A}}_\Omega = \mathcal{A}_\Omega/\{\pm 1\}$ for $\Omega \in \mathbb{H}^g$. The function we are interested in is

$$F : \tilde{\mathcal{A}}_\Omega \times \tilde{\mathcal{A}}_\Omega \times \tilde{\mathcal{A}}_\Omega \to \mathbb{C}^{2^g},$$

with components

$$F^\epsilon(X,Y,Z) = \vartheta\left[{}^{\epsilon/2}_{0}\right](2X,2\Omega) + c_1 \cdot \vartheta\left[{}^{\epsilon/2}_{0}\right](2Y,2\Omega) + c_2 \cdot \vartheta\left[{}^{\epsilon/2}_{0}\right](2Z,2\Omega), \quad (3.11)$$

This can be represented in the form

$$F(X,Y,Z) = \vec{\Theta}(X) + c_1 \cdot \vec{\Theta}(Y) + c_2 \cdot \vec{\Theta}(Z), \quad (3.12)$$

where $\vec{\Theta}(X) = \left(\vartheta\left[{}^{\epsilon/2}_{0}\right](2X,2\Omega)\right)_{\epsilon \in \mathbb{Z}^g/2\mathbb{Z}^g}$ is a representative of the Kummer point $\mathrm{Kum}(X)$ in $\mathbb{C}^{2^g}$. The coefficients are

$$c_1 = \frac{\vartheta^*(Z-X)\cdot\vartheta^*(Z+X)}{\vartheta^*(Y-Z)\cdot\vartheta^*(Y+Z)}, \quad c_2 = \frac{\vartheta^*(X-Y)\cdot\vartheta^*(X+Y)}{\vartheta^*(Y-Z)\cdot\vartheta^*(Y+Z)}, \quad (3.13)$$

where instead of considering X, Y, Z parametrized by $a, b, c, d \in \mathcal{R}$, we extend to all $X, Y, Z \in \mathcal{A}_\Omega$. For general $\Omega \in \mathbb{H}^g$, we can only consider theta functions with odd characteristics $2\mathrm{p}^*, 2\mathrm{q}^* \in \mathbb{Z}^g$ for the c_1, c_2 coefficients (there is no concept of singular characteristics for general PPAVs, since it is defined as the identical vanishing of the theta function on the Abel image of the Riemann surface).

Remark 3.1.2. *Notice that if $X = \pm Y$, then $c_2 = 0$ and $c_1 = -1$ and thus it yields $F(X,Y,Z) = 0$ for all $\Omega \in \mathbb{H}^g$. Thus, it does not provide information on whether $\mathcal{R}$ is in the Jacobi locus. The same observation applies to $X = \pm Z$. We say that the Fay identity is trivial in this case.*

Since $|2\Theta|$ is base point free, there does not exist any $X \in \mathbb{C}^g/\Lambda$ such that $\vec{\Theta}(X) = 0$ and since the Kummer map is an embedding, $\mathrm{Kum}(X) = \mathrm{Kum}(Y)$ if and only if $X = \pm Y$. Therefore, if $F(X,Y,Z) = 0$ with the condition $X \neq Y$ and $X \neq Z$ will imply that $\mathrm{Kum}(X)$, $\mathrm{Kum}(Y)$ and $\mathrm{Kum}(Z)$ are different trisecant points in $\mathbb{P}^{2^g}$.

Remark 3.1.3. *Instead, if we had considered the function $F(X,Y,Z)$ with components in the form* (3.4) *with coefficients $\lambda_1 = \vartheta^*(Y-Z)\cdot\vartheta^*(Y+Z)$, $\lambda_2 = \vartheta^*(Z-X)\cdot\vartheta^*(Z+X)$, $\lambda_3 = \vartheta^*(X-Y)\cdot\vartheta^*(X+Y)$, the vanishing of $F(X,Y,Z)$ would not imply that the Kummer images of X, Y, Z are trisecant points even if X, Y, Z are different in $\tilde{\mathcal{A}}_\Omega$. The reason is that $\lambda_1 = \lambda_2 = \lambda_3 = 0$ in a codimension-3 subset of $\tilde{\mathcal{A}}_\Omega \times \tilde{\mathcal{A}}_\Omega \times \tilde{\mathcal{A}}_\Omega$.*

3.2 Historical development

3.2.1 Schottky-Igusa modular form

The first partial solution was given by Schottky himself [Sch88] in terms of the modular form $\Sigma : \mathbb{H}^4 \to \mathbb{C}$ given in (3.15), which is now known as Schottky-Igusa modular form. Schottky showed that if $\Omega \in \mathcal{J}_g$, then $\Sigma(\Omega) = 0$. Igusa showed rigorously that the Jacobi locus is an irreducible component of the zero set of Σ (see [Igu81]),

i.e., the vanishing of $\Sigma(\Omega)$ implies that Ω is the period matrix of some suitable Riemann surface of genus g. Let us define this modular form, since it will be useful to test the accuracy of our numerical approach in genus 4.

The Schottky-Igusa modular form is a polynomial of degree 16 in the theta constants $\vartheta\left[\begin{smallmatrix} p \\ q \end{smallmatrix}\right](0)$. We follow here the presentation in [CKS19]: choose the characteristics

$$p^{(1)} = q^{(1)} = \frac{1}{2}\begin{pmatrix}1\\0\\1\\0\end{pmatrix}, \quad p^{(2)} = \frac{1}{2}\begin{pmatrix}0\\0\\0\\1\end{pmatrix}, \quad q^{(2)} = \frac{1}{2}\begin{pmatrix}1\\0\\0\\0\end{pmatrix},$$

and

$$p^{(3)} = \frac{1}{2}\begin{pmatrix}0\\0\\1\\1\end{pmatrix}, \quad q^{(3)} = \frac{1}{2}\begin{pmatrix}1\\0\\1\\1\end{pmatrix}.$$

Consider a rank 3 subgroup N of $\mathbb{Z}^8/(2\mathbb{Z}^8)$ generated by

$$n_1 = \frac{1}{2}\begin{pmatrix}0&1\\0&1\\0&1\\1&0\end{pmatrix}, \quad n_2 = \frac{1}{2}\begin{pmatrix}0&0\\0&0\\1&0\\1&1\end{pmatrix}, \quad n_3 = \frac{1}{2}\begin{pmatrix}0&1\\0&0\\1&1\\0&1\end{pmatrix}.$$

We consider the product of theta constants

$$\pi_i = \prod_{(pq)\in(p^{(i)}q^{(i)})+N} \Theta\left[\begin{smallmatrix} p \\ q \end{smallmatrix}\right](0) \tag{3.14}$$

and define the Schottky-Igusa modular form as

$$\Sigma(\Omega) = \pi_1^2 + \pi_2^2 + \pi_3^2 - \pi_1\pi_2 - \pi_1\pi_3 - \pi_2\pi_3. \tag{3.15}$$

The irreducibility of the Jacobi locus can be stated as:

Theorem 3.2.1 (Schottky-Igusa theorem)**.** *The Riemann matrix $\Omega \in \mathbb{H}^4$ is the period matrix of some Riemann surface of genus 4 if and only if the Schottky-Igusa invariant vanishes on Ω.*

Our numerical approach is analogous to (3.15) in the sense that the only input we require is the matrix $\Omega \in \mathbb{H}^g$.

3.2.2 Other characterizations

Some of the other characterizations include Matsusaka's criterion [Mat59] in terms of self intersections and Shiota's characterization in terms of soliton equations [Shi86].

Theorem 3.2.2. *A principally polarized Abelian variety of dimension g containing a curve $(C \subset X, \Theta)$ is the Jacobian of C if and only if $(g-1)! \cdot C$ is numerically equivalent to the self-intersection Θ^{g-1}.*

We show the form presented in [BL04]. Determining whether a PPAV is a Jacobian variety or not by using this criterion is hard in practice, since one would need

to give a dimension-1 subvariety $\mathcal{C}$ beforehand and then check whether it satisfies the numerical equivalence.

A very important characterization was given by Shiota [Shi86], who proved Novikov's conjecture. This idea comes from an algebro-geometric solution of the Kadomtsev-Petviashvili equation constructed by Krichever [Kri77], where he showed that there exist $U, V, W \in \mathbb{C}^g$ and $c \in \mathbb{C}$ such that the function u defined in terms of the theta function on a Jacobian variety

$$u(x,y,t) = -2(\partial_x^2 \ln \vartheta(Ux + Vy + Wt + Z, \mathbb{B}) + c), \tag{3.16}$$

solves the KP equation

$$\frac{3}{4}u_{yy} = \partial_x \left(u_t - \frac{1}{4}u_{xxx} - \frac{3}{2}uu_x \right),$$

for any $Z \in \mathbb{C}^g$. The vectors U, V, W are integrals of Abelian differentials of the second kind on the defining Riemann surface.

Novikov noticed that (3.16) does not solve the KP equation for generic $\Omega \in \mathbb{H}^g$, thus he conjectured whether this property characterizes Jacobian varieties. Shiota gave an affirmative answer to this conjecture.

Theorem 3.2.3. *Ω is a period matrix if and only if the function $u(x,y,t) = -2(\partial_x^2 \ln \vartheta(Ux + Vy + Wt, \Omega) + c)$ with $U, V, W \in \mathbb{C}^g$, $c \in \mathbb{C}$ satisfies the KP equation.*

To effectively test whether a given $\Omega \in \mathbb{H}^g$ is the period matrix of some genus-g Riemann surface, one needs to provide suitable parameters $U, V, W \in \mathbb{C}^g, c \in \mathbb{C}$ in order to determine whether Ω is in the Jacobi locus. Finding such U, V, W is not trivial.

3.2.3 Characterizations via trisecants in the Kummer variety

Some important characterizations were inspired by Fay's identity. In section 3.1 we can see that given a Riemann surface $\mathcal{R}$ and its Jacobian $\mathrm{Jac}(\mathcal{R})$, it is possible to construct a 4-dimensional family of trisecants in the Kummer variety parametrized by points in $\mathcal{R}$. Thus, one could ask whether this property characterizes Jacobian varieties amongs all PPAVs.

Gunning proved that only a one-dimensional family of trisecants would be necessary to characterize a Jacobian variety. Let us look again at Fay's identity for fixed $b, c, d \in \alpha(\mathcal{R})$, thus $r \in \alpha(\mathcal{R})$ parametrizes a one-dimensional family of distinct trisecant points

$$\mathrm{Kum}(t + b - c - d), \quad \mathrm{Kum}(t - b + c - d), \quad \mathrm{Kum}(t - b - c + d).$$

By abuse of notation and in order to agree with Gunning's notation, we denoted the Abel images of $a, b, c, t \in \mathcal{R}$ by the same letter. Let us call $2\alpha = b - c - d$, $2\beta = -b + c - d$, $2\gamma = -b - c + d$ and

$$M_{2\alpha,2\beta,2\gamma}(t) := \mathrm{rank} \left[\vec{\Theta}(\tfrac{t+2\alpha}{2}), \quad \vec{\Theta}(\tfrac{t+2\gamma}{2}), \quad \vec{\Theta}(\tfrac{t+2\gamma}{2}) \right], \tag{3.17}$$

Thus from Fay's identity we know that $M_{2\alpha,2\beta,2\gamma}(t)$ is one dimensional and in particular, at the points b, c, d, namely, $t = -\alpha - \gamma$, $t = -\beta - \gamma$, $t = -\alpha - \beta$. Gunning proved that this characterizes Jacobian varieties with certain conditions on α, β, γ.

Theorem 3.2.4 (Gunning). *An indecomposable principally polarized Abelian variety $(\mathcal{A}_\Omega, \Theta_\Omega)$ is the Jacobian variety if and only if there exist parameters $\alpha, \beta, \gamma \in \mathbb{C}^g$ such that*

- *α, β, γ represent distinct point of $\mathcal{A}_\Omega$,*
- *There are no non-zero complex multiplications F of $\mathcal{A}_\Omega$ such that $F(\alpha - \beta) = F(\beta - \gamma) = 0$,*
- $\dim_{-\alpha-\beta} M_{2\alpha,2\beta,2\gamma}(t) > 0$

Welters extended this result [Wel84] to a more general case, namely, he eliminated the condition of α, β, γ being distinct points in $\mathcal{A}_\Omega$. Thus, the existence of a one-dimensional family of flexes (namely, the trisecant points come infinitesimally close) at one point implies that $(\mathcal{A}_\Omega, \Theta_\Omega)$ is a Jacobian variety. He then conjectured whether the existence of only one trisecant would characterize Jacobian varieties amongst all PPAVs. This was solved by Krichever [Kri10].

Theorem 3.2.5 (Trisecant theorem). *The indecomposable principally polarized Abelian variety $(\mathcal{A}_\Omega, \Theta_\Omega)$ is the Jacobian of some Riemann surface of genus g if and only if there exist one trisecant point in its Kummer variety.*

Let $X, Y, Z \in \mathbb{C}^g/\Lambda$ such that $\mathrm{Kum}(X)$, $\mathrm{Kum}(Y)$, $\mathrm{Kum}(Z)$ are trisecant points. The proof was divided in three cases:

(i) All the three points coincide, i.e., $X = Y = Z$, meaning that a projective line is tangent to the Kummer variety up to order 2

(ii) Two points coincide, e.g., $X = Y$ and $X \neq Z$. This means that a projective line passes by $\mathrm{Kum}(Z)$ and it is tangent at the point $\mathrm{Kum}(X)$.

(iii) All the points are distinct, i.e., $X \neq Y \neq Z$. Namely, a projective line intersects the Kummer variety at three different points.

Thus, given a matrix $\Omega \in \mathbb{H}^g$ that defines an indecomposable PPAV, the way to determine whether it is in the Jacobi locus is by looking for trisecant points in an exhaustive manner in its Kummer variety. If a trisecant is found, then $\Omega \in \mathcal{J}_g$.

Chapter 4

Computational tools for the Schottky problem

In this chapter we present the necessary tools for the computational treatment of the Schottky problem. We will present different functions whose zeros (or global minimum) indicate the existence of trisecant points in the Kummer variety. However, all of them involve theta functions and thus, it is necessary to compute them efficiently, since it is the most expensive part of the algorithm. For this we use the method outlined in [FK16; FJK19] and consider a symplectically equivalent Riemann matrix for which the theta function shows faster convergence. Trisecant points are identified via the zeros of a function, for which one needs to impose extra constraints in order to use efficient methods that do not apply if the zero set is multidimensional, which is the case if the defining function is in $\Omega \in \mathcal{J}_g$. Then we present the algorithm to compute the zeros of these constrained functions, which would indicate the existence of trisecant points. The only input that we require for this routine is a Riemann matrix $\Omega \in \mathbb{H}^g$. Alternatively, we present real-valued functions that define trisecant points if their global minimum is zero and outline the procedure to look for such minimum.

The chapter is organized as follows. In Section 4.1 we present the algorithm to compute theta functions and their gradients in Matlab. In Section 4.2 we present Newton's method, the adaption of Fay's function in order to have a discrete set of zeros and the necessary algorithms to look for trisecant points. In Section 4.3 we present the search for trisecant points in the form of a global optimization problem and the algorithms that can be used to solve them.

4.1 Computation of theta functions

The standard way to compute the theta function (2.16) is by considering the sum

$$\vartheta(z) \approx \sum_{N \in [-\mathcal{N}_\delta, \mathcal{N}_\delta]^g} \exp\left(\pi i \langle N, \Omega N\rangle + 2\pi i \langle N, z\rangle\right), \tag{4.1}$$

where $[-\mathcal{N}_\delta, \mathcal{N}_\delta]^g := \{N \in \mathbb{Z}^g \mid -\mathcal{N}_\delta \leq N_j \leq \mathcal{N}_\delta, \quad \forall j = 1, ..., g\}$. Namely, it is a hypercube with $(2\mathcal{N}_\delta + 1)^g$ elements. The constant $\mathcal{N}_\delta$ is chosen such that all omitted terms in (2.16) are smaller in modulus than the aimed-at accuracy δ. We use the notation N instead of $\mathbf{n}$ in this chapter to indicate that we are considering a finite sum. The arrays N are g-dimensional and are expressed in column form $N = [N_1, \ldots, N_g]^\top$. Alternative methods to compute (2.16) are described in [Dec+03]

and [AC21], where they consider ellipsoids instead of a hypercube, thus giving a bound for each specific N considered in the sum.

The reason for this is that it does not add much to the computational cost, but that it simplifies a parallelization of the computation of the theta function in which we are interested.

Remark 4.1.1. *The quasi-periodicity property* (2.17) *allows us to compute* $\vartheta(\mathrm{z})$ *for any value* $\mathrm{z} \in \mathbb{C}^g$ *by considering an equivalent vector* $\mathrm{z}_0 \in \mathcal{U}_\Omega$ *and then applying the exponential factors* (2.17)*, with the lattice vector* $\lambda = \mathrm{z} - \mathrm{z}_0$*. Thus, we will always assume that* z *is in the fundamental domain of* $\mathbb{C}^g / \Lambda$*.*

Taking this into account, we get for the Riemann theta function the estimate

$$\mathcal{N}_\delta > \sqrt{-\frac{\ln \delta}{\pi y_{\min}} + \frac{1}{2}}. \tag{4.2}$$

Here $y_{\min}$ is the length of the shortest vector in the lattice defined by the imaginary part of the Riemann matrix $\mathbb{B} = X + \mathrm{i}Y$: let $Y = T^\top T$, i.e., T be the Cholesky decomposition of Y, then T defines a lattice, i.e., a discrete additive subgroup of $\mathbb{R}^g$, of the form

$$\mathcal{L}(t_1, \ldots, t_g) = \left\{ T\mathrm{N} \;\middle|\; \mathrm{N} \in \mathbb{Z}^g \right\}, \tag{4.3}$$

where $T = [t_1, t_2, \ldots, t_g] \in \mathbb{R}^{g \times g}$ has rank g. The length of the shortest vector in this lattice is denoted by $y_{\min}$, which is equivalent to the definition (2.15).

The greater the norm of the shortest lattice vector, the more rapid will be the convergence of the theta series. Note that, in general, the convergence of a theta series contrary to popular belief can be very slow, see for instance the discussion in [Dec+03]. For instance, let us consider again the case $g = 1$, with $\tau = a + \mathrm{i}b$, for some $a, b \in \mathbb{R}^+$. In this case we simply have $y_{\min} = b$ and as mentioned in Remark 2.3.5 the convergence depends mainly on $e^{-\pi b n^2}$. This factor decreases slowly if b is close to zero. However, the rate of convergence improves drastically if we consider an equivalent τ in the fundamental domain $\mathcal{F}$ given in (2.10), where $\Im(\tau) \geq \sqrt{3}/2$ for all $\tau \in \mathcal{F}$.

Siegel showed that the length of $y_{\min} \geq \sqrt{3}/2$ in the Siegel fundamental domain. Unfortunately, no algorithm is known to construct a symplectic transformation for a general Riemann matrix to this fundamental domain. But Siegel [Sie89] gave an algorithm to achieve this approximately. A problem in this context is the Minkowski ordering. Just as the identification of the shortest lattice vector, this is a problem for which only algorithms are known whose time grows exponentially with the dimension g. Therefore, the implementation of the Siegel algorithm in [Dec+03] uses an approximation to these problems known as the LLL algorithm [LLL82]. Whereas this algorithm is fast, it is not very efficient. Therefore, in [FJK19], Siegel's algorithm was implemented via an exact identification of the shortest lattice vector which leads to a more efficient computation of the theta functions. Thus, for all Riemann matrices to be considered in this work we always first apply the method outlined in [FJK19] in order to obtain faster convergent theta series. In practice, this means that an accuracy of the order $\delta \sim 10^{-12}$ can be reached with $\mathcal{N}_\delta = 5$.

Note that derivatives of theta functions are computed in an analogous way as the theta function itself since

$$\frac{\partial \vartheta\left[\begin{smallmatrix}\mathrm{p}\\ \mathrm{q}\end{smallmatrix}\right](\mathrm{z},\Omega)}{\partial \mathrm{z}_i} = 2\pi\mathrm{i}\sum_{\mathrm{N}\in\mathbb{Z}^g}(N_i+p_i)\exp\left\{\pi\mathrm{i}\left\langle \mathrm{N}+\mathrm{p},\Omega\left(\mathrm{N}+\mathrm{p}\right)\right\rangle + 2\pi\mathrm{i}\left\langle \mathrm{N}+\mathrm{p},\mathrm{z}+\mathrm{q}\right\rangle\right\}\ . \tag{4.4}$$

4.1.1 Arrays

Let $\hat{N}_{\mathrm{p}}\{I\}$ be the $(2\mathcal{N}_\delta+1)^g = (2\mathcal{N}_\delta+1)\times\cdots\times(2\mathcal{N}_\delta+1)$ array containing the I-th components of all the N considered in the sum plus the I-th component of the characteristic p. The theta function is approximated by

$$\vartheta(\mathrm{z}) = \mathtt{sum}\left(\hat{C}_{\mathrm{p}}.*\hat{T}_{\mathrm{pq}}(\mathrm{z})\right), \tag{4.5}$$

where `sum(M)` indicates the summation over all the components of the array M, the symbol "$.*$" indicates pointwise multiplication and $\hat{C}_{\mathrm{p}}$ is the array

$$\hat{C}_{\mathrm{p}} := \exp\left(\pi\mathrm{i}\sum_{\substack{I,J=1\\ I\geq I}}^{g}(1+\delta_{IJ})\Omega_{I,J}\hat{N}_{\mathrm{p}}\{I\}.*\hat{N}_{\mathrm{p}}\{I\}\right), \tag{4.6}$$

which is independent of $\mathrm{z}\in\mathbb{C}^g$; thus, for a given matrix $\Omega\in\mathbb{H}^g$ it is computed only once and then it is stored. On the other hand, the array

$$\hat{T}_{\mathrm{pq}}(\mathrm{z}) := \exp\left(2\pi\mathrm{i}\sum_{I=1}^{g}(\mathrm{z}(I)+\mathrm{q}(I))\cdot\hat{N}_{\mathrm{p}}\{I\}\right) \tag{4.7}$$

depends on z.

The construction of this array is the most expensive part of the routine that computes the theta function, but it allows the immediate computation of the derivatives. From (4.4) we see that

$$\frac{\partial \vartheta\left[\begin{smallmatrix}\mathrm{p}\\ \mathrm{q}\end{smallmatrix}\right](\mathrm{z},\mathbb{B})}{\partial \mathrm{z}_I} \approx \mathtt{sum}\left(\hat{N}_{\mathrm{p}}\{I\}.*\hat{C}_{\mathrm{p}}.*\hat{T}_{\mathrm{pq}}(\mathrm{z})\right). \tag{4.8}$$

Therefore, we compute both the theta function $\vartheta\left[\begin{smallmatrix}\mathrm{p}\\ \mathrm{q}\end{smallmatrix}\right]$ and its gradient $\nabla\vartheta\left[\begin{smallmatrix}\mathrm{p}\\ \mathrm{q}\end{smallmatrix}\right]$ using the same routine, since $\hat{C}_{\mathrm{p}}.*\hat{T}_{\mathrm{pq}}(\mathrm{z})$ is already computed in the computation of $\vartheta\left[\begin{smallmatrix}\mathrm{p}\\ \mathrm{q}\end{smallmatrix}\right]$.

4.2 Newton iteration

In this section we consider a function of the form $F:\mathbb{C}^N\to\mathbb{C}^M$ such that $F(\mathbf{x})=0$ if and only if Ω is in the Jacobi locus and describe the method to find a zero numerically.

4.2.1 Description of the method

Newton's method is a numerical method used to find zeros of locally holomorphic functions of the form $f:\mathbb{C}^M\to\mathbb{C}^N$ if the initial iterate $\mathbf{x}^{(0)}\in\mathbb{C}^M$ is sufficiently close

to a zero. If f is locally holomorphic, then it can be approximated in a neighborhood of $\mathbf{x}^{(0)}$ by a first order Taylor expansion

$$f(\mathbf{x}^{(0)} + \boldsymbol{\varepsilon}) \approx f(\mathbf{x}^{(0)}) + \mathrm{J}_f(\mathbf{x}) \cdot \boldsymbol{\varepsilon}, \tag{4.9}$$

where $\mathrm{J}(F(\mathbf{x}^{(0)}))$ denotes the Jacobian matrix of F. We approximate a zero by $f(\mathbf{x}^{(0)} + \boldsymbol{\varepsilon}) \approx 0$, then we need to solve the equation

$$J(f(\mathbf{x}^{(0)}) \cdot \boldsymbol{\varepsilon} = -f(\mathbf{x}^{(0)}). \tag{4.10}$$

This is done iteratively, thus With the choice $\mathbf{x}^{(0)} \in U \subset \mathbb{C}^M$ such that f is holomorphic on U, we find new iterates via

$$\mathbf{x}^{(n+1)} = \mathbf{x}^{(n)} - \mathrm{J}(f(\mathbf{x}^{(n)}))^{-1} f(\mathbf{x}^{(n)}), \quad n = 0, 1, \ldots; \tag{4.11}$$

However, the zero set must be discrete, otherwise $\mathrm{Jac}(F(\mathbf{x}^{(n)}))$ becomes singular.

4.2.2 Basin of attraction

Definition 4.2.1. *The basin of attraction of the zero $\mathbf{x}^*$ is defined as the subset $U^* \subset \mathbb{C}^M$ such that every initial vector $\mathbf{x}^{(0)} \in U^*$ converges to $\mathbf{x}^*$.*

For example, let us consider the function

$$\begin{aligned} f : \mathbb{C} &\to \mathbb{C}, \\ z &\mapsto z^3 - 1. \end{aligned}$$

Clearly, the zeros of this function are the roots of unity $z^* = \zeta_3^k$ for $k = 0, 1, 2$; where $\zeta_j^k = e^{2\pi k/j}$. Thus, there are three basins of attraction: the red region corresponds to $z^* = \zeta_0^k$, the green one to $z^* = \zeta_2^k$ and the blue one to $z^* = \zeta_2^k$.

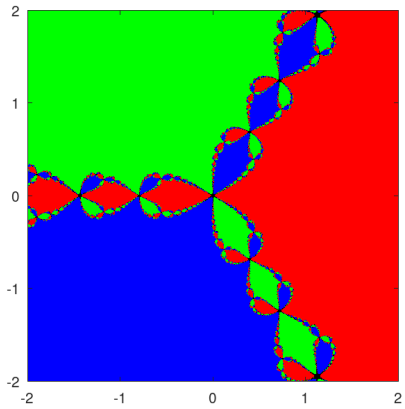

FIGURE 4.1: Basins of attraction of the zeros of $f(z) = z^3 - 1$.

However, if f is only locally holomorphic (e.g., it has poles), then there will be regions that will not converge to any of the zeros, regardless of how many iterations are carried out. For example, consider the function $f(z) = (z^3 - 1)/(1 - 2z)$, whose

zeros are also the third roots of unity, but in this case the function has a pole at $z = 1/2$. The black regions correspond to initial vectors $z^{(0)}$ that do not converge.

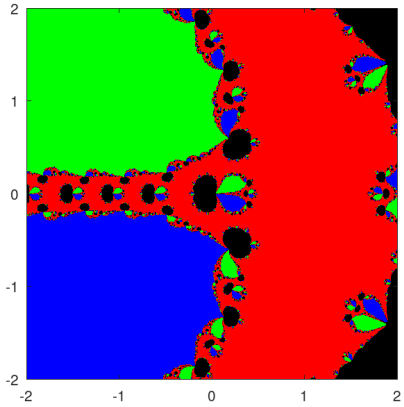

FIGURE 4.2: Basins of attraction of the zeros of $f(z) = (z^3 - 1)/(1 - 2z)$.

4.2.3 Setting up the problem

The function we are interested in is (3.11), but for computational purposes we will consider vectors X, Y, Z in the fundamental domain of $\mathcal{A}_\Omega = \mathbb{C}^g/\Lambda$, namely,

$$\begin{aligned} F : \overline{U}_\Omega \times \overline{U}_\Omega \times \overline{U}_\Omega &\to \mathbb{C}^{2^g}, \\ (X, Y, Z) &\mapsto \vec{\Theta}(X) + c_1(X, Y, Z) \cdot \vec{\Theta}(Y) + c_2(X, Y, Z) \cdot \vec{\Theta}(Z), \end{aligned} \tag{4.12}$$

where $\vec{\Theta}(Z) := \left(\vartheta\left[{}^{\epsilon/2}_{0}\right](2Z, 2\Omega)\right)_{\epsilon \in \mathbb{Z}^g/2\mathbb{Z}^g}$ is the representative of the Kummer point $\mathrm{Kum}(Z)$ in $\mathbb{C}^{2^g}$ and $\overline{U}_\Omega$ is the closure of the fundamental domain (2.6) of $\mathcal{A}_\Omega$. Additionally, we need to impose the condition that the zeros must be non-trivial.

Definition 4.2.2 (Trivial zeros)**.** *We say that (X, Y, Z) is a trivial zero if $X = \pm Z$, $Y = \pm Z$ or $X = \pm Y$, since $F(X, Y, Z) = 0$ for such cases regardless of the nature of $\Omega \in \mathbb{H}^g$.*

With the aforementioned constraint, $F(X, Y, Z) = 0$ if and only if $\mathrm{Kum}(X)$, $\mathrm{Kum}(Y)$, $\mathrm{Kum}(Z)$ are trisecant points, none of which coincide. Therefore, Welters-Krichever's result [Wel84; Kri10] can be stated in terms of F.

Theorem 4.2.3 (Trisecant theorem)**.** *Let $(\mathcal{A}_\Omega, \Theta_\Omega)$ be an indecomposable principally polarized Abelian variety. Then, it is the Jacobian of some Riemann surface $\mathcal{R}$ of genus g if and only if the function F has non-trivial zeros.*

This implies that the zero set of the constrained F is either empty or it is the four-dimensional set given by the parametrization (3.5). However, even if Ω turns out to be in the Jacobi locus, we still have to determine X, Y, Z without an Abel map, since this is generally unknown.

Adding constraints

The fact that the zero set of F is 4-dimensional if $\Omega \in \mathcal{J}_g$ is problematic, since Newton's method does not work in such cases. However, since Theorem 4.2.3 only requires the existence of one zero to conclude that Ω is in the Jacobi locus $\mathcal{J}_g$, we can add four constraints to F in such a way that the zero set of the constrained function is discrete, which will allow us to use Newton's iteration (4.11).

A simple way add such constraints is by considering the intersection of the zero set of F with the zero set of four functions of the form $f(V) = V_j - c$, where $V = (X, Y, Z) \in U_\Omega^3$ and $c \in \mathbb{C}$. This is equivalent to fixing four components of the vector V in the iterative process. Having chosen starting vectors satisfying the non-triviality condition, we fix their first components so that their iterates $X^{(n)}$, $Y^{(n)}$ and $Z^{(n)}$ remain different along the whole iteration and, in addition, fix any other component, e.g., X_2. Thus, we obtain a function of the form

$$F|_W : W \subset \mathbb{C}^{3g-4} \to \mathbb{C}^{2g}, \tag{4.13}$$

where W is the compact subset

$$W = \{(X, Y, Z) \in \overline{U}_\Omega^3 \subset \mathbb{C}^{3g} \mid X_1 = X_1^{(0)}, X_2 = X_2^{(0)}, Y_1 = Y_1^{(0)}, Z_1 = Z_1^{(0)}\}. \tag{4.14}$$

For simplicity, we drop the subscript in $F|_W$. Then, in the sequel when we refer to F we mean the constraine function (4.13). Let us denote by $\mathbf{x}$ the remaining $3g-4$ components of $V \in \overline{U}_\Omega^3$, i.e., $\mathbf{x} \in W$. The task is to find a possible zero of the function $F(\mathbf{x})$, i.e., to decide whether it can have values smaller than the specified accuracy δ. If this is the case, then the Riemann matrix is regarded as lying on the Jacobi locus within the given numerical precision.

Thus, after choosing some initial vector $V^{(0)} \in \overline{U}_\Omega^3$, fixing four components to obtain W, setting the initial iterate $\mathbf{x}^{(0)}$, we numerically identify a zero of F by applying the standard Newton iteration (4.11). Notice that $\mathrm{Jac}(F(\mathbf{x}^{(n)}))$ is composed of $3g-4$ linearly independent components of the full Jacobian matrix of (4.12). Since F is locally holomorphic in the vectors X, Y, and Z, the Jacobian can be directly computed via the derivatives $\frac{\partial F}{\partial \mathbf{x}_i}$, $i = 1, \ldots, 3g-4$. In practice we compute the full Jacobian with respect to all components of X, Y, and Z; keep the necessary components and then compute the *Newton step* $\mathrm{J}(F(\mathbf{x}^{(n)}))^{-1}F(\mathbf{x}^{(n)})$ with the Matlab command '\'. This means that the overdetermined linear system $\mathrm{J}(F(\mathbf{x}^{(n)}))\mathbf{y} = F(\mathbf{x}^{(n)})$ is solved for $\mathbf{y}$ in a least squares sense. In our context, this has the advantage that all equations in (3.11) are satisfied as required to a certain accuracy if the iteration converges.

The Jacobian matrix of F can be computed efficiently by expressing it in terms of $\vec{\Theta}(X)$, $\vec{\Theta}(Y)$, $\vec{\Theta}(Z)$; their Jacobian matrices and the functions λ_j and their gradients. Thus, the Jacobian matrix of F with respect to X, Y, Z is the following

$$\mathrm{J}(F(X, Y, Z)) = [\mathrm{J}_X F, \quad \mathrm{J}_Y F, \quad \mathrm{J}_Z F],$$

where

$$\begin{aligned}
\mathrm{J}_X F =& \mathrm{J}\vec{\Theta}(X) + \frac{1}{\lambda_1}\vec{\Theta}(Y) * \nabla_X\lambda_2 + \frac{1}{\lambda_1}\vec{\Theta}(Z) * \nabla_X\lambda_3,\\
\mathrm{J}_Y F =& \frac{\lambda_2}{\lambda_1}\mathrm{J}\vec{\Theta}(Y) + \frac{1}{\lambda_1}\vec{\Theta}(Z) * \nabla_Y\lambda_3 - \frac{1}{(\lambda_1)^2}\left[\lambda_2\vec{\Theta}(Y) + \lambda_3\vec{\Theta}(Z)\right] * \nabla_Y\lambda_1, \qquad (4.15)\\
\mathrm{J}_Z F =& \frac{1}{\lambda_1}\vec{\Theta}(Y) * \nabla_Z\lambda_2 + \frac{\lambda_3}{\lambda_1}\mathrm{J}\vec{\Theta}(Z) - \frac{1}{(\lambda_1)^2}\left[\lambda_2\vec{\Theta}(Y) + \lambda_3\vec{\Theta}(Z)\right] * \nabla_Z\lambda_1,
\end{aligned}$$

where "$*$" is the matrix product. We represent $\vec{\Theta}(X)$ in column vector form and $\nabla_X\lambda_2$ in row vector form. Recall that we consider $c_1 = \lambda_2/\lambda_1$, $c_2 = \lambda_3/\lambda_1$ with λ_j in the form in (3.4), namely, $\lambda_1 = \vartheta^*(Y-Z)\cdot\vartheta^*(Y+Z)$, $\lambda_2 = \vartheta^*(Z-X)\cdot\vartheta^*(Z+X)$, $\lambda_3 = \vartheta^*(X-Y)\cdot\vartheta^*(X+Y)$.

Remark 4.2.4. *If only $3g-4$ equations of $F=0$ are used for the Newton iteration (i.e., considering a function of the form $F:\mathbb{C}^n\to\mathbb{C}^n$), the latter in general converges to a value of $\mathbf{x}$ for which the remaining components of F do not vanish. Thus, it is important that all 2^g equations are used in the iteration.*

We recall that a Newton iteration has quadratic convergence which means that if $\tilde{\mathbf{x}}$ is the wanted zero of F, then $\|\mathbf{x}^{(n+1)} - \tilde{\mathbf{x}}\| \propto \|\mathbf{x}^{(n)} - \tilde{\mathbf{x}}\|^2$, provided $\mathbf{x}^{(n)}$ is in the so-called *basin of attraction*, which is the subset of W for which the iteration converges. Loosely speaking the number of correct digits in the iteration doubles in each step of the iteration. However, note that the convergence of the Newton iteration is local and, therefore, depends on the starting point $\mathbf{x}^{(0)}$. If this is not adequately chosen, the iteration may fail to converge.

The iteration is stopped either when $\|\mathbf{x}^{(n+1)} - \mathbf{x}^{(n)}\| < \delta$ or the residual of F is smaller than δ — in which case we speak of convergence — or else after 100 iterations, in which case the iteration is deemed to not have converged. The latter typically indicates an inadequate choice of the initial iterate, and the iteration can simply be restarted with another initial vector. When the iteration stops, we not only check whether the residual of F in (3.11) is below the aimed-at accuracy δ which would indicate that the considered Riemann matrix is in the Jacobi locus. We also compute the *singular value decomposition*[1] of the matrix formed by the three vectors $\vec{\Theta}(X)$, $\vec{\Theta}(Y)$, $\vec{\Theta}(Z)$. If the modulus of the smallest singular value of this matrix, denoted by Δ in the following, is smaller than δ, the vectors are linearly dependent and the Riemann matrix is in the Jacobi locus within numerical accuracy.

Remark 4.2.5. *It is important that we used in (3.13) ratios of theta functions instead of a form of the Fay identity free of denominators. The reason for this is that odd theta functions have co-dimension one zero sets, and the Newton iteration would converge to all factors in front of $\vec{\Theta}(X)$, $\vec{\Theta}(Y)$, $\vec{\Theta}(Z)$ being zero. The same would happen if we obtain the constants from three of the equations (3.11) in the usual definition of linear dependence of vectors. This is the reason why we also check the linear dependence of the vectors via an SVD. The many zeros of the theta functions in the denominators of (3.13) can also lead to a slow convergence of the Newton iteration for the first iterates.*

[1] The singular-value decomposition (SVD) of an $m\times n$-matrix M with complex entries is given by $M = U\Sigma V^\dagger$; here U is an $m\times m$ unitary matrix, $V^\dagger$ denotes the conjugate transpose of V, an $n\times n$ unitary matrix, and the $m\times n$ matrix Σ is diagonal (as defined for a rectangular matrix); the non-negative numbers on the diagonal of Σ are called the singular values of M.

Since the convergence of the Newton iteration depends on the choice of the initial iterate $\mathbf{x}^{(0)}$, we must consider a strategy to assure convergence. We have the following choices:

(a) Take initial vectors of the form with

$$V^{(0)} = \frac{\ell}{2}\left(\mathrm{p}^{(1)} + \Omega\mathrm{q}^{(1)}, \mathrm{p}^{(2)} + \Omega\mathrm{q}^{(2)}, \mathrm{p}^{(3)} + \Omega\mathrm{q}^{(3)}\right), \tag{4.16}$$

where $0 < \ell < 1$ and $\mathrm{p}^{(i)}, \mathrm{q}^{(i)} \in \mathbb{Z}^g/2\mathbb{Z}^g$ with $\mathrm{q}^{(i)} \neq 0$. We require $\ell \neq 0, 1$ since the Jacobian matrix of the Kummer map is singular at half-period vectors. Thus, this choice will prevent the iterates from being too close to such singular points.

(b) Take completely random vectors $X^{(0)}$, $Y^{(0)}$, $Z^{(0)}$ in the fundamental domain satisfying the non-triviality conditions.

(c) Take two random initial vectors and the third one arbitrarily close to one of them, e.g., $V^{(0)} = (X^{(0)}, \ell X^{(0)}, Z^{(0)})$ with $\ell \approx 1$ or $V^{(0)} = (X^{(0)}, X^{(0)} + \boldsymbol{\varepsilon}, Z^{(0)})$ with $\|\boldsymbol{\varepsilon}\| \approx 0$. We cannot simply set $Y = Z$, $X = Y$ or $X = Z$ because of the non-triviality condition. However, from Fay's identity and the parametrization (3.5), we know that there exists $Y \neq X$ in the neighbourhood of X making F vanish.

For reproducibility purposes, we choose initial vectors according to (4.16) with different values of ℓ. Thus, for a given Riemann matrix $\Omega_0 \in \mathbb{H}^g$, we perform the following steps:

(i) Given $\Omega_0 \in \mathbb{H}^g$, look for a modular transformation $R \in \mathrm{Sp}(2g, \mathbb{Z})$ such that $\Omega = R \cdot \Omega_0$ is approximately in the Siegel fundamental domain (the important point is to ensure that the shortest lattice vector has length greater than $\sqrt{3}/2$). This is done with the algorithm [FJK19].

(ii) Set a value for ℓ in (4.16), $\Delta\ell$, $n_{\max}$ and the precision δ. For the examples presented here, we used $\ell = 0.10$, $\Delta\ell = 0.10$, $n_{\max} = 100$ and $\delta = 10^{-10}$.

(iii) Choose starting vectors $X^{(0)}, Y^{(0)}, Z^{(0)} \in U_\Omega$ in the form (4.16) with $\mathrm{p}^{(1)} = \mathrm{q}^{(1)} = e_{g-2}$, $\mathrm{p}^{(2)} = \mathrm{q}^{(2)} = e_{g-1}$, $\mathrm{p}^{(3)} = \mathrm{q}^{(3)} = e_g$ and fix the components X_1, X_2, Y_1, Z_1.

(iv) Set up the function $F : W \subset \mathbb{C}^{3g-4} \to \mathbb{C}^{2g}$.

(v) Perform Newton's iteration (4.11) until $\|\mathbf{x}^{(n+1)} - \mathbf{x}^{(n)}\| < \delta$ or the maximum number of iterations $n_{\max}$ is reached or $\|F(\mathbf{x}^{(n)})\| < \delta$. Keep the vectors $X^{(n)}$, $Y^{(n)}$, $Z^{(n)}$ in the fundamental domain at every step.

(vi) If $\Delta^{(N)} := \min(\mathrm{svd}(\vec{\Theta}(X^N), \vec{\Theta}(Y^N), \vec{\Theta}(Z^N))) < \delta$, where N is the iteration at which the Newton iteration stopped, we conclude that Ω is in the Jacobi locus with precision δ and stop the computations.

(vii) If the iteration did not converge, replace ℓ by $\ell + \Delta\ell$ and go back to step (iii) and perform a new iteration. Stop if $\ell > \ell_{\max}$ and conclude with a precision δ that Ω is not in the Jacobi locus. We used $\ell_{\max} = 0.5$ for our examples.

We show these steps more explicitly in the pseudo code Algorithm 1.

Pseudo codes

We sumarize the latter algorithm in the following pseudo codes.

Algorithm 1 Algorithm to find trisecant points

procedure TRISECANT(Ω) ▷ Find one trisecant in the Kummer variety of X_Ω
  $\Omega \leftarrow \texttt{siegeltrans}(\Omega)$ ▷ Find Siegel's transform of Ω
  $\delta \leftarrow 10^{-10}$ ▷ Set precision δ
  $\ell \leftarrow 0.1$
  $\Delta\ell \leftarrow 0.1$
  $\texttt{max\_iter} \leftarrow 100$ ▷ Set maximum number of iterations
  $\Delta_N \leftarrow [\ \ ]$
  while $\ell \geq 0.5$ **do**
    $X \leftarrow \ell/2\left(e_{g-2} + \Omega e_{g-2}\right)$
    $Y \leftarrow \ell/2\left(e_{g-1} + \Omega e_{g-1}\right)$
    $Z \leftarrow \ell/2\left(e_g + \Omega e_g\right)$
    $\mathbf{x} \leftarrow [X(3:g); Y(2:g); Z(2:g)]$ ▷ Initial vector
    $V \leftarrow [X(1:2); Y(1); Z(1)]$ ▷ Fixed components X_1, X_2, Y_1, Z_1
    $[F, JF, \mathbf{x}, \text{res}, \Delta] \leftarrow \texttt{fay}(\mathbf{x}, V, \Omega)$
    $\boldsymbol{\varepsilon} \leftarrow -JF \backslash F$
    $\texttt{iter} \leftarrow 1$
    while $\|\boldsymbol{\varepsilon}\| < \delta$ **do** ▷ *Newton's iteration*
      $\mathbf{x} \leftarrow \mathbf{x} + \boldsymbol{\varepsilon}$
      $[F, JF, \mathbf{x}, \text{res}, \Delta] \leftarrow \texttt{fay}(\mathbf{x}, W, \Omega)$
      $\boldsymbol{\varepsilon} \leftarrow -JF \backslash F$
      if res $< \delta$ or $\texttt{iter} > \texttt{max\_iter}$ **then**
        End Newton's iteration
      end if
      $\texttt{iter} \leftarrow \texttt{iter} + 1$
    end while
    $\Delta_N \leftarrow [\Delta_N, \Delta]$ ▷ Store the smallest Δ for each ℓ
    $\Delta_{\min} \leftarrow \min(\Delta_N)$
    if $\Delta_{\min} < \delta$ **then**
      End algorithm
    end if
    $\ell \leftarrow \ell + \Delta\ell$
  end while
  return res, $\Delta_{\min}$
end procedure

The routine $\texttt{fay}(\mathbf{x}, W, \Omega)$ evaluates the function $F : W \subset \mathbb{C}^{3g-4} \to \mathbb{C}^{2g}$ at the point $\mathbf{x}$ as well as its Jacobian matrix $JF(\mathbf{x})$. The fixed components are entered as the parameter $W = [X_1; X_2; Y_1; Z_1]$. Recall that we are only interested in the compact subset $W \subset \mathbb{C}^{3g-4}$ described in (4.14), because of the quasi-periodicity properties of theta functions. However, we might observe the iteration $\mathbf{x}^{(n)}$ going out of W for some n. Thus, the position of $X^{(n)}, Y^{(n)}, Z^{(n)}$ is updated by equivalent $\hat{X}^{(n)}, \hat{Y}^{(n)}, \hat{Z}^{(n)} \in \overline{U}_\Omega$ at every step. The following pseudo code summarizes this.

Algorithm 2 Algorithm to compute the function F

procedure FAY($\mathbf{x}, V, \Omega$)
$X \leftarrow [V(1:2); \mathbf{x}(1:g-2)]$
$Y \leftarrow [V(3); \mathbf{x}(g-1:2g-3)]$
$Z \leftarrow [V(4); \mathbf{x}(2g-2:2g-4)]$
$X \leftarrow [[X]]$ ▷ Keep X, Y, Z in the fundamental domain
$Y \leftarrow [[Y]]$
$Z \leftarrow [[Z]]$
$\mathbf{x} \leftarrow [X(3:g); Y(2:g); Z(2:g)]$
$[\lambda_1, \nabla_Y\lambda_1, \nabla_Z\lambda_1] \leftarrow \texttt{lambdafun}(Y, Z, \Omega)$
$[\lambda_2, \nabla_Z\lambda_2, \nabla_X\lambda_2] \leftarrow \texttt{lambdafun}(Z, X, \Omega)$
$[\lambda_2, \nabla_X\lambda_3, \nabla_Y\lambda_3] \leftarrow \texttt{lambdafun}(X, Y, \Omega)$
$[KX, JKX] \leftarrow \texttt{kummer}(X, \Omega)$
$[KY, JKY] \leftarrow \texttt{kummer}(Y, \Omega)$
$[KZ, JKZ] \leftarrow \texttt{kummer}(Z, \Omega)$
$F \leftarrow KX + \frac{\lambda_2}{\lambda_1}KY + \frac{\lambda_3}{\lambda_1}KZ$
$J_X F \leftarrow JKX + \frac{1}{\lambda_1}KY * \nabla_X\lambda_2 + \frac{1}{\lambda_1}KZ * \nabla_X\lambda_3$
$J_Y F \leftarrow \frac{\lambda_2}{\lambda_1}JKY + \frac{1}{\lambda_1}KZ * \nabla_Y\lambda_3 - \frac{1}{(\lambda_1)^2}[\lambda_2 KY + \lambda_3 KZ] * \nabla_Y\lambda_1$
$J_Z F \leftarrow \frac{1}{\lambda_1}KY * \nabla_Z\lambda_2 + \frac{\lambda_3}{\lambda_1}JKZ - \frac{1}{(\lambda_1)^2}[\lambda_2 KY + \lambda_3 KZ] * \nabla_Z\lambda_1$
$JF = [J_X F, J_Y F, J_Z F]$
$JF(:, [1, 2, g+1, 2g+1]) \leftarrow [\quad]$ ▷ Deleting columns corresponding to X_1, X_2, Y_1, Z_1
res $\leftarrow \|F\|$ ▷ Residual of F
$\Delta \leftarrow \min(\mathrm{svd}(KX, KY, KZ))$ ▷ Linear dependence of KX KY, KZ
return $F, JF, \mathbf{x}$, res, Δ
end procedure

Here $\texttt{kummer}(X, \Omega)$ is the routine computing $\vec{\Theta}(X)$ (which is expressed as a column vector) and its Jacobian matrix $J\vec{\Theta}(X)$. The operation "$*$" is the matrix multiplication. As mentioned in Section 4.1, the array $\hat{C}_{\mathrm{p}}$ shown in (4.6) is only computed once and then stored in memory. However, for the level-two theta functions we can save memory by using the property (2.26) and representing it in terms of the zero-characteristic theta function. Namely,

$$\vartheta_2^{\epsilon}(\mathbf{z}) = \eta_{\epsilon}(\mathbf{z}) \cdot \vartheta(2\mathbf{z} + \Omega\epsilon, 2\Omega),$$

$$\nabla\vartheta_2^{\epsilon}(\mathbf{z}) = 2 \cdot \eta_{\epsilon}(\mathbf{z}) \cdot \left[\nabla\vartheta(2\mathbf{z} + \Omega\epsilon, 2\Omega) + \pi\mathrm{i} \cdot \vartheta(2\mathbf{z} + \Omega\epsilon, 2\Omega) \cdot \epsilon^{\top}\right],$$

with the factor

$$\eta_{\epsilon}(\mathbf{z}) = \exp(1/2\pi\mathrm{i}\langle\epsilon, \Omega\epsilon\rangle + 2\pi\mathrm{i}\langle\epsilon, \mathbf{z}\rangle).$$

Algorithm 3 Algorithm to compute the Kummer map

procedure KUMMER(X, Ω)
  for $I = 1 : 2^g$ **do**
    Set characteristic ϵ_I ▷ $\epsilon_I \in \{0,1\}^g$ is a column vector
    $factor \leftarrow \exp\left(\frac{1}{2}\pi\mathrm{i}\langle\epsilon_I, \Omega\epsilon_I\rangle + 2\pi\mathrm{i}\langle\epsilon_I, X\rangle\right)$
    $[t, \nabla t] \leftarrow \texttt{thetagrad}(2X + \Omega\epsilon_I, 2\Omega, 0)$
    $K(I) \leftarrow factor \cdot t$
    $JK(I,:) \leftarrow 2 \cdot factor \cdot (\nabla t + \pi\mathrm{i} \cdot t \cdot \epsilon_I^T)$
  end for
  return K, JK
end procedure

The routine $\texttt{thetagrad}(X, \Omega, C)$ computes the multidimensional theta function $\vartheta[C](X, \Omega)$ defined in (2.22) with characteristic $C = \left[\begin{smallmatrix} \mathrm{p} \\ \mathrm{q} \end{smallmatrix}\right]$, as well as its gradient $\nabla\vartheta[C](X, \Omega)$ (which is expressed as a row vector) through (4.8). Finally, the routine to compute the function $\lambda(a, b) := \vartheta^*(a + b, \Omega)\vartheta^*(a - b, \Omega)$ with an odd characteristic $2\mathrm{p}^*, 2\mathrm{q}^* \in \mathbb{Z}^g/2\mathbb{Z}^g$, as well as its gradients $\nabla_a\lambda(a, b)$, $\nabla_b\lambda(a, b)$ is the following:

Algorithm 4 Algorithm to compute the lambda coefficients

procedure LAMBDAFUN(a, b, Ω)
  $\delta_o \leftarrow [e_1/2; e_1/2]$ ▷ Default odd characteristic
  $[t_p, \nabla t_p] \leftarrow \texttt{thetagrad}(a + b, \Omega, \delta_o)$
  $[t_m, \nabla t_m] \leftarrow \texttt{thetagrad}(a - b, \Omega, \delta_o)$
  $\lambda \leftarrow t_p \cdot t_m$
  $\nabla_a\lambda \leftarrow t_m\nabla t_p + t_p\nabla t_m$
  $\nabla_b\lambda \leftarrow t_m\nabla t_p - t_p\nabla t_m$
  return $\lambda, \nabla_a\lambda, \nabla_b\lambda$
end procedure

As before, since we use the same odd characteristic throughout the whole algorithm, we enter the array $\hat{\mathrm{C}}_\mathrm{p}$ with $\mathrm{p} = e_1/2$ as an input in the computation of the odd theta function $\vartheta^*(\mathrm{z}, \Omega)$ and its gradient.

4.3 Optimization problem

In this section we set a function of the form $f : \mathbb{C}^N \to \mathbb{R}$ such that $\min_{\mathbf{x}\in\mathbb{C}^N}(f) = 0$ if and only if Ω is in the Jacobi locus.

4.3.1 Option 1

From the form (3.3) of the Fay identity, we see that (3.11) vanishes for all $\mathbf{z} \in \mathbb{C}^g$ if there exist non-repeating $X, Y, Z \in \tilde{\mathcal{A}}_\Omega$ such that

$$f(X, Y, Z) = \sum_{\epsilon\in\mathbb{Z}^g} \|\vartheta\left[{}^{\epsilon/2}_{0}\right](2X, 2\Omega) + c_1\vartheta\left[{}^{\epsilon/2}_{0}\right](2Y, 2\Omega) + c_2\vartheta\left[{}^{\epsilon/2}_{0}\right](2Z, 2\Omega)\| \quad (4.17)$$

vanishes. Then, we can use this to define a function of the form $f : \tilde{\mathcal{A}}^3_\Omega \to \mathbb{R}$. As in the previous subsections, we require $\mathbf{z}^1$, $\mathbf{z}^2$, $\mathbf{z}^3$ to be different in $\tilde{\mathcal{A}}_\Omega$. Thus, the

function to be minimized is

$$f : \tilde{\mathcal{A}}_\Omega \backslash \tilde{\Delta} \to \mathbb{R}, \tag{4.18}$$

where $f(X, Y, Z)$ is (4.17) and $\tilde{\Delta}$ is the "diagonal" in $\tilde{\mathcal{A}}_\Omega$ defined as

$$\tilde{\Delta} = \{(X, Y, Z) \in \tilde{\mathcal{A}}_\Omega \mid X \neq Y \text{ and } Y \neq Z \text{ and } X \neq Z\}.$$

4.3.2 Option 2: singular values

The other method is determining whether the Kummer points $\mathrm{Kum}(X)$, $\mathrm{Kum}(Y)$, $\mathrm{Kum}(Z)$ are collinear in $\mathbb{P}^{2^g-1}$. Namely, whether their representatives $\vec{\Theta}(X)$, $\vec{\Theta}(Y)$, $\vec{\Theta}(Z)$ are coplanar in $\mathbb{C}^{2^g}$. In this subsection we use $(\mathbf{z}^1, \mathbf{z}^2, \mathbf{z}^3)$ instead of (X, Y, Z) to facilitate the representation of some computations. Let M be the matrix

$$M(\mathbf{z}^1, \mathbf{z}^2, \mathbf{z}^3) = \left[\vec{\Theta}(\mathbf{z}^1), \quad \vec{\Theta}(\mathbf{z}^2), \quad \vec{\Theta}(\mathbf{z}^3)\right],$$

then the points $\mathrm{Kum}(\mathbf{z}^1)$, $\mathrm{Kum}(\mathbf{z}^2)$, $\mathrm{Kum}(\mathbf{z}^3)$ are collinear if and only if M is rank-deficient, i.e., $\mathrm{rank}(M) < 3$.

Therefore, we look to define a function of the form $f(\mathbf{z}^1, \mathbf{z}^2, \mathbf{z}^3) = \min(\sigma_1^2, \sigma_2^2, \sigma_3^2)$, where σ_j are the singular values of $M(\mathbf{z}^1, \mathbf{z}^2, \mathbf{z}^3)$. From now on we drop $(\mathbf{z}^1, \mathbf{z}^2, \mathbf{z}^3)$, but it should be clear that M varies with $(\mathbf{z}^1, \mathbf{z}^2, \mathbf{z}^3)$. The square of the singular values, σ_j^2, are just the eigenvalues of

$$L := M^\dagger M$$

which is a 3×3 Hermitian matrix with

$$L_{rs} = \sum_{k=0}^{2^g-1} \overline{\vartheta_2^{\epsilon_k}(\mathbf{z}^r)} \vartheta_2^{\epsilon_k}(\mathbf{z}^s) = \vec{\Theta}(\mathbf{z}^r)^\dagger \cdot \vec{\Theta}(\mathbf{z}^s). \tag{4.19}$$

Since L is Hermitian, its eigenvalues are real and they are given by the solutions of the characteristic polynomial $\mu^3 + B\mu^2 + C\mu + D = 0$, with

$$\begin{aligned} B =& -L_{11} - L_{22} - L_{33} = -\mathrm{tr}(L), \\ C =& L_{11}L_{22} + L_{11}L_{33} + L_{22}L_{33} - L_{12}L_{21} - L_{13}L_{31} - L_{23}L_{32}, \\ D =& L_{11}L_{23}L_{32} + L_{22}L_{13}L_{31} + L_{33}L_{12}L_{21} \\ & - L_{11}L_{22}L_{33} - L_{12}L_{23}L_{31} - L_{13}L_{32}L_{21} = -\det(L). \end{aligned}$$

Since

$$\begin{aligned} \mu^3 - \mathrm{tr}(L)\mu^2 + C\mu - \det(L) = 0, \\ (\mu - \mu_1)(\mu - \mu_2)(\mu - \mu_3) = 0, \end{aligned}$$

are equivalent, we can see that

$$\mu_1\mu_2\mu_3 = \det(L). \tag{4.20}$$

Then, $\min(\mu_1, \mu_2, \mu_3) = 0$ if and only if $\det(L) = 0$. Thus, we define the function f as

$$\begin{aligned} f : \tilde{\mathcal{A}}^3_\Omega \backslash \tilde{\Delta} &\to \mathbb{R}, \\ (\mathbf{z}^1, \mathbf{z}^2, \mathbf{z}^3) &\mapsto \det(L). \end{aligned} \tag{4.21}$$

Gradient

The advantage of this function is that its gradient can be computed explicitly and thus, we could use gradient-based optimization methods, increasing its efficiency with respect to methods requiring only continuity. We now show the explicit form of the gradient of f. First, notice that

$$\partial_j^n L_{rs} = \sum_k \overline{\vartheta_2^{\epsilon_k}(\mathbf{z}^r)} \partial_j^n \vartheta_2^{\epsilon_k}(\mathbf{z}^s) = \delta_{ns} \sum_k \overline{\vartheta_2^{\epsilon_k}(\mathbf{z}^r)} \partial_j \vartheta_2^{\epsilon_k}(\mathbf{z}^s), \tag{4.22}$$

where we use the notation $\partial_j^n = \partial / \partial z_j^n$. Thus, the computation of the gradient $\nabla^n L_{rs}$ be simplified since it can be expressed as

$$\begin{aligned} \nabla^n L_{rs} &= \delta_{ns} \vec{\Theta}(\mathbf{z}^r)^\dagger \cdot \mathrm{J}\vec{\Theta}(\mathbf{z}^s), \\ \overline{\nabla}^n L_{rs} &= \delta_{nr} \vec{\Theta}(\mathbf{z}^s) \cdot \overline{\mathrm{J}\vec{\Theta}(\mathbf{z}^r)}, \end{aligned}$$

where $\mathrm{J}\vec{\Theta}$ is the Jacobian matrix of the function $\vec{\Theta} : \mathbb{C}^g \to \mathbb{C}$, $M^\dagger$ is the adjoint (or conjugate transpose) of the matrix M and $\overline{M}$ indicates pointwise conjugation, i.e., $\overline{M} = (M^\dagger)^\top$. Recall that the determinant can be expressed as

$$\det(L) = \sum_{j=1}^{3} (-1)^{i+j} L_{ij} \cdot m_{ij}(L) = \sum_{j=1}^{3} (-1)^{i+j} L_{ji}, \cdot m_{ji}(L),$$

for some $i \in \{1, 2, 3\}$ and where $m_{ij}(L)$ is the minor of the matrix L. Then,

$$\begin{aligned} \nabla^k f = \nabla^k \det(L) &= \sum_j (-1)^{j+k} \cdot \nabla^k L_{jk} \cdot m_{jk}(L), \\ \overline{\nabla}^k f = \overline{\nabla}^k \det(L) &= \sum_j (-1)^{j+k} \cdot \overline{\nabla}^k L_{kj} \cdot m_{kj}(L), \end{aligned}$$

Therefore, we can express the derivatives of the complex function f in terms of the derivatives of the level-two theta functions.

For methods that to not require gradients, we can just compute the singular values of the matrix M (equivalent to computing the eigenvalues of $L = M^\dagger M$).

$$\begin{aligned} f : \tilde{\mathcal{A}}^3_\Omega \backslash \tilde{\Delta} &\to \mathbb{R}, \\ (\mathbf{z}^1, \mathbf{z}^2, \mathbf{z}^3) &\mapsto \min\left(\mathtt{eig}(L)\right). \end{aligned} \tag{4.23}$$

Instead of using the fundamental domain in the form (2.6), we express it as a subset of R^{2g} in terms of the p, q characteristics. Namely,

$$S_{\mathrm{pq}} := \left\{ \mathrm{p}, \mathrm{q} \in \mathbb{R}^g \;\middle|\; \mathrm{p}_j, \mathrm{q}_j \in (-1/2, 1/2) \right\}. \tag{4.24}$$

The closure of this set maps to the complex torus as well. Similarly to what we did in Subsection 4.2.3, we fix some components in order to avoid trivial solutions. Thus we set,

$$\begin{aligned} S := \Big\{ (\mathrm{p}^{(1)}, \mathrm{q}^{(1)}, \mathrm{p}^{(2)}, \mathrm{q}^{(2)}, \mathrm{p}^{(3)}, \mathrm{q}^{(3)}) \in \overline{S}_{\mathrm{pq}} \times \overline{S}_{\mathrm{pq}} \times \overline{S}_{\mathrm{pq}} \mid \cdots \\ \mathrm{p}_1^{(j)} = const., \mathrm{q}_1^{(j)} = const.; \text{ for } j = 1, 2, 3 \Big\}. \end{aligned} \tag{4.25}$$

This is similar to the definition of (4.14), except for the fourth constraint. The reason is that there are optimization methods that do not rely on the derivatives of the function f, but it can be added since the set of zeros of F are precisely the set of global minima of f. The domain (4.25) is compact.

Thus, the three optimization problems presented above can be rewritten as

$$f : S \subset \mathbb{R}^{6g} \to \mathbb{R}. \tag{4.26}$$

Therefore, the trisecant theorem can be rewritten in terms of any of these functions.

Theorem 4.3.1. *Let $(\mathcal{A}_\Omega, \Theta_\Omega)$ be an indecomposable principally polarized Abelian variety. Then, it is the Jacobian of some Riemann surface $\mathcal{R}$ of genus g if and only if the global minimum of the function f is zero, i.e.,* $\min_{\mathbf{x} \in S}(f) = 0$.

4.3.3 Global optimization methods

In global optimization we are interested in finding the global minimum of real-valued continuous functions

$$f : S \subset \mathbb{R}^d \to \mathbb{R}, \tag{4.27}$$

on a compact subset S of $\mathbb{R}^d$ and f. Namely, we want to find

$$f_* := f(\mathbf{x}_*) = \min_{\mathbf{x} \in S} f(\mathbf{x}),$$

namely, a global optimization problem in S. This means that we are looking for the optimal vector $\mathbf{x}_* \in S$ such that $f(\mathbf{x}_*) \leq f(\mathbf{x})$ for all $\mathbf{x} \in S$. Moreover, we are interested to know whether the global minimum is zero.

Gradient-based methods are popular optimization tools, but get trapped in regions with local minima, namely, the iterations stop when the function converge to a local minimum. To address this problem the following options are usually followed:

- Two-phase methods: where gradient-based methods are used to carry out a local search on multiple starting vectors $\mathbf{x}^{(0)} \in S$. The smallest $f(\mathbf{x}_*)$ is taken as the most optimal value in the whole process.
- Random search methods: randomly generated points following a distribution probability.

The first choice does not have any advantage for our specific problem and is less optimal, so we only discuss the latter. One of the most popular methods for global optimization is *simulated annealing*. This method is more flexible than gradient-based methods in accepting new iterations. In gradient-based methods the new iterations $\mathbf{x}^{(n+1)}$ are only accepted if $f(\mathbf{x}^{(n+1)}) < f(\mathbf{x}^{(n)})$. However, in simulated

annealing an iterate for which $f(\mathbf{x}^{(n+1)}) < f(\mathbf{x}^{(n)})$ is accepted with a probability $P_n(f(\mathbf{x}^{(n)}), f(\mathbf{x}^{(n+1)}))$ that decreases as n increases. This allows the iteration to "escape" from the neighborhood of local minima [Rub81; KGV83] at the beginning of the iterative process and eventually fall into the basin of attraction of a global minimum.

The basic algorithm for this random search is the following:

0 Choose a starting vector $\mathbf{x}^{(0)} \in S$

1 Choose a vector $\epsilon^{(n)}$ such that $\mathbf{x}^{(n)} + \epsilon^{(n)} \in S$

2 Choose a new vector $\mathbf{y}^{(n+1)} = \mathbf{x}^{(n)} + \epsilon^{(n)}$

3 With a probability $\beta(\mathbf{x}^{(n)}, \mathbf{y}^{(n+1)})$, set $\mathbf{x}^{(n+1)} = \mathbf{y}^{(n+1)}$

4 Set $n = n + 1$

5 Go back to step [1] or stop if $n > n_{max}$ $f(\mathbf{x}^{(x+1)}) < \delta$

Which we summarize in the pseudo code

Algorithm 5 Algorithm to find a global minimum

```
procedure SIMULATEDANNEALING(Ω)
    Ω ← siegeltrans(Ω)
    δ ← 10^{-10}                          ▷ Set precision δ
    x = InitialVector()
    y = x
    n ← 0, N ← n_max
    fx ← Fun(x, Ω)
    while n < N do
        ε ← UpdateFun(x)
        y ← x + ε
        fy ← Fun(y, Ω)
        T = Temperature(n)
        if rand() < Beta(fx, fy, T) then
            x ← y
        end if
    end while
    f_min ← min(fx, fy)
    return f_min
end procedure
```

Where $\texttt{Beta}(fx, fy, T)$ is known as the acceptance probability function. The classical choice for this function is the so-called Metropolis criterion [RS94]

$$\beta_T(\mathbf{x}, \mathbf{y}) = \min(1, e^{[f(\mathbf{y}) - f(\mathbf{x})]/T}),$$

assuring an acceptance when $f(\mathbf{x}^{(n+1)}) < f(\mathbf{x}^{(n)})$. Thus we set $\texttt{Beta}(fx, fy, T) = \exp((fy - x)/T)$.

The *temperature function* T_n is a decreasing function that takes values in the set $(0, 1]$ and $T_n \to 0$ as $n \to \infty$. This is chosen heuristically and some of the common

choices include $T_n = \alpha^n$ with $\alpha \approx 1$ and $T_n = 1/\ln(n+1)$. This means that at the beginning of the iteration, the acceptance probability functions is flexible in accepting candidates $y^{(n+1)}$ that do not decrease the value of the function f, which is done in order to do an exhaustive search in the whole domain; but as n increases the acceptance probability is more strict since $\beta_T(\mathbf{x}, \mathbf{y}) \to 0$ when $T \to 0$, thus the search becomes local.

The routine $\texttt{Fun}(\mathbf{x}, \Omega)$ computes the function f, for example the norm of the *Fay function* (4.17) or the function to determine the singular values (4.21) with the domain.

The iteration is updated by $\mathbf{x}^{(n+1)} = \mathbf{x}^{(n)} + \epsilon^{(n)}$, where $\epsilon^{(n)}$ is chosen randomly with a distribution centered on $\mathbf{x}^{(n)}$. The distribution to be used must be included in the routine `UpdateFun`.

There many options for the acceptance functions $\beta_T(\mathbf{x}, \mathbf{y})$, the temperature functions T_n, as well as for the distribution functions to update the iterates. However, as mentioned in [RS94], the choice of these values is done heuristically. This means this approach would not assure an efficient search for trisecants for general $\Omega \in \mathbb{H}^g$. The other downside is that it has slow convergence (in the order of thousands or millions of iterations depending on the complexity of the function), since it does not consider the smoothness of the functions f. Therefore, the local search of zeros using the Newton method described in Section 4.2 is our best choice, considering that it is several orders of magnitude faster than simulated annealing. In Newton's iteration we do not need other functions inside the routine in a heurisitc way, thus making it sufficiently general to study any point $\Omega \in \mathbb{H}^g$.

Chapter 5

Numerical determination of trisecant points

In this chapter we present some numerical experiments for the Schottky problem up to genus 7. The only input of the routine that looks for distinct trisecant points in the Kummer variety is the Riemann matrix $\Omega \in \mathbb{H}^g$ that defines the PPAV. We start by carrying out some computations for a family of Riemann matrices in $\mathbb{H}^4$, since this allows the comparison with the Schottky-Igusa form, the only direct way of determining whether a given $\Omega \in \mathbb{H}^g$ with $g \geq 4$ defines a Jacobian variety. The algorithm is stable and fast convergence is observed. Adding small perturbations to known period matrices $\Omega \in \mathcal{J}_g$ sends them out of the Jacobi locus, and this is observed numerically in several tests. Moreover, the size of the smallest attained residual is an indicator of the precision of the considered matrices if they are only known in numerical form.

The chapter is organized as follows. In Section 5.1 we study the stability of the code and then compare the outcomes of our algorithm to the Schottky-Igusa form in $g = 4$. In Section 5.2 we apply the algorithm to several PPAVs up to $g = 7$ in order to look for trisecant points.

5.1 Examples in genus 4

In this section we study known examples in genus 4 since the Schottky-Igusa form gives the identification of the Jacobi locus in genus 4. This provides interesting tests for our approach. We start by studying the stability of the code by considering the Riemann matrix of Bring's curve, as well as images of the Abel map (which are computed numerically). We use the algorithm described above, but with perturbations of the Abel vectors as initial iterates. We expect quadratic convergence from the beginning since the initial iterates are in the vicinity of zeros.

5.1.1 Bring's curve

Bring's curve is the curve with the highest number of automorphisms in genus 4, see [BN12] for the computation of its Riemann matrix. It can be defined by the algebraic curve

$$\{(x, y) \in \mathbb{C}^2 \quad | \quad xy^5 + x + x^2y^2 - x^4y - 2y^3 = 0\}. \tag{5.1}$$

For a given algebraic curve, the Riemann matrix can be computed via the symbolic approach by Deconinck and van Hoeij [DH01] implemented in Maple or in Sage [SD16] or the purely numerical approach [FK16], see also the respective chapters in

[Be11]. We use here the approach of [FK16] and find after applying Siegel's algorithm in the form [FJK19] the Riemann matrix

```
RieMat =

  -0.5000 + 0.8685i  -0.0000 + 0.0649i  -0.5000 - 0.2678i   0.5000 - 0.2678i
   0.0000 + 0.0649i  -0.5000 + 0.8685i   0.5000 + 0.2678i  -0.5000 + 0.2678i
  -0.5000 - 0.2678i   0.5000 + 0.2678i  -0.0000 + 1.0714i   0.5000 - 0.2678i
   0.5000 - 0.2678i  -0.5000 + 0.2678i   0.5000 - 0.2678i  -0.5000 + 0.8685i.
```

Note that the accuracy of the computed matrix is estimated to be better than 10^{-14}, but for the ease of readability, we give only four digits here. For this matrix, we get for the Schottky-Igusa form $|\Sigma| = 1.04 \times 10^{-15}$, i.e., a value of the order of the rounding error as expected. This is to ensure that we are indeed testing with a matrix Ω in the Jacobi locus.

To test the computation of the Abel map and the Fay identity, we consider the points covering 2.5 on the sheets 1 to 4 of Bring's curve. The code [FK16] gives

```
AbelMap =

  -0.7052 + 0.3692i   0.0545 + 0.0278i   0.0293 + 0.0775i  -0.0607 + 0.1180i
   0.1286 - 0.2662i   0.2747 + 0.2456i  -0.4068 + 0.4113i   0.0318 + 0.2067i
  -0.4351 + 0.2906i  -0.2108 + 0.0422i   0.0250 + 0.2906i   0.0823 - 0.2451i
   0.4519 - 0.6915i   0.0718 + 0.0915i  -0.0126 - 0.0140i   0.0487 + 0.0493i.
```

Before testing the algorithm with starting vectors of the form (4.16), we first study the stability of the iteration. This is done by setting $X^{(0)}$, $Y^{(0)}$, $Z^{(0)}$ as linear combinations of the computed Abel vectors in the shape given by (3.5). The residual of the function F in (3.11) for this Abel map is of the order of 10^{-10}, and the minimal singular value of the matrix with the vectors $\vec{\Theta}(X)$, $\vec{\Theta}(Y)$ and $\vec{\Theta}(Z)$ is $\Delta \sim 10^{-11}$. This indicates that the Abel map is computed to an accuracy of the order of 10^{-11}. After one Newton iteration, the difference between the new and old vector is of the order 10^{-11}, and the residual of $F \sim 10^{-14}$ and $\Delta \sim 10^{-14}$. This shows that the iteration is stable (the numerical error in the Abel map is 'corrected' by the Newton iteration), and that a similar residual of F is reached in this example as for the Schottky-Igusa form.

The stability of the iteration is also shown by perturbing the initial vector. We multiply the above $\mathbf{x}$ by a factor 1.1, i.e., we keep the entries $X_1^{(0)}$, $X_2^{(0)}$, $Y_1^{(0)}$, $Z_1^{(0)}$ and multiply the remaining ones by 1.1. After 7 iterations, we get the same residual, minimal singular value Δ and final vector $\mathbf{x}$ as before. The same behaviour is observed for $0.9\mathbf{x}$ as the initial iterate.

It is known that Matlab timings are not very precise since they strongly depend on how many precompiled commands are used in the coding, but they provide an indication of actual computing times for a given task. On a standard laptop, the above examples take a few seconds.

To finish the tests with Bring's curve, we choose the same $X_1^{(0)}$, $X_2^{(0)}$, $Y_1^{(0)}$, $Z_1^{(0)}$ as before, but the remaining components are chosen randomly with the condition that $X^{(0)}$, $Y^{(0)}$, $Z^{(0)}$ must be in the fundamental domain. The algorithm finally produces a residual for F smaller than 10^{-12}, but finds a vector $\mathbf{x}$ different from the one produced by the Abel map. This is because the zero set of $F|_W$, with W given by (4.14), does not necessarily have a unique element.

5.1.2 Family of genus 4 Riemann matrices

We now turn to the family of Riemann matrices studied in [CKS19], which correspond to the genus 4 algebraic curves

$$\{(x,y)\in\mathbb{C}^2 \quad | \quad y^6 = x(x+1)(x-t)\}, \tag{5.2}$$

parametrized by $t\in\mathbb{P}^1\backslash\{0,1,\infty\}$. Their period matrices are given by [GM18], i.e. $\Omega_\tau = A^{-1}B$, where

$$(A|B) = \begin{pmatrix} \tau & \tau & 0 & -\tau-1 & 1 & 1 & 0 & -1 \\ \zeta^2-1 & 1 & -\zeta^2+1 & 1 & 1 & -\zeta^2 & \zeta^2 & -\zeta^2+1 \\ \zeta^3-\zeta & -\zeta^3 & -2\zeta^3+2\zeta^2+\zeta-1 & \zeta^2-\zeta & 1 & \zeta^2-1 & \zeta^3-\zeta^2-2\zeta+2 & \zeta^2 \\ -\zeta^3+\zeta & \zeta^3 & 2\zeta^3+2\zeta^2-\zeta-1 & \zeta^2+\zeta & 1 & \zeta^2-1 & -\zeta^3-\zeta^2+2\zeta+2 & \zeta^2 \end{pmatrix}, \tag{5.3}$$

with $\zeta = e^{2\pi i/12}$ and $t=\mu(\tau)$ for some $\mu:\mathbb{H}\to\mathbb{P}^1$.

Let us first look at the convergence rate of the iteration for one specific Riemann matrix, e.g., Ω_τ with $\tau = 1+i$. In Figure 5.1 we observe that as soon as the vector $\mathbf{x}^{(n)}$ falls into a basin of attraction, it converges to a zero very rapidly. Recall that N is the step at which the iteration stops. Thus, $\|F(\mathbf{x}^{(N)})\|$ is the best residual achieved by the iteration corresponding to the starting vectors $X^{(0)}, Y^{(0)}, Z^{(0)}$. For this test, we chose the starting vectors according to Algorithm 1. In contrast, notice that with a small perturbation of the form

$$\Omega_{\tau,s} = \Omega_\tau + s\cdot\mathrm{diag}[2,3,5,7], \quad \text{with } s=0.01; \tag{5.4}$$

the smallest value of $\|F(\mathbf{x}^{(N)})\|$ is above 10^{-4} (although this lower bound will depend on how small s is). Thus, for these particular examples there are at least six orders of magnitude of difference in the smallest attained residuals.

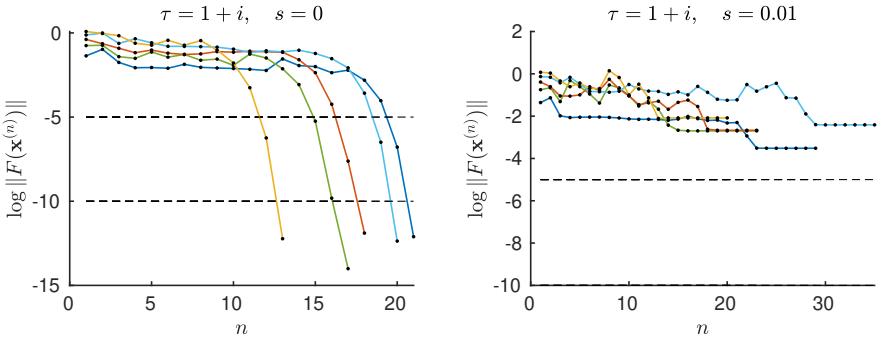

FIGURE 5.1: Residual of the function F, corresponding to the matrix $\Omega_{\tau,s}$, in dependence of the n-th iteration.

Remark 5.1.1. *Using Algorithm 1, but with randomly chosen initial vectors, the iterations converge with a frequency of approximately* 90% *when* $\mathbb{B}$ *is in the Jacobi locus. We attain the residuals shown in Figure 5.2 for 1000 different tests for the same matrix* Ω_τ*, i.e., 1000 iterations with different randomly chosen initial vectors* $X^{(0)}, Y^{(0)}, Z^{(0)}$ *attained* $\Delta^{(N)} < 10^{-10}$ *896 times. In contrast, none of the tests attained a value below* 10^{-5} *when the considered matrix is* $\Omega_{\tau,s}$ *with* $s = 0.1$.

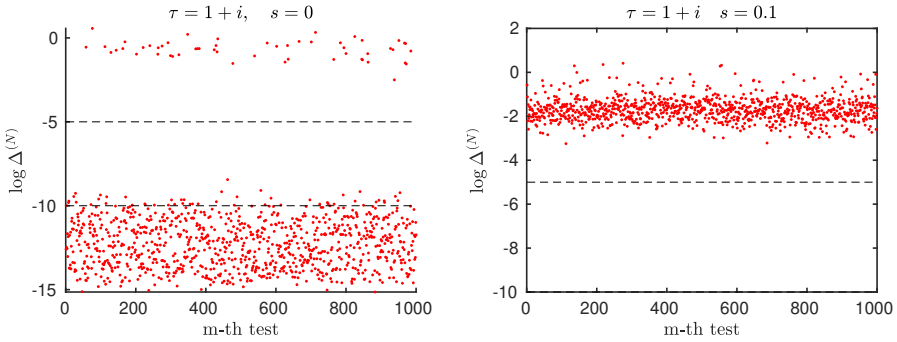

FIGURE 5.2: Attained values of $\Delta^{(N)}$ for randomly chosen initial vectors. The left-hand side corresponds to $\Omega_{\tau,s}$ with $s = 0$ and the right-hand side to $s = 0.1$.

Let us consider the family of Riemann matrices of the form (5.4) parametrized by $s \in [-1/2, 1/2]$ and $\tau = x + \mathrm{i}$, with $x \in [0, 1]$. We expect the Schottky-Igusa form of every $\Omega_{\tau,s}$ and the residual $\|F(\mathbf{x}^{(N)})\|$ (or its associated minimum singular value) obtained with Algorithm 1 to be within the same order of magnitude. This is indeed what we observe in Figure 5.3. With this algorithm, we conclude with precision $\delta = 10^{-10}$ that the Riemann matrices $\Omega_{\tau,s}$ with $s \neq 0$ are not in the Jacobi locus, agreeing with the Schottky-Igusa form.

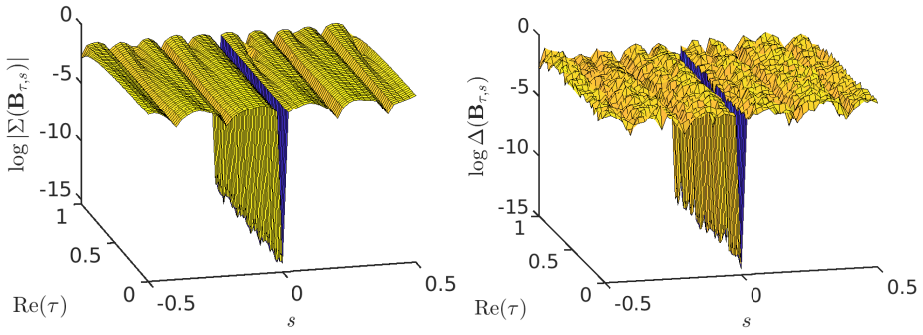

FIGURE 5.3: On the left the Schottky-Igusa form and on the right the minimum singular value $\Delta^{(N)}$, both in dependence of the Riemann matrices $\Omega_{\tau,s}$.

The matrices Ω_τ considered above are in exact form, thus the smallest residual is expected to be zero to machine precision, i.e., approximately 10^{-14} with Matlab. However, the smallest $\|F(\mathbf{x}^{(N)})\|$ might be considered as an indicative of the precision of its input matrix Ω, if this is not in exact form. For example, let us consider the matrices $\Omega_{\tau,s} = \Omega_\tau + s(M + \mathrm{i}M)$ where M is the symmetric matrix with coefficients $M_{jk} = (j + k)/5$, $\tau = 1 + \mathrm{i}$ and $s \in [10^{-15}, 10^{-1}]$ are small perturbations. Thus, $\Omega_{\tau,s}$ can be seen as the Riemann matrices of the curve (5.2) with an accuracy of the order s. We remove the stopping criterion $\|F(\mathbf{x}^{(N)})\| < \delta$ for this particular example in order to visualize the smallest residual we can achieve with Matlab's precision.

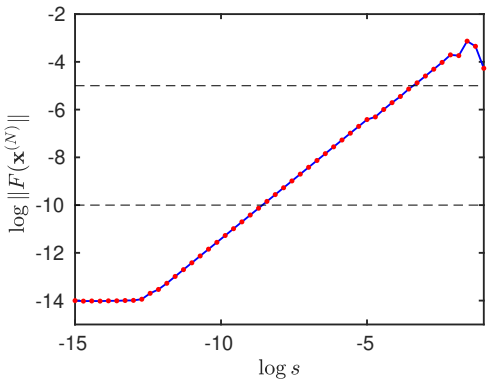

FIGURE 5.4: Smallest residuals of period matrices with accuracy s.

We can observe in the figure that we attain a residual to machine precision if the matrices are within a precision of approximately 10^{-13} and, in particular, the residual is below $\delta = 10^{-10}$ if the Riemann matrix is within a precision of the order δ. This is important, since some of the Riemann matrices in higher dimensions are only known numerically.

5.2 Examples in higher genus

We perform similar tests with matrices in higher genus such as, for example, the period matrices of hyperelliptic curves of arbitrary genus given by [Sch93]. In this paper we only show examples corresponding to the curve

$$\{(x,y) \in \mathbb{C}^2 \quad | \quad y^2 = x(x^{2g+1} - 1)\}, \tag{5.5}$$

but similar results are obtained with the period matrices of other hypereliptic curves. The period matrix of (5.5) is

$$\mathbb{B}_{jk} = 1 + \frac{1}{\tau_1} \sum_{l=1}^{j} \tau_l \tau_{k-j+l} \quad \text{for } 1 \leq j \leq k \leq g, \tag{5.6}$$

where $\tau_1 = (-1)^g \zeta_{2g+1}^{g^2}$ with $\zeta_m^n = \exp(2\pi i m/n)$ and

$$\tau_{j+1} = \frac{\tau_1}{1 + \zeta_{2g+1}^j} \left(1 - \sum_{l=2}^{j} \zeta_{2g+1}^{g-j+l-1} \tau_l \tau_{j-l+2} \right), \quad j = 1, ..., g-1.$$

We use these matrices for tests up to $g = 7$, but we also consider period matrices of non-hyperelliptic curves. For $g = 6$ let us consider the period matrix of the Fermat curve

$$\{[X : Y : Z] \in \mathbb{P}^2 \quad | \quad X^m + Y^m = Z^m\}, \tag{5.7}$$

with $m = 5$, making (5.7) a genus 6 curve. With the numerical approach [FK16], we get after applying the algorithm [FJK19] the Riemann matrix

```
RieMat =
```

```
  Columns 1 through 4

-0.3735 + 0.9276i  -0.3574 + 0.4580i  -0.4578 + 0.3092i  -0.2891 + 0.3705i
-0.3574 + 0.4580i   0.1365 + 1.0006i  -0.0161 + 0.4697i   0.1104 - 0.1415i
-0.4578 + 0.3092i  -0.0161 + 0.4697i   0.3474 + 1.0079i  -0.2630 - 0.3894i
-0.2891 + 0.3705i   0.1104 - 0.1415i  -0.2630 - 0.3894i  -0.3152 + 1.1305i
 0.0905 + 0.4390i  -0.4616 + 0.4201i   0.3635 + 0.5382i  -0.3735 - 0.2479i
-0.4417 - 0.1605i  -0.3313 - 0.3020i   0.2891 - 0.3705i  -0.1725 + 0.0496i

  Columns 5 through 6

 0.0905 + 0.4390i  -0.4417 - 0.1605i
-0.4616 + 0.4201i  -0.3313 - 0.3020i
 0.3635 + 0.5382i   0.2891 - 0.3705i
-0.3735 - 0.2479i  -0.1725 + 0.0496i
-0.4839 + 1.0692i  -0.3796 - 0.0685i
-0.3796 - 0.0685i  -0.4095 + 0.8023i.
```

For this curve, we could again compute an Abel map, but we are interested also in perturbations of this Riemann matrix not in the Jacobi locus.
Analogously to (5.4), we add diagonal perturbations of the form $\Omega_s = \mathbb{B} + s \cdot \mathrm{diag}[2, ..., g+1]$ with $s \in [-1/2, 1/2]$. As in the previous example, we observe several orders of magnitude of difference between the case $s = 0$ and the cases $s \neq 0$. Although a similar behaviour to Figure (5.4) is to be expected for small values of s.

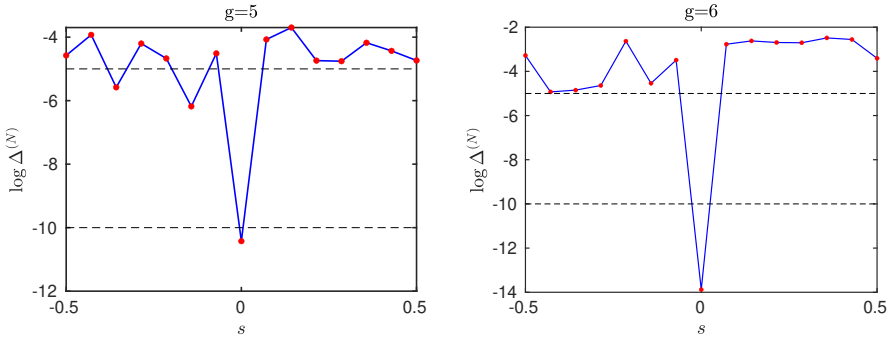

FIGURE 5.5: Minimum $\Delta^{(N)}$ obtained for the matrices $\Omega_s \in \mathbb{H}^g$ for $g = 5$ and $g = 6$.

The Fricke-Macbeath curve [Fri99; Mac65] is a curve of genus 7 with the maximal number $84(g-1) = 504$ of automorphisms. It can be defined via the algebraic curve

$$\{(x, y) \in \mathbb{C}^2 \quad | \quad 1 + 7yx + 21y^2x^2 + 35x^3y^3 + 28x^4y^4 + 2x^7 + 2y^7 = 0\}. \tag{5.8}$$

After applying the algorithm from [FJK19], the code [FK16] leads to the Riemann matrix

```
RieMat =

  Columns 1 through 4
```

```
  0.3967 + 1.0211i   0.0615 - 0.1322i   0.0000 - 0.0000i   0.4609 + 0.2609i
  0.0615 - 0.1322i   0.3967 + 1.0211i  -0.3553 + 0.5828i   0.3386 - 0.1933i
  0.0000 - 0.0000i  -0.3553 + 0.5828i   0.2894 + 1.1656i   0.0905 + 0.2450i
  0.4609 + 0.2609i   0.3386 - 0.1933i   0.0905 + 0.2450i   0.3967 + 1.0211i
 -0.3553 + 0.5828i  -0.4776 + 0.1287i  -0.4776 + 0.1287i  -0.4776 + 0.1287i
 -0.1838 - 0.3219i  -0.2743 - 0.5669i   0.3871 - 0.3736i   0.0167 - 0.3895i
  0.3386 - 0.1933i   0.3386 - 0.1933i  -0.1223 - 0.4541i   0.0615 - 0.1322i

Columns 5 through 7

 -0.3553 + 0.5828i  -0.1838 - 0.3219i   0.3386 - 0.1933i
 -0.4776 + 0.1287i  -0.2743 - 0.5669i   0.3386 - 0.1933i
 -0.4776 + 0.1287i   0.3871 - 0.3736i  -0.1223 - 0.4541i
 -0.4776 + 0.1287i   0.0167 - 0.3895i   0.0615 - 0.1322i
  0.2894 + 1.1656i  -0.1671 - 0.7115i   0.0905 + 0.2450i
 -0.1671 - 0.7115i   0.4414 + 1.2784i  -0.3386 + 0.1933i
  0.0905 + 0.2450i  -0.3386 + 0.1933i   0.3967 + 1.0211i.
```

The accuracy of this matrix is estimated to be of the order of 10^{-10}.

Fast convergence when $\mathbf{x}^{(n)}$ falls into a basin of attraction is still observed in higher genus. For example, let us observe the convergence of the residual of F corresponding to the period matrix of Fermat curve for $g = 6$ and the period matrix of the Fricke curve for $g = 7$. The dimension of the domain of F increases linearly with g, thus it might take more steps for the iteration to find a basin of attraction, but when it does, fast convergence is assured.

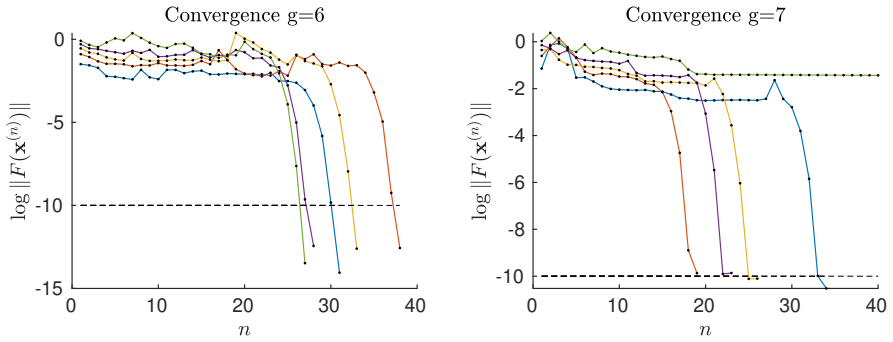

FIGURE 5.6: Residual of the function F in dependence of the n-th iteration.

It is worth mentioning that the convergence is slower if the matrix Ω corresponds to the hyperelliptic example, as we can see in Figure 5.7 for the curve (5.5) with $g = 6$ and $g = 7$. This might be due to the extra symmetries in their matrix elements, which makes the convergence slower. However, these are just special cases amongst all the possible matrices in $\mathbb{H}^g$.

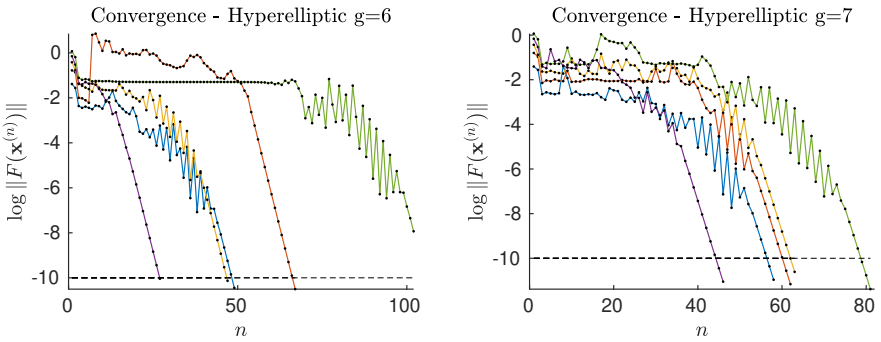

FIGURE 5.7: Residual of the function F in dependence of the n-th iteration.

The computation per step becomes more expensive as g increases since the number of summands in the approximation of every theta function is $(2\mathcal{N}_\delta + 1)^g$. Besides that, we need to compute 2^g even and 6 odd theta functions in each step. This increases the computational time of the whole algorithm. As a reference, the computational time for the tests in Figures 5.1 and 5.6 consisting of 5 iterative processes are

g	time
4	6 s
6	28 min
7	19 h

However, since it suffices finding only one zero, the computations can also be terminated as soon as we find a vector with $\|F(\mathbf{x}^{(n)})\| < \delta$, thus reducing these times. The total computational time of the five iterative processes for the hyperelliptic examples are

g	time
4	14 s
5	98 s
6	56 min
7	30 h

Chapter 6

Ernst equation and stationary axisymmetric spacetimes

In this chapter we present a family of solutions of the Ernst equation in terms of theta functions with characteristics. The proof [KKS04] that they solve the Ernst equation is based on Fay's identity. The Ernst equation is particularly important in general relativity, since it is equivalent to the Einstein field equations on a stationary axisymmetric vacuum spacetime. We briefly present the astrophysical importance of solutions of this type, since it models rotating black holes, such as the one observed for the very first time [EHT19]. We present the Weyl-Lewis-Papapetrou metric, whose coefficients can be obtained via solutions of the Ernst equation. These solutions are obtained on the Jacobian varieties of real hyperelliptic curves and they are given in terms of theta functions. Then we discuss how to obtain the metric coefficients from the Ernst solutions in the particular case when they are constructed on elliptic curves.

The chapter is organized as follows. In Section 6.1 we show the physical importance of stationary axisymmetric spacetimes. In Section 6.2 we introduce the Ernst equation and how its solutions provide the metric functions. In Section 6.3 we introduce a special type of hyperelliptic curves for its use in the solution of the Ernst equation. In Section 6.4 we show a family of solutions of the Ernst equation in terms of theta functions on hyperelliptic curves. In Section 6.5 we discuss the special case of the solutions on elliptic curves.

6.1 Stationary axisymmetric vacuum spacetimes in nature

The Einstein field equations relate the geometry of a curved spacetime with the distribution of matter. Recall that a spacetime is the pair $(\mathcal{M}, \mathbf{g})$, where $\mathcal{M}$ is a four-dimensional differentiable manifold with a Lorentzian metric $\mathbf{g}$, namely a metric whose corresponding quadratic form is symmetric and has 1 negative and 3 positive eigenvalues, whe say that it has signature $(-1, +1, +1, +1)$ in this case.

The metric components $g_{\mu\nu}$ describing the curvature of the spacetime must satisfy Einstein field equations

$$R_{\mu\nu} - \frac{1}{2} R g_{\mu\nu} = 8\pi \frac{G}{c^4} T_{\mu\nu}, \tag{6.1}$$

where $R_{\mu\nu}$ is the Ricci tensor, R is the scalar curvature, $g_{\mu\nu}$ is the metric tensor, G is the gravitational constant, c is the speed of light and $T_{\mu\nu}$ is the stress-energy tensor, see [MTW73; Wal84; Har03] for the precise definition of these tensors and further

discussions. We will not show them here since we are interested in a different approach rather than solving the equations (6.1) in an explicit manner. However, we recall some of the results that have been obtained in this way. The Minkowski metric, whose line element $ds^2 = \sum_{\mu\nu} g_{\mu\nu} dx^\mu dx^\nu$ in Cartesian coordinates is

$$ds^2 = -dt^2 + dx^2 + dy^2 + dz^2, \tag{6.2}$$

is a trivial solution, since it models a flat spacetime (absence of gravity) in vacuum. Vacuum spacetime means that $T_{\mu\nu} = 0$, so (6.1) reduces to $R_{\mu\nu} = 0$. The first non-trivial solution of the Einstein equations was found in 1916 by Karl Schwarzschild, corresponding to a static spherically symmetric vacuum spacetime,

$$ds^2 = \left(1 - \frac{2m}{r}\right) dt^2 + \left(1 - \frac{2m}{r}\right)^{-1} dr^2 + r^2 d\theta^2 + r^2 \sin^2\theta d\phi^2. \tag{6.3}$$

This solution reduces to (6.2) in spherical coordinates when $m = 0$, and it is asymptotically flat, i.e., it tends to the Minkowski metric when $r \to \infty$. The first stationary axisymmetric solution of the Einstein equations was found almost half a century later by Roy Kerr (see [Ker63]). The line element of the Kerr metric in the Boyer-Lindquist coordinates is

$$ds^2 = -\frac{\Delta}{\Sigma^2}\left[dt - a_m \sin^2\theta d\phi\right]^2 + \frac{\sin^2\theta}{\Sigma^2}\left[(r^2 + a_m^2)d\phi - a_m dt\right]^2 + \frac{\Sigma^2}{\Delta} dr^2 + \Sigma^2 d\theta^2, \tag{6.4}$$

with

$$\Delta(r) := r^2 - 2mr + a_m^2 \quad \& \quad \Sigma^2(r,\theta) := r^2 + a_m^2 \cos^2\theta,$$

where $a_m = J/m$ is the angular momentum per unit mass (ranging from 0 to m), m the mass of the spacetime. In the following we will work with physical units, i.e., $c = G = 1$. The expression (6.4) reduces to the Schwarzschild metric in the limiting case $a_m \to 0$ (the case $a_m = m$ is known as the extreme Kerr solution) and it is asymptotically flat as well. The Kerr metric is interpreted as the solution of a rotating black hole. Further discussions about the physical interpretations of (6.4) can be found in [MTW73].

Black holes have been an interesting topic since a long time, but it was originally considered as a mathematical curiosity rather than an actual physical object. However, several observations have proven their existence, such as the stars orbiting around the center of the Milky Way (the supermassive black hole Sagittarius A* or SgrA*) and the merging of two black holes that produced the first direct detection of gravitational waves.
In April 2019, the Event Horizon Telescope (EHT) Collaboration made an astounding announcement: they had taken the picture of the shadow of a black hole for the first time, confirming not only that black holes exist but also that the horizon (discussed in Section 7.1.1) is a true physical feature.

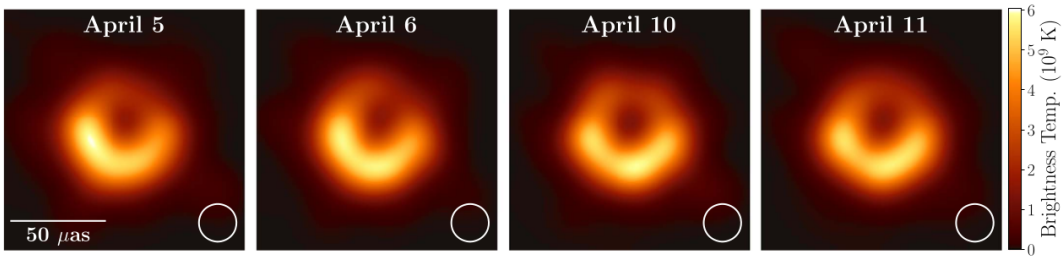

FIGURE 6.1: Pictures of the black hole at the center of the galaxy M87.
Source: [EHT19]

The EHT Collaboration collected data of the black hole at the center of the galaxy M87 in April 2017 and after two years, they published the pictures appearing in Figure 6.1. Among other important tools, the relativistic ray tracing method was used to simulate the visualization of the accretion of matter around a black hole, which we explain in Chapter (7). The axially symmetric solution of the Einstein equations played an important role in those simulations, since black holes are thought to be rotating objects. In fact, the EHT Collaboration [EHT19] tested the observations with different angular momenta and concluded that the non-rotating case is an unlikely situation, showing the importance of the Kerr metric and more importantly for us, the potential physical relevance of other stationary axisymmetric spacetimes.

6.2 Weyl-Lewis-Papapetrou metric

It is convenient to work in the Weyl-Lewis-Papapetrou coordinates since the Einstein field equations in vacuum $R_{\mu\nu} = 0$ reduce to the Ernst equation (see [Ern68; KR05]) when time and axial symmetries are assumed.

The relation with the Cartesian coordinates is just

$$t = t, \quad \rho = \sqrt{x^2 + y^2}, \tag{6.5a}$$

$$\zeta = z, \quad \phi = \arctan(y/x). \tag{6.5b}$$

The line element in this coordinate system can be expressed in the form

$$ds^2 = -f(dt + ad\phi)^2 + \frac{1}{f}\left[e^{2k}(d\rho^2 + d\zeta^2) + \rho^2 d\phi^2\right], \tag{6.6}$$

where $f = f(\rho, \zeta)$, $a = a(\rho, \zeta)$ and $k = k(\rho, \zeta)$. The Ernst equation is

$$\Re(\mathcal{E})\Delta\mathcal{E} = (\nabla\mathcal{E})^2, \tag{6.7}$$

where the Laplacian Δ and the gradient ∇ are the usual operators in cylindrical coordinates. Namely,

$$(\mathcal{E} + \overline{\mathcal{E}})\left[\mathcal{E}_{\zeta\zeta} + \rho^{-1}\mathcal{E}_\rho + \mathcal{E}_{\rho\rho}\right] = 2(\mathcal{E}_\rho^2 + \mathcal{E}_\zeta^2), \tag{6.8}$$

where the solution $\mathcal{E}$ is known as the Ernst potential. The metric coefficients are related to the Erst potential with the relation $f = \Re(\mathcal{E})$ and the line integration of

$$a_\xi = 2\rho \frac{(\mathcal{E} - \overline{\mathcal{E}})_\xi}{(\mathcal{E} + \overline{\mathcal{E}})^2}, \quad k_\xi = 2\mathrm{i}\rho \frac{\mathcal{E}_\xi \mathcal{E}_{\bar{\xi}}}{(\mathcal{E} + \overline{\mathcal{E}})^2}, \tag{6.9}$$

where $\xi = \zeta + \mathrm{i}\rho$. Thus, rather than solving the field equation (6.1) directly, we will be interested in the Ernst equation and then constructing the metric coefficients via (6.9). Such integrals are not trivial as we will see later, but they can be treated analytically for some specific cases or numerically in general.

6.2.1 Complex form of the Ernst equation

We will also be interested in the complex form of the Ernst equation. Considering $\xi = \zeta + i\rho$, the equation (6.7) translates to

$$(\mathcal{E} + \overline{\mathcal{E}}) \left(\mathcal{E}_{\xi\bar{\xi}} - \frac{1}{2(\bar{\xi} - \xi)} \left(\mathcal{E}_{\bar{\xi}} - \mathcal{E}_\xi \right) \right) = 2\mathcal{E}_\xi \mathcal{E}_{\bar{\xi}}, \tag{6.10}$$

Thus, $\mathcal{E}$ depends on $\xi, \bar{\xi}$. The metric coefficients are constructed via $f = \Re(\mathcal{E})$ and the line integration of

$$a_\xi = (\xi + \bar{\xi}) \frac{(\mathcal{E} - \overline{\mathcal{E}})_\xi}{(\mathcal{E} + \overline{\mathcal{E}})^2}, \quad k_\xi = (\xi - \bar{\xi}) \frac{\mathcal{E}_\xi \mathcal{E}_{\bar{\xi}}}{(\mathcal{E} + \overline{\mathcal{E}})^2}. \tag{6.11}$$

6.3 Hyperelliptic curves

It is known that algebraic curves including points at infinity (i.e. projective curves) define compact Riemann surfaces. Thus everything we introduced in Section 2 applies here.

The period matrix $\mathbb{B}$ of an algebraic curve $\mathcal{L}$ is defined as the matrix with components $\mathbb{B}_{jk} = \int_{b_j} \omega_j$, where $\{a_1, b_1, ..., a_g, b_g\}$ is a canonical basis of the first homology group, and $\{\omega_1, ..., \omega_g\}$ is a basis of holomorphic differentials normalized with respect to the a_j cycles, i.e., $\int_{a_j} \omega_k = \delta_{jk}$. The cycles are usually taken as curves on the multi-sheeted coverings of the complex plane. Then, $\mathbb{B}$ is complex symmetric matrix with positive definite imaginary part and defines a Jacobian variety $\mathrm{Jac}(\mathcal{L}) = \mathbb{C}^g / \Lambda$ with lattice $\Lambda = \mathbb{Z}^g + \mathbb{B}\mathbb{Z}^g$.

A curve $\mathcal{L}$ is mapped into $\mathbb{C}^g$ through the Abel map $\alpha : p \mapsto \int_{p_0}^p \omega$, for a base point $p_0 \in \mathcal{L}$. Although $\alpha(p)$ depends on the path, it is unique in $\mathbb{C}^g$ modulo Λ. For simplicity, we use the notation $\int_{p_1}^{p_2} := \alpha(p_2) - \alpha(p_1)$. Notice that the difference is independent of the base point p_0.

In particular, let us consider the family of hyperelliptic curves parametrized by $\xi \in \mathbb{C}$ via the assignment $\xi \to \mathcal{L}_\xi$,

$$\mathcal{L}_\xi = \{(x, y) \in \mathbb{C}^2 | y^2 = (x - \xi)(x - \bar{\xi}) \prod_{j=1}^{g} (x - E_j)(x - F_j)\}. \tag{6.12}$$

In order to satisfy the connectedness condition of a Riemann surface, the branch points $E_j, F_j \in \mathbb{C}$ must not repeat. Additionaly, we will only be considering real hyperelliptic curves, i.e., curves whose branch points satisfy $E_j = \bar{F}_j$ or $E_j, F_j \in \mathbb{R}$.

We consider the following choice of cycles: a_j are the cycles encircling the branch cuts $[E_j, F_j]$ in clockwise direction and b_j are those going from $[E_j, F_j]$ to $[\xi, \bar{\xi}]$ on the $+$-sheet (as shown in Figure 6.2). In the following, the $\pm$ scripts indicate whether we are considering the $+$ or $-$ covering sheet of $\mathcal{L}_\xi$ as fixed at some base point.

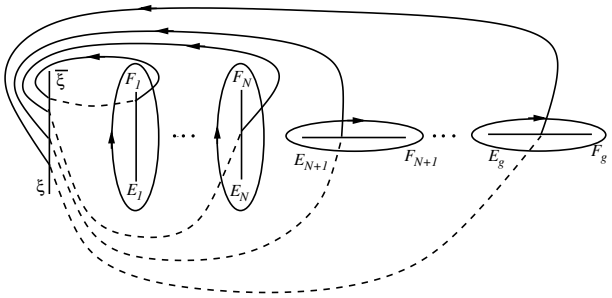

FIGURE 6.2: Choice of cycles.

6.3.1 Theta functions on hyperelliptic curves

Unlike the definition in Chapter 2, we consider the multidimensional theta function

$$\vartheta\left[\begin{smallmatrix}\mathrm{p}\\ \mathrm{q}\end{smallmatrix}\right](\mathbf{z}, \mathbb{B}) := \sum_{\mathbf{n}\in\mathbb{Z}^g} \exp\left(\pi\mathrm{i}\langle \mathbf{n}+\mathrm{p}, \mathbb{B}(\mathbf{n}+\mathrm{p})\rangle + 2\pi\mathrm{i}\langle \mathbf{n}+\mathrm{p}, \mathbf{z}+\mathrm{q}\rangle\right), \tag{6.13}$$

with characteristics $\mathrm{p} \in \mathbb{R}^g$ and $\mathrm{q} \in \mathbb{C}^g$. The function $\vartheta\left[\begin{smallmatrix}\mathrm{p}\\ \mathrm{q}\end{smallmatrix}\right]$ is still an entire function in $\mathbb{C}^g$ with such characteristics. The matrices $\mathbb{B}$ will be the period matrices of the hyperelliptic curves (6.12). This curve will be purely imaginary in the special case where $E_j = \bar{F}_j$ for all $j = 1, \ldots, g$. The quasi-periodicity property we will be using is

$$\vartheta\left[\begin{smallmatrix}\mathrm{p}\\ \mathrm{q}\end{smallmatrix}\right](\mathbf{z}+\mathbf{m}, \mathbb{B}) = e^{2\pi\mathrm{i}\langle \mathrm{p}, \mathbf{m}\rangle}\vartheta\left[\begin{smallmatrix}\mathrm{p}\\ \mathrm{q}\end{smallmatrix}\right](\mathbf{z}, \mathbb{B}), \tag{6.14}$$

where $\mathbf{m} \in \mathbb{Z}^g$ is a lattice vector. The theta function on $\mathcal{L}$ is given by

$$\begin{aligned}\vartheta : \mathcal{L} &\to \mathbb{C},\\ P_1 &\mapsto \vartheta\left[\begin{smallmatrix}\mathrm{p}\\ \mathrm{q}\end{smallmatrix}\right](\alpha(P_1) + c, \mathbb{B}),\end{aligned}$$

for some $c \in \mathbb{C}$, where $\alpha(P_1)$ is the Abel map (2.3). Summarizing, to every point $\xi \in \mathbb{C}$, we associate the period matrix $\mathbb{B}_\xi$ of the curve $\mathcal{L}_\xi$, as well as the Abel maps $\int_\xi^{\infty^\pm}$, which enter the arguments of the theta functions.

6.4 Solution of the Ernst equation

In this section, we show that the potential

$$\mathcal{E}(\xi) = e^{-2\pi\mathrm{i}\langle \mathrm{p}, \Re(\int_{\infty^-}^{\infty^+})\rangle}\frac{\vartheta\left[\begin{smallmatrix}\mathrm{p}\\ \mathrm{q}\end{smallmatrix}\right]\left(\int_\xi^{\infty^+}, \mathbb{B}_\xi\right)}{\vartheta\left[\begin{smallmatrix}\mathrm{p}\\ \mathrm{q}\end{smallmatrix}\right]\left(\int_\xi^{\infty^-}, \mathbb{B}_\xi\right)}, \tag{6.15}$$

solves the Ernst equation (6.10) with arbitrary but fixed characteristics $\mathrm{p} \in \mathbb{R}^g$, $\mathrm{q} \in \mathbb{C}^g$ satisfying a "reality condition". We start by expressing the real part of (6.15) in a simple form through Fay's identity, which still holds for theta functions with characteristics by considering the quasi-periodicity properties (2.23).

6.4.1 Real part of the Ernst potential

The following proposition is needed in order to use Fay's identity.

Proposition 6.4.1. *Let $\mathcal{E}(\xi)$ be the potential defined by* (6.15) *with characteristics $\mathrm{p} \in \mathbb{R}^g$, $\mathrm{q} \in \mathbb{C}^g$ satisfying the reality condition*

$$\Re(\mathrm{q} + \mathbb{B}\mathrm{p}) = \frac{1}{2}\mathrm{diag}(\Re(\mathbb{B})). \tag{6.16}$$

Then, its complex conjugate is

$$\overline{\mathcal{E}(\xi)} = e^{-2\pi \mathrm{i}\langle \mathrm{p}, \Re(\int_{\infty^-}^{\infty^+})\rangle} \frac{\vartheta\left[\begin{smallmatrix}\mathrm{p}\\ \mathrm{q}\end{smallmatrix}\right]\left(\int_{\bar{\xi}}^{\infty^+}, \mathbb{B}_\xi\right)}{\vartheta\left[\begin{smallmatrix}\mathrm{p}\\ \mathrm{q}\end{smallmatrix}\right]\left(\int_{\bar{\xi}}^{\infty^-}, \mathbb{B}_\xi\right)}. \tag{6.17}$$

Proof. From the definition (6.13) with $\mathrm{p} \in \mathbb{R}^g$ and $\mathrm{q} \in \mathbb{C}^g$, we see that in general

$$\overline{\vartheta\left[\begin{smallmatrix}\mathrm{p}\\ \mathrm{q}\end{smallmatrix}\right](\mathbf{z}, \mathbb{B})} = \vartheta\left[\begin{smallmatrix}\mathrm{p}\\ \mathrm{q}\end{smallmatrix}\right](-\bar{\mathbf{z}} - 2\Re(\mathrm{q} + \mathbb{B}\mathrm{p}), \mathbb{B} - 2R),$$

for any $\mathbf{z} \in \mathbb{C}^g$ and $\mathbb{B} \in \mathbb{H}^g$, where $R = \Re(\mathbb{B})$. Additionally, if

$$\begin{pmatrix} \mathbb{I}_g & -2R \\ 0 & \mathbb{I}_g \end{pmatrix} \in \mathrm{Sp}(2g, \mathbb{Z}),$$

which is the case for the curves we are interested in, then $\mathbb{B} - 2R$ is symplectically equivalent to $\mathbb{B}$. The latter is equivalent to the conditions: $2\Re(\mathbb{B}) \in M_{g\times g}(\mathbb{Z})$ and $\Re(\mathbb{B}) = \Re(\mathbb{B})^\top$. Thus, using the modular transformation of theta functions, we obtain

$$\overline{\vartheta\left[\begin{smallmatrix}\mathrm{p}\\ \mathrm{q}\end{smallmatrix}\right](\mathbf{z}, \mathbb{B})} = c \cdot \vartheta\left[\begin{smallmatrix}\mathrm{p}\\ \mathrm{q}\end{smallmatrix}\right](-\bar{\mathbf{z}} - 2\Re(\mathrm{q} + \mathbb{B}\mathrm{p}) + \mathrm{diag}(R), \mathbb{B}).$$

for all $\mathbf{z} \in \mathbb{C}^g$ and for some constant $c \in \mathbb{C}$ independent of $\mathbf{z}$. The conditions on $\Re(\mathbb{B})$ are satisfied by the period matrices $\mathbb{B}_\xi$ of hyperelliptic curves of the form (6.12) with the choice of cycles mentioned above (see [Bel+94]). Moreover, with the condition (6.16), we get

$$\overline{\vartheta\left[\begin{smallmatrix}\mathrm{p}\\ \mathrm{q}\end{smallmatrix}\right](\mathbf{z}, \mathbb{B}_\xi)} = c \cdot \vartheta\left[\begin{smallmatrix}\mathrm{p}\\ \mathrm{q}\end{smallmatrix}\right](-\bar{\mathbf{z}}, \mathbb{B}_\xi).$$

The next step is expressing the complex conjugate $\overline{\int_\xi^{\infty^\pm}}$ in terms of the Abel map of $\bar{\xi}$. Notice that $\bar{\mathbf{z}} = 2\Re(\mathbf{z}) - \mathbf{z}$ for any $\mathbf{z} \in \mathbb{C}^g$, then

$$\overline{\int_\xi^{\infty^\pm}} = 2\Re\left(\int_\xi^{\infty^\pm}\right) - \int_\xi^{\infty^\pm} - \int_{\bar{\xi}}^{\xi} + \int_{\bar{\xi}}^{\xi} = 2\Re\left(\int_\xi^{\infty^\pm}\right) + \int_{\bar{\xi}}^{\xi} - \int_{\bar{\xi}}^{\infty^\pm}.$$

With the homology basis shown in Figure 6.2, it is known that $2\Re\left(\int_\xi^{\infty^\pm}\right) = \pm\frac{1}{2}\sum_j A_j = \pm\int_{\bar\xi}^{\xi}$ (see [Bel+94]), namely, a half-lattice vector. Thus,

$$\overline{\int_\xi^{\infty^+}} = 2\int_{\bar\xi}^{\xi} - \int_{\bar\xi}^{\infty^+}, \quad \overline{\int_\xi^{\infty^-}} = -\int_{\bar\xi}^{\infty^-}.$$

Considering the property (6.14) and the fact that $2\Re\left(\int_{\infty^-}^{\infty^+}\right) = 2\int_{\bar\xi}^{\xi}$ is a lattice vector, we obtain

$$\begin{aligned}\overline{\mathcal{E}(\xi)} &= e^{2\pi i\langle \mathrm{p},\Re(\int_{\infty^-}^{\infty^+})\rangle}\frac{\vartheta\left[\begin{smallmatrix}\mathrm{p}\\ \mathrm{q}\end{smallmatrix}\right]\left(\int_{\bar\xi}^{\infty^+} - 2\Re(\int_{\infty^-}^{\infty^+}), \mathbb{B}_{\bar\xi}\right)}{\vartheta\left[\begin{smallmatrix}\mathrm{p}\\ \mathrm{q}\end{smallmatrix}\right]\left(\int_{\bar\xi}^{\infty^-}\right), \mathbb{B}_{\bar\xi}}, \\ &= e^{2\pi i\langle \mathrm{p},\Re(\int_{\infty^-}^{\infty^+}\rangle} e^{-2\pi i\langle \mathrm{p},2\Re(\int_{\infty^-}^{\infty^+})\rangle}\frac{\vartheta\left[\begin{smallmatrix}\mathrm{p}\\ \mathrm{q}\end{smallmatrix}\right]\left(\int_{\bar\xi}^{\infty^+}, \mathbb{B}_{\bar\xi}\right)}{\vartheta\left[\begin{smallmatrix}\mathrm{p}\\ \mathrm{q}\end{smallmatrix}\right]\left(\int_{\bar\xi}^{\infty^-}, \mathbb{B}_{\bar\xi}\right)}.\end{aligned}$$

□

This implies that $\mathcal{E}(\xi) + \overline{\mathcal{E}(\xi)}$ can be simplified with Fay's identity. First, notice that

$$\mathcal{E}(\xi) + \overline{\mathcal{E}(\xi)} = e^{-2\pi i\langle \mathrm{p},\Re(\int_{\infty^-}^{\infty^+})\rangle}\left[\frac{\vartheta\left[\begin{smallmatrix}\mathrm{p}\\ \mathrm{q}\end{smallmatrix}\right](\int_\xi^{\infty^+})\vartheta\left[\begin{smallmatrix}\mathrm{p}\\ \mathrm{q}\end{smallmatrix}\right](\int_{\bar\xi}^{\infty^-}) + \vartheta\left[\begin{smallmatrix}\mathrm{p}\\ \mathrm{q}\end{smallmatrix}\right](\int_{\bar\xi}^{\infty^+})\vartheta\left[\begin{smallmatrix}\mathrm{p}\\ \mathrm{q}\end{smallmatrix}\right](\int_\xi^{\infty^-})}{\vartheta\left[\begin{smallmatrix}\mathrm{p}\\ \mathrm{q}\end{smallmatrix}\right](\int_\xi^{\infty^-})\vartheta\left[\begin{smallmatrix}\mathrm{p}\\ \mathrm{q}\end{smallmatrix}\right](\int_{\bar\xi)}^{\infty^-}}\right],$$

and considering Fay's identity (3.1) with $z = 0$, $a = \xi$, $b = \bar\xi$, $c = \infty^-$, $d = \infty^+$; the lemma

$$\frac{E(\infty^-,\xi)E(\infty^+,\bar\xi)}{E(\infty^-,\bar\xi)E(\xi,\infty^+)}) = 1,$$

which is proved in [KKS04]; and the property $E(x,y) = -E(y,x)$ of the prime forms, we obtain

$$\begin{aligned}&\vartheta\left[\begin{smallmatrix}\mathrm{p}\\ \mathrm{q}\end{smallmatrix}\right](\int_\xi^{\infty^+})\vartheta\left[\begin{smallmatrix}\mathrm{p}\\ \mathrm{q}\end{smallmatrix}\right](\int_{\bar\xi}^{\infty^-}) + \vartheta\left[\begin{smallmatrix}\mathrm{p}\\ \mathrm{q}\end{smallmatrix}\right](\int_{\bar\xi}^{\infty^+})\vartheta\left[\begin{smallmatrix}\mathrm{p}\\ \mathrm{q}\end{smallmatrix}\right](\int_\xi^{\infty^-}) = \\ &\quad\frac{E(\infty^-,\infty^+)E(\xi,\bar\xi)}{E(\xi,\infty^-)E(\bar\xi,\infty^+)}\vartheta\left[\begin{smallmatrix}\mathrm{p}\\ \mathrm{q}\end{smallmatrix}\right](0)\vartheta\left[\begin{smallmatrix}\mathrm{p}\\ \mathrm{q}\end{smallmatrix}\right](\int_\xi^{\infty^+} + \int_{\bar\xi}^{\infty^-}).\end{aligned}$$

Thus, the real part of the Ernst potential is

$$\Re(\mathcal{E}(\xi)) = e^{-2\pi i\langle \mathrm{p},\Re(\int_{\infty^-}^{\infty^+})\rangle}Q\frac{\vartheta\left[\begin{smallmatrix}\mathrm{p}\\ \mathrm{q}\end{smallmatrix}\right](0)\vartheta\left[\begin{smallmatrix}\mathrm{p}\\ \mathrm{q}\end{smallmatrix}\right](\int_{\bar\xi}^{\xi})}{\vartheta\left[\begin{smallmatrix}\mathrm{p}\\ \mathrm{q}\end{smallmatrix}\right](\int_\xi^{\infty^-})\vartheta\left[\begin{smallmatrix}\mathrm{p}\\ \mathrm{q}\end{smallmatrix}\right](\int_{\bar\xi}^{\infty^-})}, \tag{6.18}$$

where

$$Q = Q(\xi,\bar\xi) = \frac{1}{2}\frac{E(\infty^-,\infty^+)E(\xi,\bar\xi)}{E(\xi,\infty^-)E(\bar\xi,\infty^+)} = \frac{\Theta(\int_\xi^{\infty^-})\Theta(\int_{\bar\xi}^{\infty^-})}{\Theta(0)\Theta(\int_\xi^{\bar\xi})}.$$

The latter equality is obtained from the fact that $\mathcal{E}(\xi) \equiv 1$ if $\mathrm{p},\mathrm{q} = 0$.

6.4.2 Solution to the Ernst equation

An equivalent form of the Ernst equation is given by

$$(\mathcal{E}+\overline{\mathcal{E}})\Delta\mathcal{E} = 8\mathcal{E}_{\xi}\mathcal{E}_{\bar{\xi}}. \tag{6.19}$$

As mentioned above, $\Re(\int_{\infty^-}^{\infty^+})$ is independent of ξ and $\bar{\xi}$ if the homology basis is chosen appropriately, such as the choice in Figure 6.2. Thus, the derivatives $\mathcal{E}_{\xi}$, $\mathcal{E}_{\bar{\xi}}$ and the Laplacian $\Delta\mathcal{E}$ are just those shown in [KKS04] multiplied by an exponential factor. Namely,

$$\mathcal{E}_{\xi} = \frac{c_2(\infty^-,\xi,\infty^+)}{2} e^{-2\pi i\langle \mathrm{p},\Re(\int_{\infty^-}^{\infty^+})\rangle} \frac{\vartheta\left[\begin{smallmatrix}\mathrm{p}\\ \mathrm{q}\end{smallmatrix}\right](0)}{\vartheta\left[\begin{smallmatrix}\mathrm{p}\\ \mathrm{q}\end{smallmatrix}\right]^2(\int_{\xi}^{\infty^-})} D_{\xi}\vartheta\left[\begin{smallmatrix}\mathrm{p}\\ \mathrm{q}\end{smallmatrix}\right](0),$$

$$\mathcal{E}_{\bar{\xi}} = \frac{c_2(\infty^-,\bar{\xi},\infty^+)}{2} e^{-2\pi i\langle \mathrm{p},\Re(\int_{\infty^-}^{\infty^+})\rangle} \frac{\vartheta\left[\begin{smallmatrix}\mathrm{p}\\ \mathrm{q}\end{smallmatrix}\right](\int_{\bar{\xi}}^{\xi})}{\vartheta\left[\begin{smallmatrix}\mathrm{p}\\ \mathrm{q}\end{smallmatrix}\right]^2(\int_{\xi}^{\infty^-})} D_{\bar{\xi}}\vartheta\left[\begin{smallmatrix}\mathrm{p}\\ \mathrm{q}\end{smallmatrix}\right](\int_{\xi}^{\bar{\xi}}),$$

$$\Delta\mathcal{E} = -\frac{(c_2(\infty^-,\xi,\infty^+))^2}{Q} e^{-2\pi i\langle \mathrm{p},\Re(\int_{\infty^-}^{\infty^+})\rangle} \frac{\vartheta\left[\begin{smallmatrix}\mathrm{p}\\ \mathrm{q}\end{smallmatrix}\right](\int_{\bar{\xi}}^{\infty^-})}{\vartheta\left[\begin{smallmatrix}\mathrm{p}\\ \mathrm{q}\end{smallmatrix}\right]^3(\int_{\xi}^{\infty^-})} D_{\bar{\xi}}\vartheta\left[\begin{smallmatrix}\mathrm{p}\\ \mathrm{q}\end{smallmatrix}\right](\int_{\xi}^{\bar{\xi}}) D_{\xi}\vartheta\left[\begin{smallmatrix}\mathrm{p}\\ \mathrm{q}\end{smallmatrix}\right](0),$$

where the coefficient $c_2(\infty^-,\xi,\infty^+)$ is a function defined in terms of prime forms. Thus, the Ernst equation (6.19) is solved by the potential (6.15) for all $\mathrm{p}\in\mathbb{R}^g$, $\mathrm{q}\in\mathbb{C}^g$ satisfying $\Re(\mathrm{q}+\mathbb{B}\mathrm{q}) = \frac{1}{2}\mathrm{diag}(\Re(\mathbb{B}))$.

Remark 6.4.2. *The class of solutions* (6.15) *is equivalent to*

$$\mathcal{E}(\xi) = e^{-2\pi i\langle \mathrm{p},\Re(\int_{\infty^-}^{\infty^+})\rangle} \frac{\vartheta\left[\begin{smallmatrix}\mathrm{p}\\ \mathrm{q}\end{smallmatrix}\right]\left(\int_{\xi}^{\infty^+}+\frac{1}{2}\Delta,\mathbb{B}_{\xi}\right)}{\vartheta\left[\begin{smallmatrix}\mathrm{p}\\ \mathrm{q}\end{smallmatrix}\right]\left(\int_{\xi}^{\infty^-}+\frac{1}{2}\Delta,\mathbb{B}_{\xi}\right)}, \tag{6.20}$$

for all $\mathrm{q}\in\mathbb{R}$, $\mathrm{q}\in\mathbb{C}^g$ *subject to the reality condition* $\Re(\mathrm{q}+\mathbb{B}\mathrm{q}) = 0$, *where* $\Delta = \mathrm{diag}(\Re(\mathbb{B}))$, *which is independent of* ξ *and* $\bar{\xi}$.

6.5 Discussion of the elliptic case

In this section we are going to discuss the computation of the period matrices, the Abel maps and other necessary quantities for the elliptic case, as well as the calculation on some specific regions, see [Kor91] for other discussions (we use σ instead of α to avoid confusion with the Abel map we use throughout the thesis). The objective is to use them as a testbed for future purely numerical computations, but first we will look at its ergosphere (see Chapter 7 for further descriptions of this hypersurface).

Let us consider the special case $y^2 = (x-\xi)(x-\bar{\xi})(x-E)(x-\bar{E})$, with $E\in\mathbb{H}$ and $\xi = \zeta+\mathrm{i}\rho$. Without loss of generality, let $E = ia$. Let us consider the Ernst potential with $\mathrm{p}=0$ and $\mathrm{q}=\mathrm{i}\sigma$, for some $\sigma\in\mathbb{R}$,

$$\mathcal{E} = \frac{\vartheta(\int_{\xi}^{\infty^+}-i\sigma)}{\vartheta(\int_{\xi}^{\infty^+}+i\sigma)}. \tag{6.21}$$

Thus, its real part is

$$\Re(\mathcal{E}) = Q\frac{\vartheta(i\sigma)\vartheta(\int_{\bar{\xi}}^{\xi} + i\sigma)}{\vartheta(\int_{\xi}^{\infty^+} + i\sigma)\vartheta(\int_{\bar{\xi}}^{\infty^+} + i\sigma)} = Q\frac{\vartheta(i\sigma)\vartheta(1/2 + i\sigma)}{\vartheta(\int_{\xi}^{\infty^+} + i\sigma)\vartheta(\int_{\xi}^{\infty^+} + i\sigma + 1/2)},$$

with

$$Q = \frac{\vartheta(\int_{\xi}^{\infty})\vartheta(\int_{\bar{\xi}}^{\infty})}{\vartheta(0)\vartheta(\int_{\bar{\xi}}^{\xi})} = \frac{\vartheta(\int_{\xi}^{\infty^+})\vartheta(\int_{\xi}^{\infty^+} + 1/2)}{\vartheta(0)\vartheta(1/2)}.$$

6.5.1 Ergospheres

The zero of Riemann theta function for a fixed $\mathbb{B}$ is located at $z_0 = 1/2 + \mathbb{B}/2$. Thus ergosphere of the the spacetime defined by (6.21) is given by the zero locus of $\vartheta(\sigma + 1/2, \mathbb{B})$, since the other theta functions do not vanish. Thus,

$$\Re(\mathcal{E}) = 0 \quad \Leftrightarrow \quad \mathbb{B}_n = \frac{2\sigma}{2n-1},$$

for some $n \in \mathbb{N}$. This implies that σ must be positive in order for an ergosphere to exist.

Since the spacetime is axisymmetric, the ergospheres have toroidal shapes, as we can see in Figure 6.3. The radius of the tube goes to zeros as σ decreases, the limiting case being a ring.

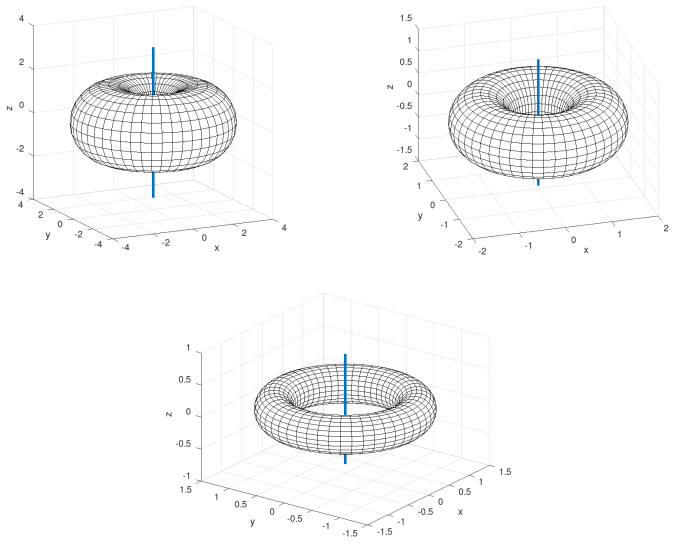

FIGURE 6.3: Three-dimensional representation of the outer ergospheres for different σ.

For the numerical study of this spacetime, we can simulate the picture of this ergosphere in the same way we do the simulations in Section 7.

Analytical values

Recall that any elliptic curve $y^2 = (x-a)(x-b)(x-c)(x-d)$ is equivalent to $y^2 = x(x-1)(x-\lambda)$, which is known as the Legendre form of elliptic curves with parameter $\lambda \in \mathbb{P}$. This parameter is obtained by $\lambda = \frac{(c-a)(b-d)}{(b-a)(c-d)}$, see for instance [Sil09].

Thus, all the curves yielding the same λ are equivalent and therefore have the same period matrix Ω. Notice that the definition of λ depends on the order of the points and the image of the cross-ratio map is $\mathbb{P}\backslash\{0,1,\infty\}$. Upon permutation, we obtain the following equivalent cross-ratios λ, $1-\lambda$, $\frac{1}{\lambda}$, $\frac{\lambda-1}{\lambda}$, $\frac{1}{1-\lambda}$, $\frac{\lambda}{\lambda-1}$.

Considering the order $\xi, \bar{\xi}, E, \bar{E}$ for the points defining the elliptic curves we are interested in, we obtain

$$\begin{aligned}\lambda &= \frac{(E-\xi)(\bar{\xi}-\bar{E})}{(\bar{\xi}-\xi)(E-\bar{E})},\\ &= \frac{(z+i\rho-ia)(z-i\rho+ia)}{(2i\rho)(2ia)} = \frac{\|z+i(\rho-a)\|^2}{-4a\rho},\end{aligned}$$

from this, we observe that the set of points satisfying the following equation define the same λ and thus the same $\mathbb{B}$.

$$\zeta^2 + (\rho-\rho_0)^2 = R^2, \tag{6.22}$$

with $\rho_0 = a(1-2\lambda)$ and $R^2 = 4a^2(\lambda^2-\lambda)$, where R is the radius of the tube of the torus in Figure 6.3.
Notice that $\lambda \in \mathbb{R}$. Moreover $\lambda \leq 0$, since we defined a, ρ to be non-negative. This in turn implies that $\rho_0 \geq a$ and $R \geq 0$.

In order to compare the numerical and analytical results, let us consider the map

$$\lambda_0(\mathbb{B}) = \frac{\vartheta_2^4(\mathbb{B})}{\vartheta_3^4(\mathbb{B})},$$

where $\vartheta_2(\Omega) = \vartheta\left[\begin{smallmatrix}1/2\\0\end{smallmatrix}\right](0,\Omega)$ and $\vartheta_3(\Omega) = \vartheta\left[\begin{smallmatrix}0\\0\end{smallmatrix}\right](0,\Omega)$. In terms of the previously defined λ we have $\lambda_0 = (\lambda-1)/\lambda$, thus

$$\lambda(\mathbb{B}) = \frac{\vartheta_3^4(\mathbb{B})}{\vartheta_3^4(\mathbb{B}) - \vartheta_2^4(\mathbb{B})}. \tag{6.23}$$

With this we can see the radius of the n-th ergosphere is

$$R_n = 2a\sqrt{\lambda(\mathbb{B}_n)^2 - \lambda(\mathbb{B}_n)} \tag{6.24}$$

However, this radius decreases exponentially with n, thus in practice we will only observe the first ergospheres.

6.5.2 Explicit computations for elliptic solution

For the computation of the Abel maps, period matrices and other necessary values, we can use standard theory of elliptic curves [Sil09]. We use the cut-system 6.2. Let us denote the points $P_4 = \bar{P}_2 = \xi$, $P_3 = \bar{E}$ and $P_1 = E$. Writing the differential of the

first kind as $\omega = Adx/y$ we get the normalization factor

$$1 = 2A \int_{P_3}^{P_1} \frac{dx}{y}, \tag{6.25}$$

and with the transformation (this transformation is invertible if the K_i do not coincide)

$$t = \frac{(K_1 - K_2)(x - K_3)}{(K_1 - K_3)(x - K_2)}, \quad x - K_2 = \frac{(K_2 - K_3)(K_1 - K_2)}{(K_1 - K_3)t - (K_1 - K_2)}, \tag{6.26}$$

the integral is brought into normal form

$$1 = -\frac{A}{\sqrt{(K_1 - K_2)(K_4 - K_3)}} \int_0^1 \frac{dt}{\sqrt{t(1-t)(1-k^2t)}}, \tag{6.27}$$

for $K_3 = F$, $K_1 = E$, $K_4 = \xi$ and $K_2 = \bar{\xi}$, and with

$$m = k^2 = \frac{(K_4 - K_2)(K_1 - K_3)}{(K_4 - K_3)(K_1 - K_2)} = \frac{(\xi - \bar{x}i)(E - \bar{E})}{(\xi - \bar{E})(E - \bar{\xi})},$$

Thus, k^2 is real (this is $-\lambda$ computed in the previous subsection). Since we assumed that $a > 0$, we have $k \in [0, 1]$. For $\xi = E$, we have $k = 1$. We thus get for the (6.27),

$$A = -\frac{\sqrt{(K_1 - K_2)(K_4 - K_3)}}{2K} = -\frac{\sqrt{(E - \bar{\xi})(\xi - \bar{E})}}{2K}, \tag{6.28}$$

where K is the complete elliptic integral of the first kind. It follows from $\mathbb{B} = -2(\alpha(\bar{E} - \alpha(\bar{\xi}))$ that

$$\mathbb{B} = -\frac{2A}{\sqrt{(K_1 - K_2)(K_4 - K_3)}} \int_0^\infty \frac{dt}{\sqrt{t(1-t)(1-k^2t)}} = \frac{iK'}{K}. \tag{6.29}$$

This is the standard form of the modul of elliptic theta functions. Another quantity of interest is $\alpha(\infty^+)$,

$$\alpha(\infty^+) - \alpha(\xi) = -\frac{A}{\sqrt{(K_1 - K_2)(K_4 - K_3)}} \int_{1/k^2}^{\frac{K_1 - K_2}{K_1 - K_3}} \frac{dt}{t(1-t)(1-k^2t)} = \frac{1}{2K}(\gamma - K - \mathrm{i}K), \tag{6.30}$$

where $\mathrm{sn}^2\gamma = (K_1 - K_2)/(K_1 - K_3) = (E - \bar{\xi})/(E - \bar{E})$. Since $\alpha(\bar{E}) = -(1 + \mathrm{i}K'/K)/2$, we can express the Ernst potential in the form

$$\mathcal{E} = \frac{\vartheta(\alpha(\infty^+) - \alpha(\xi) - \mathrm{i}\sigma)}{\vartheta(\alpha(\infty^+) - \alpha(\xi) + \mathrm{i}\sigma)} = \frac{\vartheta_1(\tilde{\gamma} - \mathrm{i}\sigma)}{\vartheta_1(\tilde{\gamma} + \mathrm{i}\sigma)} e^{-2\pi\mathrm{i}\sigma}, \tag{6.31}$$

where $\vartheta_1(t) = \vartheta\left[\begin{smallmatrix}1/2\\1/2\end{smallmatrix}\right](t)$ is the standard Jacobi theta function and $\tilde{\gamma} = \gamma/(2K)$. The Abel map is chosen such that it has a jump for $\zeta = 0$ and $\rho < \Im(E)$, but is continuous for $\rho > \Im(E)$. This is achieved by adding a b-period to the standard definition of the Abel map for $\rho > \Im(E)$ and $\zeta < 0$.

On the axis it follows from (6.27) that $k = 0$ which implies $K = \pi/2$ whereas K' diverges. Thus $\mathbb{B}$ becomes infinite. However, the quantity γ remains finite and can

be calculated via $\sin^2\gamma = (E-\bar{\xi})/(E-\bar{E})$. Thus,

$$e^{2\mathrm{i}\gamma} = e^{2\pi\mathrm{i}\tilde{\gamma}} = \mathrm{i}\left(-\frac{\zeta}{a} + \sqrt{\left(\frac{\zeta}{a}\right)^2 + 1}\right). \tag{6.32}$$

Notice that $e^{2\mathrm{i}\pi\tilde{\gamma}}$ is purely imaginary in this case. To study the behaviour of the theta quotient it is sufficient to perform the limit $\mathbb{B} \to \infty$ in the theta series if one remembers that (6.38) contains $\mathbb{B}$ too. Notice that the expansion of all quantities in ρ is smooth whereas $\mathbb{B}$ has an expansion of the form $\mathbb{B} = 2\ln\rho + \sum_{n=0}^{\infty} c_n\rho^n$. Thus we get for $\zeta > 0$

$$\mathcal{E} = \frac{1 - e^{2\pi\mathrm{i}\tilde{\gamma}}e^{2\pi\sigma}}{1 - e^{2\pi\mathrm{i}\tilde{\gamma}}e^{-2\pi\sigma}}. \tag{6.33}$$

Considering (6.32) we get

$$f = \Re(\mathcal{E}) = \frac{1 - (e^{2\pi\mathrm{i}\tilde{\gamma}})^2}{1 - (e^{2\pi\mathrm{i}\tilde{\gamma}-2\pi\sigma})^2}. \tag{6.34}$$

From (6.33) we can compute the asymptotic expansion for large ζ,

$$\mathcal{E} = 1 - \frac{\mathrm{i}a}{\zeta}\sinh(2\pi\sigma) + \mathcal{O}(1/\zeta^2), \tag{6.35}$$

from which is deduced that the mass is purely imaginary. For $\zeta < 0$ we get accordingly

$$\mathcal{E} = \frac{1 - e^{-2\pi\mathrm{i}\tilde{\gamma}}e^{-2\pi\sigma}}{1 - e^{-2\pi\mathrm{i}\tilde{\gamma}}e^{-2\pi\sigma}}, \tag{6.36}$$

and thus the same mass as in (6.35) is obtained. With this choice of the Abel map, infinity is a regular point for the Ernst potential. With the formulas $k' = \sqrt{1-k^2}$ and $K'(k) = K = (k')$, it is sufficient to consider only K. For $k \ll 1$ we have

$$K = \frac{\pi}{2}\left(1 + \left(\frac{1}{2}\right)^2 k^2 + \left(\frac{1\cdot 3}{2\cdot 4}\right)^2 k^4 + \ldots\right). \tag{6.37}$$

And for $k' \ll 1$ we have

$$K = \ln\frac{4}{k'} + \left(\frac{1}{2}\right)^2\left(\ln\frac{4}{k'} - \frac{2}{1\cdot 2}\right) + \ldots \tag{6.38}$$

Thus, the only singular term in the expansion of K'/K is $\ln(4/k')$, implying that $\mathbb{B} \to 0$ for $\xi \to E$. For the Ernst potential we get

$$\mathcal{E} \sim \frac{1 + e^{-2\pi\sigma}e^{2\pi\mathrm{i}\tilde{\gamma}}}{1 + e^{2\pi\sigma}e^{2\pi\mathrm{i}\tilde{\gamma}}}, \tag{6.39}$$

where $\tilde{\gamma} = 1/2$ in the limit.

The metric function af follows from

$$(a - a_0)f = D_\infty \ln\frac{\vartheta_3(\sigma(\infty^-) - \sigma(\xi) + \mathrm{i}\sigma)}{\vartheta_4(\sigma(\infty^-) - \sigma(\xi) + \mathrm{i}\sigma)}, \tag{6.40}$$

where $a_0 = const.$ and $\vartheta_4 = \vartheta\left[\begin{smallmatrix} 0 \\ 1/2 \end{smallmatrix}\right]$ is a Jacobi theta function. On the axis we get for $\zeta > a$

$$(a - a_0)f = 2\mathrm{i}\sqrt{\zeta^2 + a^2}\frac{2e^{2\pi\sigma}e^{-2\pi\mathrm{i}\tilde{\gamma}}}{1 - (e^{2\pi\sigma}e^{-2\pi\mathrm{i}\tilde{\gamma}})^2}. \tag{6.41}$$

These values can be used to test the numerical computations in higher genus, since the computations for $g > 1$ are note only more difficult but impractical for the purposes of numerical simulations, since the analytical computation of all these values are less efficient than using purely numerical approaches.

Chapter 7

Ray-tracing in stationary axisymmetric vacuum spacetimes

In this chapter we present some numerical techniques to compute the geodesics in spacetimes whose metric functions are given by locally smooth functions, such as the solutions of the Ernst equation in [Kor88] and [FK01b]. One of the reasons that this type of solutions has not been extensively studied is that their metric coefficients are theta functions and thus their computation is expensive and impractical for simulations that require a large number of evaluations of both the metric coefficients and their derivatives. An example for this is the generation of pictures, which is done by solving the equations of motion of individual photons iteratively. This process is repeated for a large number of photons. Thus an efficient method to compute the derivatives is needed.

We start by studying the Kerr solution constructed from a solution of the Ernst equation as a toy model, which is given by algebraic functions. Thus the computation of its explicit derivatives is straightforward. We are interested in doing simulations using *ray-tracing* techniques, for which we need to solve the initial value problems (IVP) modeling light rays. In these simulations we expect to observe the frame-dragging effect of the rotating black hole. This is observed in the simulation of the picture of one special hypersurface of the black hole known as the ergosphere as well as in the picture of an ideal disk on the equatorial plane of the black hole. The issue we would need to address in order to do numerical simulations in more general spacetimes is the efficient differentiation of the metric functions. This is done by combining two efficient approximation techniques that take advantage of the smoothness of the metric functions. We approximate the derivatives on a grid by using *spectral methods* and then interpolate all the other necessary derivatives for the solution using numerically stable and efficient *barycentric interpolation*.

The chapter is organized as follows. In Section 7.1 we present the Kerr metric in Weyl coordinates, which is obtained through the Ernst equation and discuss some of its important features. In Section 7.2 we discuss how to compute the geodesics in Weyl coordinates. In Section 7.3 we present the ray-tracing technique to simulate pictures in curved spacetimes. In Section 7.4 we show the simulation of the ergosphere and an ideal disk for several parameters of the Kerr solution. In Section 7.5 we introduce a completely numerical approach in order to apply the ray-tracing technique to general solutions of the Ernst equation.

7.1 Kerr's solution

The most prominent solution of the Ernst equation from the physical point of view is the Kerr metric leading to the Ernst potential

$$\mathcal{E} = \frac{e^{-i\varphi} r_+ + e^{i\varphi} r_- - 2m\cos\varphi}{e^{-i\varphi} r_+ + e^{i\varphi} r_- + 2m\cos\varphi}, \tag{7.1}$$

where $r_\pm = \sqrt{(\zeta \pm m\cos\varphi)^2 + \rho^2}$, while m, φ are parameters of the solution. As mentioned in the previous section, it leads to the most important observable phenomenona, since it models rotating black holes.

Physically, m is the mass of the black hole (which is usually normalized to $m = 1$) and φ is a parameter that indicates how fast the black hole spins and takes values $\varphi \in [0, \pi/2]$. The angular momentum of the black hole is $J = m^2 \sin\varphi$. The metric functions f, a and e^{2k} can be obtained explicitly,

$$\begin{aligned} a &= \frac{2m\sin\varphi(1-Y^2)(1+X\cos\varphi)}{\cos^2\varphi X^2 + \sin^2\varphi Y^2 - 1}, \\ f &= \frac{\cos^2\varphi X^2 - 1 + \sin^2\varphi Y^2}{(\cos\varphi X + 1)^2 + \sin^2\varphi Y^2}, \\ e^{2k} &= \frac{m^2}{r_+ r_-}\left[\sin^2\varphi(Y^2-1) + \cos^2\varphi(X^2-1)\right], \end{aligned}$$

where X and Y are

$$X = \frac{r_+ + r_-}{2m\cos\varphi}, \quad Y = \frac{r_+ - r_-}{2m\cos\varphi}.$$

The relation of the variables X and Y with ζ and ρ is given by

$$\begin{aligned} \zeta/(m\cos\varphi) &= XY, \\ \rho/(m\cos\varphi) &= \sqrt{(X^2-1)(1-Y^2)}, \\ r_\pm &= (X \pm Y) m\cos\varphi. \end{aligned}$$

Notice that,

$$h(\rho,\zeta) := \frac{e^{2k}}{f} = \frac{(\cos\varphi X + 1)^2 + \sin^2\varphi Y^2}{(X^2 - Y^2)\cos^2\varphi}, \quad \text{if} \quad f \neq 0. \tag{7.2}$$

The behavior can be inferred by looking at the three-dimensional visualizations of $f(\rho,\zeta)$, $a(\rho,\zeta)$ and $e^{2k}(\rho,\zeta)$. For instance, the metric function g_{03} gives an indication of how fast a test particle would rotate in the vicinity of the black hole; thus a vanishes on the axis and at infinity.

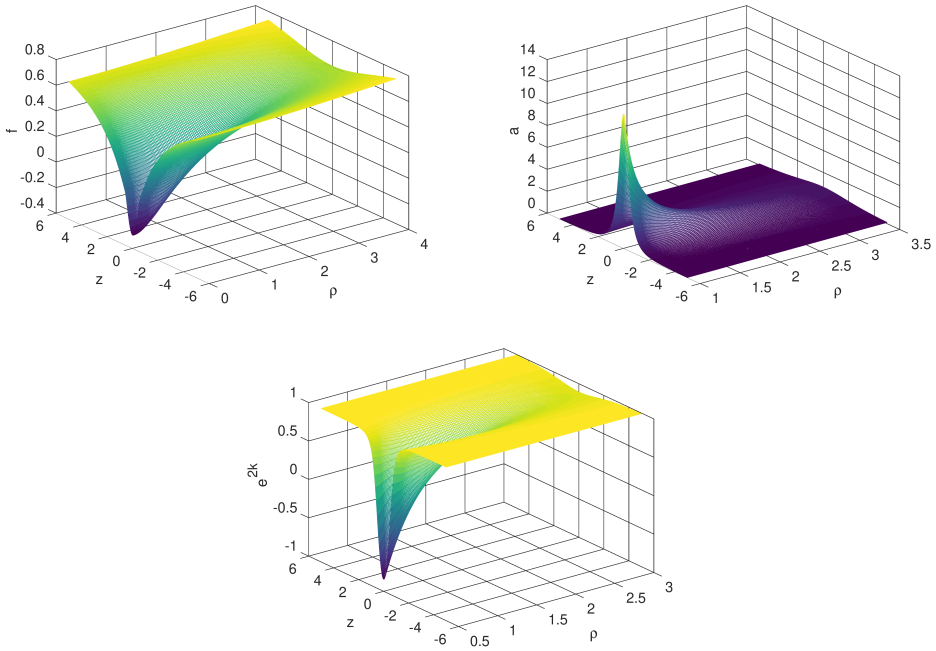

FIGURE 7.1: Three-dimensional plots of $f(\rho,\zeta)$, $a(\rho,\zeta)$ and $e^{2k}(\rho,\zeta)$ corresponding to $\varphi = 1.0$.

7.1.1 Horizon and ergosphere

Two hypersurfaces we are especially interested in are the horizon and the ergosphere. A *horizon* is defined to be a hypersurface whose normal vectors $\mathbf{b}$ are null, namely, $g_{\mu\nu}b^\mu b^\nu = 0$. The horizon turns out to be the region of space where $g_{rr} \to \infty$ in (6.3), which is a coordinate singularity. The Schwarzschild horizon is a spherical shell with radius $r_s = 2m$, known as the Schwarzschild radius. Massive particles and photons can fall inside the horizon, but they can never emerge from it.
The Kerr black hole (6.4) has a horizon as well, which is the ellipsoid described by $r_H = M + \sqrt{M^2 - a^2}$. However, a rotating black hole has another special feature: the ergosphere, which is the region bounded by the horizon and the surface described by $r_E = M + \sqrt{M^2 - a^2\cos^2\theta}$ in the Boyer-Lindquist coordinates. The outer surface of the ergosphere is called static limit, which is defined to be the limit in which an observer could remain static relative to a frame at rest at infinity [MTW73]. Once the observer crosses this limit, it becomes impossible to remain static and it will necessarily co-rotate with the black hole. It is common to refer to the outer surface as the ergosphere and to the inner region as the ergoregion. The section of these special hypersurfaces are shown in Figure 7.2 in the Boyer-Lindquist coordinates. Due to the spacetime we are working with, these surfaces are axially symmetric and they do not change over time.

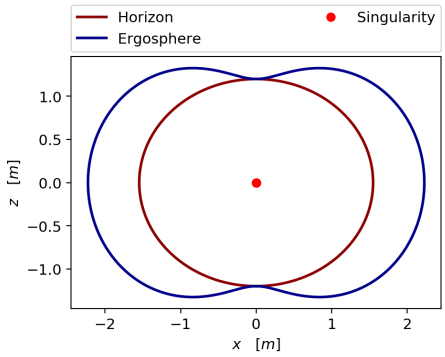

FIGURE 7.2: Special features of a Kerr black hole in the Boyer-Lindquist coordinates.

Horizon in Weyl coordinates

The horizon of the black hole for the metric (6.6) is on the axis, between $\zeta = -m\cos\varphi$ and $\zeta = m\cos\varphi$ (see [KR05]). The values of the metric functions can be computed on the horizon, since $X = 1$ and $Y = \zeta/(m\cos\varphi)$,

$$f = \left(1 - \frac{2}{(1-Y^2)}\cot(\varphi/2)\right)^{-1}$$

$$a = -2m\cot(\varphi/2), \quad e^{2k} = -\tan^2(\varphi).$$

Ergosphere

The static limit is the hypersurface where the time component of the metric vanishes, i.e., $g_{tt} = f = 0$. This is given by the solution of

$$\cos^2\varphi X^2 - 1 + \sin^2\varphi Y^2 = 0.$$

This surface is axially symmetric and its cross section is shown in Figure 7.3. For $\varphi = 0$, the ergosphere is simply a line on the ζ axis, going from $-m$ to m. As φ increases, the radius of the ergosphere at the equator expands and its height decreases, being a sphere when $\varphi = \pi/4$. Finally, if $\varphi \in (\pi/4, \pi/2]$ the ergosphere has the shape of a pumpkin, as we can see in Figure 7.3c.

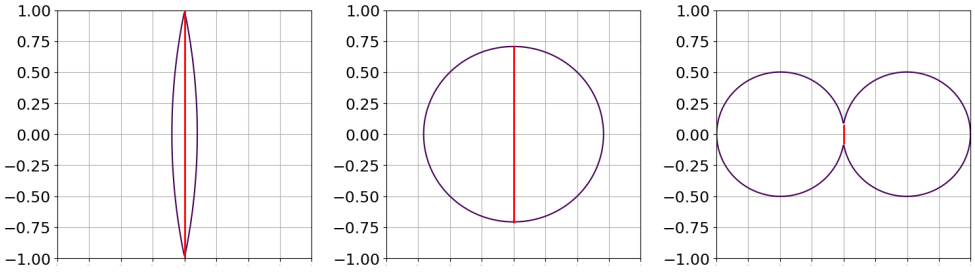

(A) $\varphi = 0.10$ (B) $\varphi = \pi/4$ (C) $\varphi = 1.50$

FIGURE 7.3: Cross section of the ergosphere (purple) and the horizon (red) for different values of the parameter φ. The radius of the ergosphere at the equator is $m \sin \varphi$, then it is bigger if the black hole rotates faster.

As φ increases (and consequently, the angular momentum J of the black hole), the horizon gets smaller and smaller until $\varphi = \pi/2$, the extreme Kerr solution, where it is just a point. In order to have a better visualization of the picture of the ergosphere using ray-tracing techniques, we color them in the following way.

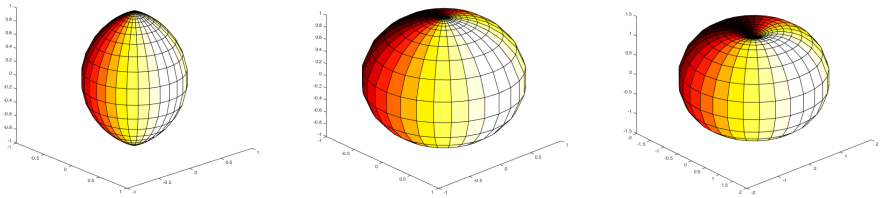

FIGURE 7.4: Three-dimensional representation of the ergospheres with $\varphi < \pi/4$, $\varphi = \pi/4$ and $\varphi > \pi/4$ respectively.

Having $g_{tt} \to 0$ means that the coordinate time goes to infinity as the photon approaches the ergosphere. A stopping criterion we use for the numerical integration is: if $f < \epsilon$ for a small ϵ, then we stop the iteration.

7.2 Equations of motion

The motion of a particle or a photon is governed by the geodesic equation, namely

$$\frac{d^2x^\mu}{ds^2} + \Gamma^\mu_{\alpha\beta}\frac{dx^\alpha}{ds}\frac{dx^\beta}{ds} = 0,$$

where $(x^0, x^1, x^2, x^3) = (t, \rho, \zeta, \phi)$, $\Gamma^\mu_{\alpha\beta}$ are the Christoffel symbols and s is an affine parameter. These equations are obtained using the Euler-Lagrange equations [Wal84]

$$\frac{d}{ds}\frac{\partial \mathfrak{L}}{\partial \dot{x}^\mu} = \frac{\partial \mathfrak{L}}{\partial x^\mu}, \tag{7.3}$$

for the Lagrangian

$$\mathfrak{L} = \frac{1}{2} g_{\mu\nu}\dot{x}^\mu \dot{x}^\nu. \tag{7.4}$$

This quantity gives essentially the rest mass of the test particle, in such a case it is normalized to $\mathfrak{L} = 1$, so it is a conserved quantity. For massless particles, such as photons, we have $\mathfrak{L} = 0$. Since (6.6) is independent of t and ϕ, we have the conserved quantities $E := -d\mathfrak{L}/d\dot{t}$ and $L := d\mathfrak{L}/d\phi$. Thus, the system of ODEs describing the motion of test particles or photons is reduced to

$$\begin{aligned}
\frac{dt}{ds} &= \frac{E}{\rho^2}\left(\frac{\rho^2}{f} - fa^2\right) - \frac{fa}{\rho^2}L, \\
\frac{d\phi}{ds} &= \frac{f}{\rho^2}(aE + L), \\
\frac{d^2\rho}{ds} &= \frac{1}{2h}\left[-f_\rho(\dot{t})^2 - h_\rho(\dot{\rho})^2 + h_\rho(\dot{\zeta})^2 + F_\rho(\dot{\phi})^2 - 2(fa)_\rho \dot{t}\dot{\phi} - 2h_\zeta \dot{\rho}\dot{\zeta}\right], \\
\frac{d^2\zeta}{ds} &= \frac{1}{2h}\left[-f_\zeta(\dot{t})^2 + h_\zeta(\dot{\rho})^2 - h_\zeta(\dot{\zeta})^2 + F_\zeta(\dot{\phi})^2 - 2(fa)_\zeta \dot{t}\dot{\phi} - 2h_\rho \dot{\rho}\dot{\zeta}\right],
\end{aligned} \tag{7.5}$$

where $h := e^{2k}/f$ and $F := \rho^2/f - fa^2$. We are interested in studying light rays (the trajectory of photons) so we consider $\mathfrak{L} = 0$ in the sequel.

7.2.1 Numerical solution

In order to obtain the trajectory of each photon, we solve the system of first-order ordinary differential equations with an initial value

$$\begin{cases} \frac{d\mathbf{y}}{ds} = \mathbf{f}(s, \mathbf{y}), \\ \mathbf{y}(0) = \mathbf{y}_o, \end{cases} \tag{7.6}$$

namely, an initial value problem (IVP). To make (7.5) a system of first-order ODEs, we add the two auxiliary variables $d\zeta/ds = p^\zeta$ and $d\rho/ds = p^\rho$. Thus, the variables of the system are $\mathbf{y} = (t, \rho, p^\rho, \zeta, p^\zeta, \phi)$.

The initial condition for each photon is its location $(t_0, \rho_0, \zeta_0, \phi_0)$ in the spacetime and its four-momentum $(p_0^t, p_0^\rho, p_0^\zeta, p_0^\phi)$ at that point. Recall that for a photon we require $g_{\mu\nu}p_0^\mu p_0^\nu = 0$ for the initial four-momentum.

Since the system of ODEs is highly non-linear, we solve the IVP numerically. Given the value of $\mathbf{y}_n$, the fourth-order Runge-Kutta method gives the numerical value of $\mathbf{y}_{n+1}$ by the formula

$$\mathbf{y}_{n+1} = \mathbf{y}_n + \frac{h}{6}\left(\mathbf{k}_1 + 2\mathbf{k}_2 + 2\mathbf{k}_3 + \mathbf{k}_4\right), \tag{7.7}$$

(see [BF10]). The quantity $h = \psi(s_n)$ is the stepsize (which is updated at every iteration) and

$$\begin{aligned}
\mathbf{k}_1 &= \mathbf{f}\left(s_n, \mathbf{y}_n\right), \\
\mathbf{k}_2 &= \mathbf{f}\left(s_n + \frac{h}{2}, \mathbf{y}_n + \frac{h}{2}\mathbf{k}_1\right), \\
\mathbf{k}_3 &= \mathbf{f}\left(s_n + \frac{h}{2}, \mathbf{y}_n + \frac{h}{2}\mathbf{k}_2\right), \\
\mathbf{k}_4 &= \mathbf{f}\left(s_n + h, \mathbf{y}_n + h\mathbf{k}_3\right).
\end{aligned}$$

7.3 Ray-tracing

Ray tracing is a useful method in general relativity, it is used to calculate light rays in curved spacetimes, namely, the trajectories of photons. We are going to determine the light rays by integrating the equations of motion of photons, i.e., the geodesic equations for null vectors.

The idea is to determine what a camera could see at a certain distance from the black hole. In ray-tracing we do the computations backwards, namely, we consider the updating function as

$$\mathbf{y}_{n-1} = \mathbf{y}_n - \frac{h}{6}\left(\mathbf{k}_1 + 2\mathbf{k}_2 + 2\mathbf{k}_3 + \mathbf{k}_4\right). \tag{7.8}$$

7.3.1 Pinhole camera

One straightforward technique is to place a pinhole camera at a distance $\vec{R}_c$ pointing directly to the black hole. The notation with an arrow will denote a vector in space. Each light ray enters the aperture (or "pinhole") and hits the screen at the point $\vec{p}_0$, as shown in the figure 7.5. The vector $\vec{R}_c$ could have any direction, but since (6.6) is axisymmetric, we will place the camera in the direction $\vec{R}_c = (x_c, 0, z_c)$ in the coordinate system S. However, it is easier to visualize the direction of the light rays in a system S' where $\vec{R}_c = (R_c, 0, 0)$. The components of a vector in the system S' and S are related by

$$\vec{v} = R_y(\alpha)\vec{v}',$$

where $R_y(\alpha)$ is the rotation matrix about the y-axis in counterclockwise direction with an angle α (the inclination of the camera).

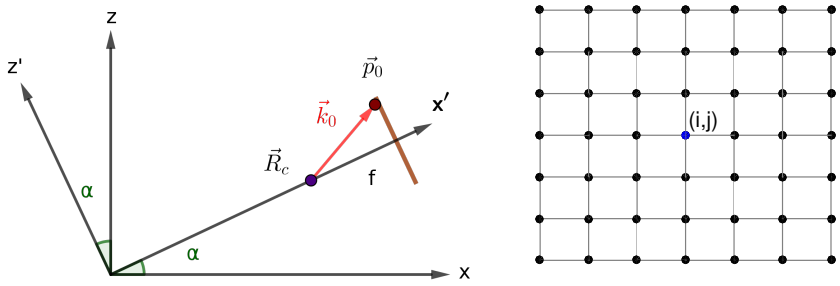

FIGURE 7.5: The left-hand side picture shows a pinhole camera of focal length f_L at the position $\vec{R}_c$ in the system S' and the right-hand side one shows the screen divided in dots representing each pixel. The screen is always perpendicular to the axis x'.

The screen has width d_W, height d_H, horizontal and vertical resolution I and J, respectively. The position $\vec{p}_0$ of each pixel (i, j) in the coordinate system S' is given

by

$$\begin{aligned} x_0 =& Rc + f_L, \\ y_0 =& \frac{d_W}{2}\left[2\frac{(i-1)}{(I-1)} - 1\right], \\ z_0 =& \frac{d_H}{2}\left[1 - 2\frac{(j-1)}{(J-1)}\right], \end{aligned}$$

and the direction $\vec{k}_0$ of each light ray in a flat spacetime would be

$$\vec{k}_0 = \left(\frac{f_L}{r_c}, \frac{y_0}{r_c}, \frac{z_0}{r_c}\right),$$

where $r_c = \sqrt{f_L^2 + y_0^2 + z_0^2}$, since $|\vec{k}_0| = 1$. However, the light ray is in the curved spacetime described by the metric (6.6), so its speed is less than $c = 1$. A good approximation of its actual speed is βc, where β is the factor $\beta = v(r)/c$ as shown in Figure 7.6. This factor is obtained as follows: assume a light ray falling radially into the black hole, then its radial velocity $v(r) = dr/dt$ can be obtained from the relation $g_{\mu\nu}u^\mu u^\nu = 0$, so

$$v(r) = \frac{dr}{dt} = \sqrt{-\frac{g_{tt}}{g_{rr}}},$$

where g_{rr} is

$$g_{rr} = \frac{d\rho}{dr}g_{\rho\rho} + \frac{d\zeta}{dr}g_{\zeta\zeta} = \frac{(\rho+\zeta)}{r}\frac{e^{2k}}{f}; \qquad r^2 = \rho^2 + \zeta^2.$$

The speed $v(r)$ is shown in the following figure. For simplicity, we have set $\zeta = 0$ so $v(r) = v(\rho)$. Then,

$$v(\rho) = \sqrt{-\frac{g_{tt}}{g_{\rho\rho}}} = \frac{f}{e^k}.$$

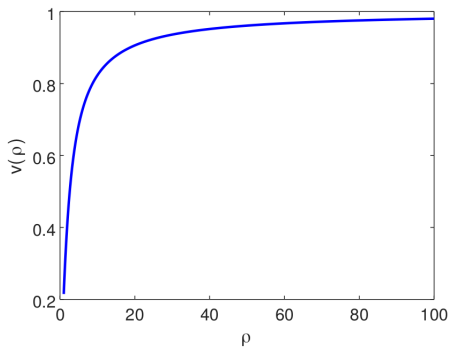

FIGURE 7.6: Speed of light in the presence of gravity. In this case, $\beta = v(\rho)$ since we are using units in which $c = 1$.

Thus, the direction of the light ray in the curved space-time is

$$\vec{k} = (k^x, k^y, k^z) = \beta_0 R_y(\alpha)\vec{k}_0, \tag{7.9}$$

where $\beta_0 = v(r_0)$, corresponds to the speed of light at the point $\vec{p} = R_y(-\alpha)\vec{p}_0$ and $r_0 = |\vec{p}|$. Then, the four-position and four-velocity in cartesian coordinates are

$$\mathbf{x} = \left(t, R_y(\alpha)\vec{p}_0\right), \tag{7.10a}$$

$$\mathbf{u} = \left(1, \beta_0 R_y(\alpha)\vec{k}_0\right). \tag{7.10b}$$

Finally, the initial data corresponding to each pixel (i, j) in the Weyl-Lewis-Papapetrou coordinates is obtained using the transformation formula

$$u^{\mu'} = \frac{dx^{\mu'}}{dx^{\nu}} u^{\nu},$$

where the relation between the coordinate systems is given in (6.5). Therefore, the components of $\mathbf{u}$ in the Weyl-Lewis-Papapetrou coordinates are

$$u^t = 1, \tag{7.11a}$$

$$u^\rho = \cos\phi k^x + \sin\phi k^y, \tag{7.11b}$$

$$u^\zeta = k^z, \tag{7.11c}$$

$$u^\phi = \frac{\cos\phi}{\rho} k^y - \frac{\sin\phi}{\rho} k^x. \tag{7.11d}$$

7.4 Ray-tracing pictures

The settings for the "camera" are as follows: we placed it with its focal length directed towards the origin and an inclination $\alpha = \pi/4$. Since it is directed towards the origin, the picture should be centered if there is no frame-dragging effect, as we can observe in the case $\varphi = 0$. However, we notice a shift as φ changes. Coloring the pixels according to the color of the ergospheres shown in Figure 7.4, we get the following pictures.

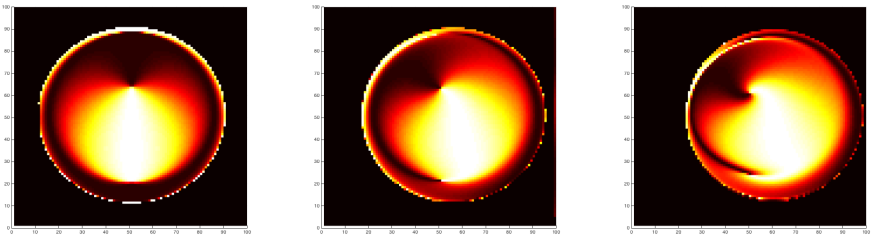

FIGURE 7.7: Picture of colored ergospheres with $\varphi = 0, \varphi = 0.5$ and $\varphi = 1.0$ respectively.

In order to visualize the equatorial symmetry and also the frame-dragging effect, we place the "camera" on the plane, i.e., we choose $\alpha = 0$. With this choice, we obtain the following simulation for the ergospheres of four black holes with different angular momenta.

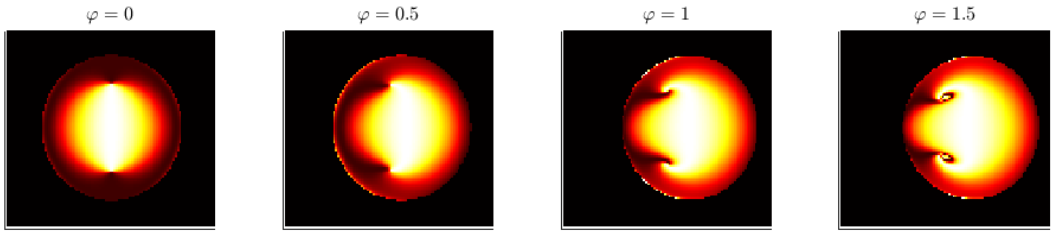

FIGURE 7.8: Pictures with $\alpha = 0$.

And for a better visualization on where the ergosphere is hit by the light ray, we can also paint the ergosphere with a checkerboard pattern.

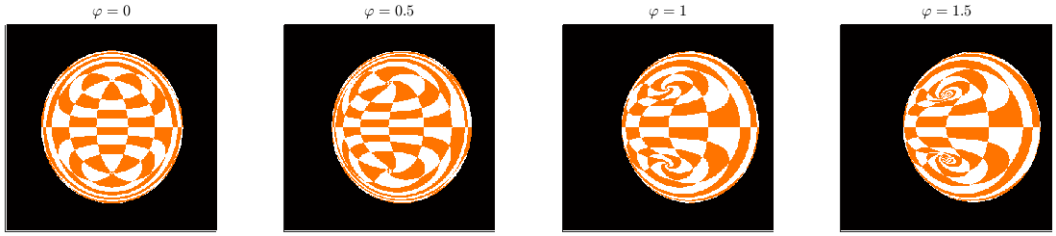

FIGURE 7.9: Pictures with $\alpha = 0$ with a checkerboard coloring.

Remark 7.4.1. *In the computation of the trajectories of the photons, we keep all the positions. However, in ray-tracing we are only interested in the source. Thus, from the computational perspective it is more convenient just updating the variable containing the information about the position at the n-th step.*

7.4.1 Thin disk

In order to test the method for the dust disk type of solutions given by the Ernst equation [KR05; Kle03; NM95], we place an ideal thin disk around the Kerr black hole, namely a bidimensional disk on the equatorial plane with inner radius R_{in}, outer radius R_{out}. For the simulations in this section, we will always use the values

$$R_{\text{in}} = 3, \quad R_{\text{out}} = 7$$

We color the pixels if their corresponding light rays hit the disk and for visualization purposes, we color the disk with a checkerboard pattern. We assign a color to a given pixel depending on the color its light ray hits.

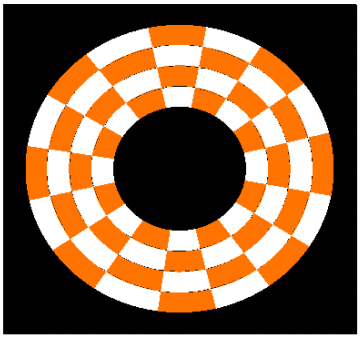

FIGURE 7.10: Checkerboard coloring of the ideal disk.

Consider, for example, the following light rays associated to some pixels. Some of them "hit" the ergosphere and others hit the disk. The rest escape to infinity. We consider the rotation parameter $\varphi = \pi/4$, which yields a spherical ergosphere.

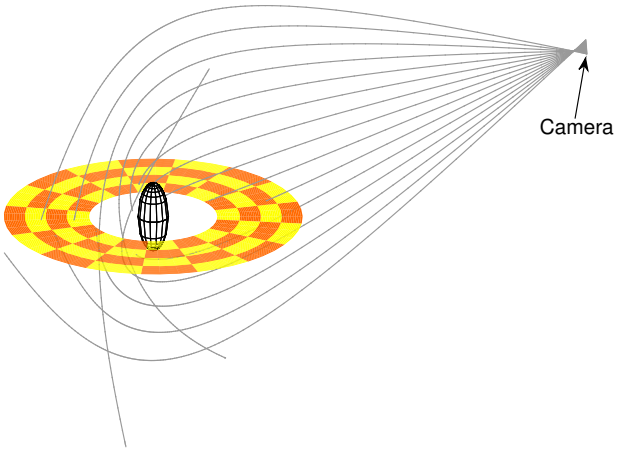

FIGURE 7.11: Three-dimensional trajectory of some light rays in a Kerr spacetime with parameter $\varphi = \pi/4$.

The parameters for the camera we used for this example, as well as for the other simulations in this section, are chosen to be

$$\begin{cases} \alpha = \frac{\pi}{18}\text{rad}, & R_c = 20, & f_L = 0.55, \\ d_W = 0.55, & d_H = 0.40, & I = J = 400. \end{cases}$$

Notice that since light is bent around the ergosphere, different pixels can hit the same spot on the disk and thus showing certain portions twice, as we observe in Figure 7.13. In the following xy-plane view, we observe the frame-dragging effect of the Kerr spacetime on the individual light-rays.

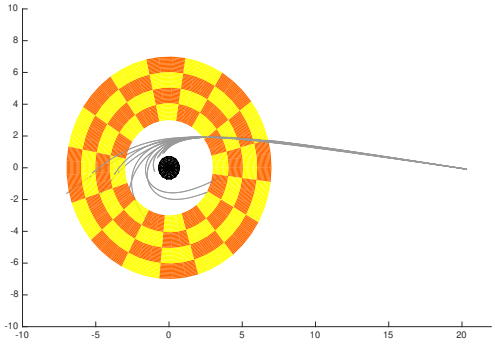

FIGURE 7.12: Trayectory of some light rays in a Kerr spacetime with parameter $\varphi = \pi/4$.

Since the light rays correspond to numerical integration of a system of ODEs via an iterative method, we need to set some stopping criteria:

- Stop if $s_n > T_{\max}$: the integration stops if the affine parameter surpasses this threshold. We use $T_{\max} = 25$ for the examples.
- Stop if $|g_{tt}| < \epsilon$: the integration stops if the light rays get close to the ergosphere. We use $\epsilon = 0.1$ for the examples in this section.
- Stop if the light rays hit the disk. Moreover, color the associated pixel depending on where the light ray hits the disk.

We observe in Figure 7.11 that the integration stops precisely with one of these stopping criteria. Now we show the full simulation of the picture of a disk in Kerr spacetimes with different parameters. We start with $\varphi = 0$, which is the Schwarzschild black hole and then continue with $\varphi = 0.5$, $\varphi = 1.0$ and finish with $\varphi = 1.5$, which is close to the extreme black hole $\varphi = \pi/2$.

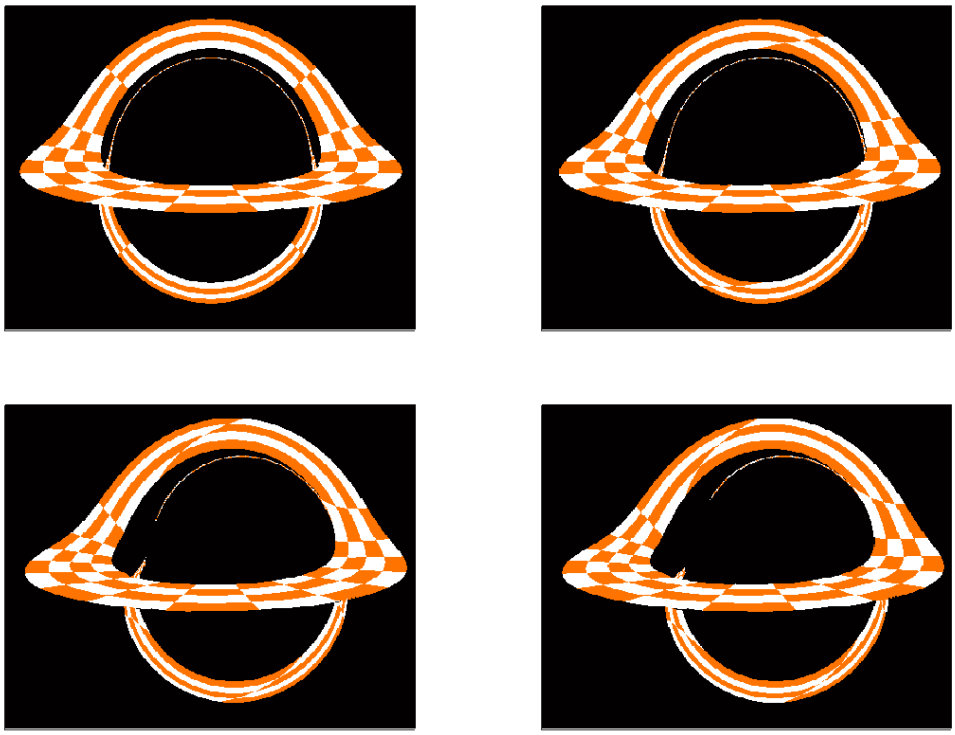

FIGURE 7.13: Simulation of the picture of thin disks in Kerr space-times with parameters $\varphi = 0$, $\varphi = 0.5$, $\varphi = 1.0$ and $\varphi = 1.5$.

Since light is curved in the vicinity of the black hole, we could be able to see objects behind it. As Figure 7.13 shows, a camera near the plane is able to record the whole accretion disk but strongly distorted. Moreover, we can clearly observe that the most distant part of the disk is recorded twice. It can be seen in Figure 7.11 that when the light rays cross the equatiorial plane, the dragging-effect pull them back, and they eventually hit the disk. This is a simulation of what we would visualize if we were able to take a picture pointed at the black hole with an inclination of $\alpha = \pi/18$ (namely, 10^o) with respect to the equatorial plane of the black hole (or $\pi - \alpha$ with respect to the rotational axis).

Another interesting consequence of the frame-dragging effect is that there might be photons with the right initial conditions that the light will orbit around the black hole. This can be observed in the *ring*, which correspond to light rays that hit the disk after several orbits. The full picture of the ring is missing in Figure 7.13 since the parameters $\varphi = 1.0$ and $\varphi = 1.5$ imply a stronger dragging-effect. Thus the light will take more time to finally hit the disk, since it will orbit the black hole more times.

7.5 Numerical derivatives

We are also interested in computing geodesics by using numerical values for the derivatives of the metric functions. These derivatives can be easily computed in an

explicit manner for Kerr, since the metric coefficients are given by algebraic function. However, as we saw in the previous chapter, in general this can be done only approximately, since the solutions of the Ernst equation are given by theta functions. To optimize this process, we take advantage of the smoothness of the metric coefficients and compute the derivatives via spectral methods, a highly efficient method to approximate derivatives on a grid.

The goal is to obtain the spectral derivatives of the functions on a bi-dimensional Chebyshev grid and then, using barycentric interpolation to approximate the derivative inside the boundaries of such grid. For example, let $f : [x_a, x_b] \times [y_a, y_b] \subset \mathbb{R}^2 \to \mathbb{R}$ be a smooth function on the compact set $[x_a, x_b] \times [y_a, y_b]$. We evaluate its values on a bi-dimensional Chebyshev grid 7.14 and store them in the array $v_{ij} = f(x_i, y_j)$. Its spectral derivatives will be given by

$$\partial_x f \approx (D_x \otimes \mathbb{I}_y)v,$$
$$\partial_y f \approx (\mathbb{I}_x \otimes D_y)v,$$

where $\otimes$ is the Kronecker product [Tre00] and D_x, D_y are the one dimensional spectral derivatives with respect to x and y respectively.

7.5.1 Barycentric interpolation

On the other hand, we can compute the values of a function $\psi : [x_a, x_b] \times [y_a, y_b] \to \mathbb{R}$ with known values on a grid on any arbitrary point $(x, y) \in [x_a, x_b] \times [y_a, y_b]$ via barycentric interpolation, i.e.,

$$\psi(x, y) \approx \frac{1}{a(x)b(y)} \sum_{i=0}^{N_x} \sum_{j=0}^{N_y} \frac{w_i^x w_j^y}{(x - x_i)(y - y_j)} \psi_{ij}, \tag{7.12}$$

where $a(x) = \sum_i w_i^x/(x - x_i)$, $b(y) = \sum_j w_j^y/(y - y_j)$ and w_i^x (resp. w_j^y) are the weights on the grid $[x_a, x_b]$ (resp. $[y_a, y_b]$).
In matrix form, let Ψ the matrix with entries $\Psi_{ij} = \psi(x_i, x_j)$ and A, B the column vectors with entries $A_i(x) = w_i^x/(x - x_i)$, $B_j(y) = w_j^y/(y - y_j)$. Thus,

$$\psi(x, y) \approx \frac{1}{\sum_i A_i(x) \sum_j B_j(y)} A(x)^\top \Psi B(y). \tag{7.13}$$

In general, the weights are given by $w_j = \prod_{k \neq j}(x_k - x_j)$, but for the Chebyshev grid it takes the simple form $w_j = (-1)^j(2 - \delta_{j,0} - \delta_{j,N})/2$. Although the weight formula depends on the limits x_a, x_b, the barycentric formula does not. Thus, we can use this formula for any limit [BT04]. Thus, to compute the values of the function ψ, it suffices to compute $A_i(x)$ and $B_j(y)$ at the point (x, y), which is easy to do, and then apply the formula (7.13).

Combining spectral differentiation with barycentric interpolation. Let $\phi(x, y) = \partial_x^r \partial_y^s f(x, y)$ be a smooth function on a compact domain $[x_a, x_b] \times [y_a, y_b]$, for some smooth funciton f on the same domain. Then, we approximate the derivatives of $\partial_x^r \partial_y^s f(x, y)$ at any point $(x, y) \in [x_a, x_b] \times [y_a, y_b]$ by obtaining the value on a grid of ψ via spectral differentiation $\psi = (D_x^r \otimes D_y^s)v$ and then applying the barycentric

interpolation formula (7.13) on (x, y). This is useful for functions whose derivatives have a complicated form, such as the metric functions described in Chapter 6.

7.5.2 Numerical derivatives of the metric coefficients

For the metric coefficients, assume that

$$g_{\mu\nu} = \sum_k \frac{P_k(\rho,\zeta)}{Q_k(\rho,\zeta)},$$

for piecewise smooth functions $P_k, Q_k : S \subset \mathbb{R}^2 \to \mathbb{R}$ for a compact square domain $S \subset \mathbb{R}^2$. The functions obtained from the Ernst equation in Chapter 6 have this form. In order to avoid numerical inaccuracies when $Q_k(\rho,\zeta) \to 0$, e.g., when we approach an ergosphere, we express the derivatives in the form

$$\partial_\sigma g_{\mu\nu} = g_{\mu\nu}\left[\frac{\partial_\sigma P}{P} - \frac{\partial_\sigma Q}{Q}\right], \tag{7.14}$$

where $\sigma = \rho, \zeta$. For ease of representation, let us assume that $g_{\mu\nu} = P(\rho,\zeta)/Q_k(\rho,\zeta)$. Thus to compute its derivatives, first compute the derivatives of P and Q and then use the formula (7.14). Namely,

- First, we need to compute the grid values of P and Q on a bidimensional grid $[\rho_{\min}, \rho_{\max}] \times [\zeta_{\min}, \zeta_{\max}]$ with resolution $N \times N$.
- Then, we compute the spectral derivatives of such functions, i.e., $\partial_\rho P \approx (D_\rho \otimes \mathbb{I}_\zeta)P$ and $\partial_\zeta \approx (\mathbb{I}_x \otimes D_\zeta)P$ and similarly for Q.
- We approximate the derivatives $\partial_\rho P, \partial_\zeta P$ at any point (ρ,ζ) using the barycentric interpolation formula (7.13). We do the same for $\partial_\rho Q$ and $\partial_\rho Q$.
- Finally, compute $\partial_\sigma g_{\mu\nu}$ with (7.14).

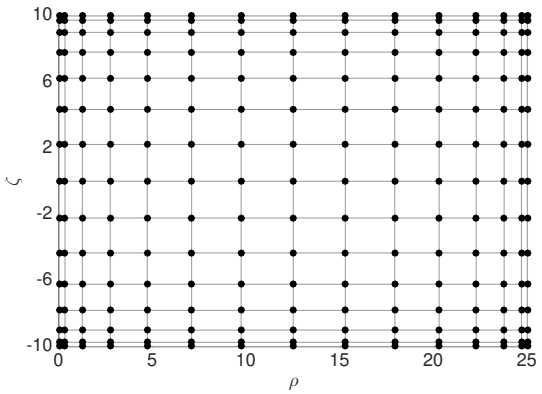

FIGURE 7.14: Chebyshev grid on $[\rho_a, \rho_b] \times [\zeta_a, \zeta_b]$.

Remark 7.5.1. *The metric functions of the Kerr example have discontinuities in the derivatives on the axis since they involve the term* $r_\pm = \sqrt{(\zeta - m\cos\varphi)^2 + \rho^2}$*, which is discontinuous at* $(\rho,\zeta) = (0, \pm m\cos\varphi)$*. Thus, we need to choose* $\rho_{\min} > 0$*. However, if the*

metric we are interested in does not have discontinuities, we can choose $\rho_{\min} = 0$*. Figure 7.15 shows the comparison between the trajectories obtained with the explicit form of the derivatives and with barycentric interpolation. Another option is using multiple domains.*

7.5.3 Geodesics with the approximated derivatives

For the following examples we chose a grid resolution $N = 50$. For the angular momentum parameter $\varphi = 0$ we use the domain $[\rho_{\min}, \rho_{\max}] \times [\zeta_{\min}, \zeta_{\max}] = [0.05, 25] \times [-10, 10]$ and for $\varphi = 0.5$ we use $[\rho_{\min}, \rho_{\max}] \times [\zeta_{\min}, \zeta_{\max}] = [0.4, 25] \times [-10, 10]$.

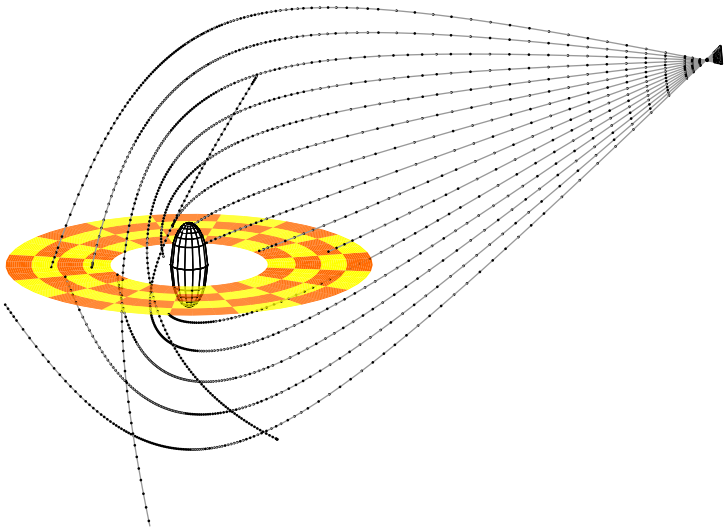

FIGURE 7.15: Some light rays obtained with both the explicit derivatives (grey lines) and the numerical ones (black dots).

As observed, this method is able to reproduce the same light rays without the explicit expression for the derivatives.

Bibliography

[AC21] D. Agostini and L. Chua. "Computing theta functions with Julia. Journal of Software for Algebra and Geometry". In: 11 (2021).

[Be11] A.I. Bobenko and C. Klein (ed.) *Computational Approach to Riemann Surfaces*. Lect. Notes Math. Springer, 2011.

[Bel+94] E.D. Belokolos et al. *Algebro-geometric approach to nonlinear integrable equations*. Springer, 1994.

[BF10] R. Burden and J. Faires. *Numerical Analysis, 9th ed*. Cengage Learning, 2010.

[Bia94] L. Bianchi. *Lezioni di geometria differenziale*. Enrico Spoerri, Pisa, 1894.

[BL04] C. Birkenhake and H. Lange. *Complex Abelian varieties*. GMW. Springer, 2004.

[BN12] H.W. Braden and T.P. Northover. "Bring's Curve: its Period Matrix and the Vector of Riemann Constants". In: *SIGMA* 8.65 (2012).

[BT04] J.P. Berrut and L.N. Trefethen. "Barycentric Lagrange Interpolation". In: *SIAM Review* 46.3 (2004), pp. 501–517.

[CKS19] L. Chua, M. Kummer, and B. Sturmfels. "Schottky Algorithms: Classical meets Tropical". In: *Mathematics of computation* 88 (2019).

[Con] K. Conrad. $SL_2(\mathbb{Z}$. URL: https://kconrad.math.uconn.edu/blurbs/grouptheory/SL(2,Z).pdf. (accessed: 03.04.2023).

[Dec+03] B. Deconinck et al. "Computing Riemann theta functions". In: *Mathematics of Computation* 73 (2003), pp. 1417–1442.

[DH01] B. Deconinck and M. van Hoeij. "Computing Riemann matrices of algebraic curves". In: *Physica D* 28 (2001), pp. 152–153.

[Dub81] B.A. Dubrovin. "Theta functions and non-linear equations". In: *Usp. Mat. Nauk. 36, No. 2, 11-80 (English translation: Russ. Math. Surv. 36, No. 2, 11–92* (1981).

[EHT19] EHT: Event Horizon Telescope Collaboration. "The Event Horizon Telescope Collaboration. First M87 Event Horizon Telescope Results. I. The Shadow of the Supermassive Black Hole". In: *The Astrophysical Journal Letters* 875.L1 (2019).

[Ern68] F. Ernst. "New formulation of the axially symmetric gravitational field problem". In: *Phys. Rev.* 167 (1968), p. 1175.

[Fay73] J.D. Fay. *Theta functions on Riemann surfaces*. Lect. Notes in Math. **352**. Springer, 1973.

[FJK19] J. Frauendiener, C. Jaber, and C. Klein. "Efficient computation of multidimensional theta functions". In: *J. Geom. Phys.* 141 (2019).

[FK01a] H. M. Farkas and I. Kra. *Theta constants, Riemann surfaces and the modular group*. Graduate Studies in Mathematics. American Mathematical Society, 2001.

[FK01b] J. Frauendiener and C. Klein. "Exact relativistic treatment of stationary counterrotating dust disks: Physical properties". In: *Phys. Rev. D* 63.8 (2001).

[FK16] J. Frauendiener and C. Klein. "Computational approach to compact Riemann surfaces". In: *Nonlinearity* 30.1 (2016), p. 138.

[FK80] H. M. Farkas and I. Kra. *Riemann surfaces*. Graduate Texts in Mathematics 71. Springer-Verlag, Berlin - Heidelberg - New York, 1980.

[Fri99] R. Fricke. "Über eine einfache Gruppe von 504 Operationen". In: *Mathematische Annalen* 52.23 (1899), pp. 321–339.

[GM18] S. Grushevsky and M. Möller. "Explicit formulas for infinitely many Shimura curves in genus 4". In: *Asian J. Math.* 22.2 (2018).

[Gru11] S. Grushevsky. "The Schottky problem". In: *Current developments in algebraic geometry, Math. Sci. Res. Inst. Publ.* 59 (2011), pp. 129–164.

[Gun82] R.C. Gunning. "Some curves in abelian varieties". In: *Invent. Math.* 66.3 (1982), pp. 377–389.

[Har03] J. Hartle. *Gravity: an Introduction To Einstein's General Relativity*. Addison Wesley, 2003.

[Igu72] J.I. Igusa. *Theta Functions*. GMW. Springer, 1972.

[Igu81] J.I. Igusa. "On the irreducibility of Schottky's divisor". In: *J. Fac. Sci. Univ. Tokyo Sect. IA Math.* 28 (1981), pp. 531–545.

[Ker63] R. Kerr. In: *Phys. Rev.* 11.5 (1963), p. 237.

[KGV83] S. Kirkpatrick, C. Gelatt Jr., and M. Vecchi. "Optimization by simulated annealing". In: *Science* 20 (1983), pp. 671–680.

[KKS04] C. Klein, D. Korotkin, and V. Shramchenko. "Ernst equation, Fay identities and variational formulas on hyperelliptic curves". In: *Mathematical Research Letters* 9 (2004), pp. 27–45.

[Kle03] C. Klein. "Exact relativistic treatment of stationary black-hole–disk systems". In: *Phys. Rev. D: Particles and Fields* 68.2 (2003).

[Kor88] D. Korotkin. "Finite-gap solutions of the stationary axisymmetric Einstein equation in vacuum". In: *Theor. Math. Phys.* 77 (1988), p. 1018.

[Kor91] D. Korotkin. "Solutions of the vacuum Einstein equation having toroidal infinite red-shif surface". In: *Class. Quantum Grav.* 8.L219 (1991).

[Kow88] S. Kowalevski. "Sur le problème de la rotation d'un corps solide autour d'un point fixe". In: *Acta Math.* 12 (1888), pp. 177–232.

[KR05] C. Klein and O. Richter. *Ernst Equation and Riemann Surfaces*. Lecture Notes in Physics, Vol. 685. Springer, 2005.

[Kri10] I. Krichever. "Characterizing Jacobians via trisecants of the Kummer variety". In: *Ann. of Math.* 172.1 (2010), pp. 485–516.

[Kri77] I. Krichever. "Methods of algebraic geometry in the theory of nonlinear equations". In: 32.6 (1977), pp. 185–213.

[LLL82] A.K. Lenstra, H.W. Lenstra Jr., and L. Lovász. "Factoring polynomials with rational coefficients". In: *Math. Ann.* 261 (1982).

[Mac65] A. Macbeath. "On a curve of genus 7". In: *Proceedings of the London Mathematical Society* 15 (1965), pp. 527–542.

[Mat59] T. Matsusaka. "On a characterization of a Jacobian variety". In: *Mem. Coll. Sci. Univ. Kyoto Ser. A. Math.* 32 (1959), pp. 1–19.

[Min11] H. Minkowski. "Gesammelte Abhandlungen". In: *Leipzig-Berlin: Teubner* 107 (1911).

[Min91] H. Minkowski. "Über die positiven quadratischen Formen und über kettenbrucha ähnliche Algorithmen". In: *J. Reine und Angewandte Math* 107 (1891), pp. 278–297.

[Mir94] R. Miranda. *Riemann Surfaces and Algebraic Curves*. Graduate Studies in Mathematics. American Mathematical Society, 1994.

[MTW73] C. Misner, K. Thorne, and J. Wheeler. *Gravitation*. W.H. Freeman, 1973.

[Mum83] D. Mumford. *Tata lectures on theta II*. Progress in Mathematics 29. Birkhäuser, Boston, MA, 1983.

[NM95] G. Neugebauer and R. Meinel. "General relativistic gravitational field of the rigidly ro-tating disk of dust: Solution in terms of ultraelliptic functions". In: *Phys. Rev. Lett.* 75 (1995), pp. 3046–3048.

[RS94] E. Romeijn and R.L. Smith. "Simulated annealing for constrained optimization". In: *Journal of Global Optimization* 5 (1994), pp. 101–126.

[Rub81] R.Y. Rubinstein. *Simulation and the Monte Carlo Method*. Wiley, New York, NY, 1981.

[Sch88] F. Schottky. "Zur Theorie der Abelschen Funktionen von vier Variabeln". In: *J. reine angewandte Mathematik* 102 (1888), pp. 304–352.

[Sch93] B. Schindler. "Period Matrices of Hyperelliptic Curves". In: *Manuscr. Math.* 78 (1993), pp. 369–380.

[SD16] C. Swierczewski and B. Deconinck. "Computing Riemann theta functions in Sage with applications". In: *Mathematics and Computers in Simulation* 127 (2016), pp. 263–272.

[Shi86] T. Shiota. "Characterization of Jacobian varieties in terms of soliton equations". In: *Invent. Math.* 83.2 (1986), pp. 333–382.

[Sie89] C.L. Siegel. "Topics on Complex Function Theory". In: *John Wiley & Sons* III (1989).

[Sil09] J. Silverman. *The arithmetic of elliptic curves, 2nd edition*. Springer, 2009.

[Tai97] I.A. Taimanov. "Secants of Abelian Varieties, Theta Functions and Soliton Equations". In: *Russ. Math. Surv.* 52 (1997).

[Tre00] L.N. Trefethen. *Spectral Methods in MATLAB*. Society for Industrial and Applied Mathematics, 2000.

[Wal84] R. Wald. *General Relativity*. U. Chicago Press, 1984.

[Wel84] G.E. Welters. "A criterion for Jacobi varieties". In: *Ann. of Math.* 120.3 (1984), pp. 497–504.